Abstract

Title of Dissertation: Studies of SOHO Comets

Matthew Manning Knight, Doctor of Philosophy, 2008

Dissertation directed by: Professor Michael F. A'Hearn
Department of Astronomy

We present here a study of the Kreutz, Marsden, and Kracht comets observed by SOHO including photometric reductions and analysis, numerical modeling, and physical modeling. We build off the work of Biesecker *et al.* (2002) and analyze the results of our photometric study of more than 900 lightcurves of Kreutz comets observed by SOHO. We find that they do not have a bimodal distance of peak brightness as previously reported, but instead peak from 10.5–14 $R_\odot$ (prior to perihelion), suggesting there is a continuum of compositions rather than two distinct subpopulations. The lightcurves have two rates of brightening, typically $\propto r^{-7.3\pm2.0}$ when first observed by SOHO then rapidly transitioning to $\sim r^{-3.8\pm0.7}$ between 20–30 $R_\odot$. It is unclear at what distance the steeper slope begins, but it likely does not extend much beyond the SOHO field of view. We derive nuclear sizes up to ∼50 meters in radius for the SOHO observed comets, with a cumulative size distribution of $N(>R)\propto R^{-2.2}$ for comets larger than 5 meters in radius. This size distribution cannot explain the six largest members of the family seen from the ground, suggesting that either the family is not collisionally evolved or that the distribution is not uniform around the orbit. The total mass of the distribution up to the largest expected size (∼500 meters) is $\sim 4\times10^{14}$g, much less than the estimated mass of the largest ground observed members. After correcting for the changing discovery circumstances, the flux of comets reaching perihelion has increased since 1996, and the increase is seen in comets of all sizes.

We consider the Marsden and Kracht comets together due to their apparent dynamical linkage (e.g. Ohtsuka *et al.* (2003); Sekanina and Chodas (2005)). Seasonal effects of the viewing geometry make it impossible to build a characteristic lightcurve of either group. Many are seen to survive perihelion and most reach a peak brightness within ∼6 hours of perihelion with no preference for peaks before or after perihelion. Most are barely above the threshold for detection, and the largest is probably smaller than 30 meters in radius. Our dynamical simulations suggest that the orbital distribution of the Kracht group can be produced by low velocity fragmentation events and close approaches to Jupiter over the last 50–250 years. We construct fragmentation trees for the Marsden and Kracht groups and predict that 7–8 comets in each group may be visible on their next perihelion passage.

This research was supported by NASA Planetary Atmospheres grants NAG513295 and NNG06GF29G.

Studies of SOHO Comets

by

Matthew Manning Knight

Dissertation submitted to the Faculty of the Graduate School of the
University of Maryland at College Park in partial fulfillment
of the requirements for the degree of
Doctor of Philosophy
2008

Advisory Committee:

Professor Michael F. A'Hearn, chair
Doctor Douglas A. Biesecker
Professor Douglas P. Hamilton
Professor Derek C. Richardson
Professor Paul D. Feldman
Professor James Farquhar

Preface

The work presented here has not been published, but has been presented as posters and talks at the 2004–2007 AAS Division of Planetary Science meetings, the 2005 Asteroids, Comets, and Meteors meeting, and the January 2008 American Astronomical Society meeting. It has made use of the University of Maryland's time at Kitt Peak National Observatory and has benefited from collaboration with scientists from Laboratoire d'Astronomie Spatiale in Marseille, France, NASA's Goddard Space Flight Center, and the Naval Research Laboratory.

Due to the quantity of data produced, the work included herein will be published in multiple places. More than 20,000 reduced and calibrated images of Kreutz comets observed by SOHO have been submitted to the Planetary Data System for archiving and will be made public after passing peer review. Later updates will include the Kreutz comets observed since 2005 and the non-Kreutz comets. The photometry discussed here will be published in International Comet Quarterly and the Planetary Data System. The analysis of the Kreutz comets will be submitted to *Icarus* shortly, and the analysis of the Marsden and Kracht comets will be submitted to *Icarus* either independently or jointly with the Marseille group.

To my parents, John and Nancy Knight, whose support and encouragement have allowed me to follow my dreams and made me who I am today.

Acknowledgements

Thanks to my advisor, Michael A'Hearn for helping me reach my potential as a scientist. He has encouraged me to explore my scientific interests, indulged my desires to travel, and allowed me to make mistakes along the way. He has matched deep insight with a quick wit to keep me terrified of disappointing him for the better part of a decade. I can't tell you how many times I've been proud of myself for coming up with some great idea only to flip through my notebook and find a suggestion from Mike 10 months ago that told me to do just that. Thanks also to Doug Hamilton and Doug Biesecker for serving as co-advisors and helping me with the occasional topics Mike doesn't know everything about.

I am indebted to the many planetary scientists who have taken me under their wings and helped me to feel like I am among friends at conferences and telescopes. These include Beatrice Müller, Nalin Samarasinha, Yan Fernandez, Laura Woodney, Tony Farnham, Lucy McFadden, Casey Lisse, Derek Richardson, Donna Pierce, Jianyang Li, Dennis Wellnitz,

Olivier Groussin, and Amy Lovell. Astronomy is immensely more rewarding when you work with friends.

Thanks to the graduate students, postdocs, professors, and staff who have made all these years of graduate school so much more fun than I thought they'd be. I couldn't possibly name everyone, but the following people deserve special notice: Nicholas Chapman, Kevin Walsh, Rahul Shetty, Rob Piontek, Vanessa Lauburg, Stephanie Zonak, Franziska Koeckert, Lisa Wei, John Vernaleo, Claudia Knez, David Garofalo, Ke Zhang, David Rupke, Cole Miller, Kayhan Gültekin, Glen Petitpas, Chul Gwon, Ji Hoon Kim, Woong-Tae Kim, and Nikolas Volgenau. Special thanks to all the Dirty Snowballs past, present, and future for indulging my sports star fantasies. We may never have won an IM title, but I hope you all had as much fun as I did.

Thanks to Aung, Kyaw, and everyone at Mandalay. I am already longing for chicken 11 and I haven't even moved away yet!

Thanks to all the teachers who inspired and challenged me along the way, most notably Miss Robertson, Mr. Kreisa, Mr. Lynch, Mr. Wallace, Professor Deaver, and Professor Elzinga.

Thanks to my family for their love, encouragment, hot meals, and free laundry. I am particularly grateful to my uncle Don Manning for all those free tickets and for his longstanding offer to proofread my papers. I also wish to remember my late grandfather, Bus Knight, from whom I apparently inherited the only bit of science genes in the family.

I have found that lying on the floor in the sun next to a purring cat makes all of life's troubles less important. Thanks to all those cats who

have given me a new perspective on life.

Finally, thanks to my wife, Stacy Teng. She has put up with my being "No Fun Matthew" for months on end and has managed to make me smile whenever I've needed it.

Contents

List of Tables

List of Figures

Chapter 1

Introduction

1.1 A Brief History of Sungrazing Comets

Comets have been seen by sky watchers around the world for millennia. There are written records of 1P/Halley on every apparition since 240 BCE. A silk book found in Mawangdui, China which dates from about 168 BCE depicts 29 types of comets, indicating that the Chinese had already been recording comet appearances for centuries. The significance of comets throughout history is reflected in the abundance of clay tablets, rock art, coins, and paintings depicting comets (Yeomans 1991). A small number of these comets were seen near the Sun (see e.g. England (2002); Hasegawa (1979); Hasegawa and Nakano (2001); Kronk (1999); Strom (2002) and references therein). These comets were often quite spectacular, some bright enough to be seen during the day and others having tails which stretched for tens of degrees across the sky.

The first comet which was recognized as having a sungrazing orbit was C/1680 V1 (Newton (1687), Halley (1705), and others) which was also historically significant

as the first comet to have its orbit calculated using Newton's theory of gravitation[1]. Several other bright comets were seen near the Sun in the next few decades, however no further obvious sungrazers were observed until the 1800s when C/1826 U1 (1826 V), C/1843 D1 (1843 I = "The Great March Comet"), C/1880 C1 (1880 I = 1880a = "The Great Southern Comet"), X/1882 K1 ("Eclipse Comet" or "Tewfik"), C/1882 R1 (1882 II = 1882b = "The Great September Comet"), and C/1887 B1 (1887 I = 1887a) were observed. C/1843 D1 and C/1882 R1 were two of the brightest comets of the nineteenth century. C/1882 R1 was observed to split into at least five fragments, the brightest of which persisted for more than eight months after perihelion (Kronk 1999; Marsden 2005).

While a number of authors had previously speculated about apparent linkages between sungrazing comets (see Marsden (2005) and Kronk (1999, 2003) for detailed discussions of these works), Kreutz (1888, 1891, 1901) was the first to rigorously show dynamical linkages. He calculated periods for the individual fragments of C/1882 R1 ranging from 671.3 to 955.2 years. This suggested that C/1882 R1 was likely the return of the famous comet of 1106 (X/1106 C1, which was observed by people around the world). Kreutz concluded that many of the other bright sungrazers observed during the preceding 250 years (C/1668 E1, C/1843 D1, C/1880 C1, X/1882 K1, and possibly X/1702 D1 and C/1887 B1) were related to these comets via splitting[2]. It should be noted that while the group bears Kreutz's name, Kirkwood (1880) had earlier argued that C/1843 D1 and C/1880 C1 were fragments

[1]While there is no formal definition for what constitutes a sungrazing comet (or sungrazer), in this paper we include all comets which reach perihelion within $\sim$15 $R_\odot$ (1 $R_\odot$ = 0.0046524 AU). This includes nearly all the comets discovered by SOHO and excludes most comets seen from the ground

[2]Ironically, this study showed that C/1680 V1, the first identified sungrazer, was not likely a member of the Kreutz family!

of the same parent comet. He suggested that the parent may have been the comet of 372 BCE which was allegedly observed to break up close to the Sun (attributed alternatively to Aristotle and the Greek historian Ephorus–see the discussion in Kronk (1999) for more information). While no orbit can reliably be computed for this comet, the idea that this comet was the progenitor of the Kreutz family persists.

The twentieth century yielded four more bright sungrazers (C/1945 X1 = 1945 VII = 1945g = Du Toit, C/1963 R1 = 1963 V = 1963e = Pereyra, C/1965 S1 = 1965 VIII = 1965f = Ikeya-Seki, and C/1970 K1 = 1970 VI = 1970f = White-Ortiz-Bolelli), all of which were members of the Kreutz group (Hasegawa 1966; Kresák 1966; Marsden 1967, 1989). Ikeya-Seki was perhaps the most spectacular comet of the twentieth century, reaching magnitude –10 or –11 and being visible during the day. It displayed a 20–25° tail for several weeks, and was observed to split very near perihelion[3]. Orbital integrations strongly suggest it fragmented from C/1882 R1 around 1100 CE, quite possibly being observed as the comet of 1106 (X/1106 C1). Orbital elements of probable members of the Kreutz family seen from the ground can be found in Table A.1.

The next advance in the understanding of sungrazing comets came with the discovery of 16 Kreutz comets by the space-based coronagraphs Solar Maximum Mission (SMM) and Solwind from 1979–1989[4]. Solwind operated from 1979 to 1985, discovering six comets. The first (and brightest) of these was C/1979 Q1 (1979 X) which reached a peak magnitude of –3.5 (Michels *et al.* 1982; Sheeley *et al.* 1982) and may have been detected from the ground (Chochol *et al.* 1983). The Coronagraph/Polarimeter instrument on the Solar Maximum Mission operated

[3]http://www.cometography.com/lcomets/1965s1.html

[4]Four additional comets – three Kreutz and one non-group – were found by Rainer Kracht in archival Solwind images in 2005 (Kracht and Marsden 2005a,b,c).

for six months in 1980 and then continuously from 1984 to 1989. It discovered 10 comets and also observed one comet which was discovered by Solwind. Interestingly, all but one of these arrived within a 2 year stretch, suggesting arrivals were "highly episodic" (MacQueen and St. Cyr 1991). The SMM and Solwind comets were much fainter than those seen from the ground, and implied a much a larger population of smaller Kreutz comets than was previously known. Orbital elements of the Kreutz comets observed by SMM and Solwind can be found in Table A.2.

Another leap forward in the understanding of sungrazing comets came with the launch of NASA's SOlar and Heliospheric Observatory (SOHO) in late 1995. SOHO's unprecedented sensitivity at small solar elongations opened a window into an even fainter realm of sungrazing comets. As of May 2008, it has discovered more than 1400 comets, including more than 1200 Kreutz sungrazers, three new groups of near-Sun comets: the Marsden, Kracht, and Meyer groups (Kracht *et al.* 2002; Meyer *et al.* 2002), the first periodic comet seen by SOHO (Hönig 2006), and more than 50 as-yet unlinked comets. See Table 1.1 for an overview of the comets discovered by SOHO, and Tables A.3– A.4 for orbital elements of all the Marsden and Kracht comets observed by SOHO from 1996–2005 (in the interest of space the Kreutz and Meyer elements are not included). Nearly all of these comets are faint, with only a few as bright as those seen by Solwind and SMM. They are believed to be small, probably less than 50 meters in size, and many have arrived within a few hours of each other. These discoveries have demonstrated that rather than consisting of only a few isolated members separated by months to decades, the Kreutz group is made up of a nearly continuous trail of small comets of varying sizes. The discovery of the additional groups of sungrazing comets has shown that the near-Sun environment is a much more populous area than was previously known, and provides an opportunity to observe split comets on a regular basis.

Group	Number[a]	q (AU)[b]	e[c]	ω (°)	Ω (°)	i (°)	Period (yr)
Kreutz	1225	0.0056	>0.9999	80.0	0.4	143.2	500–1000
Marsden	32	0.048	0.984	24.2	79.0	26.5	5.30–6.10
Kracht	31	0.045	0.984	58.8	43.8	13.4	4.81–5.81
Meyer	85	0.0358	1.0	57.4	73.1	72.6	unknown
P/2007 R5	4	0.054	0.978	48.6	0.0	12.7	3.99
Non-group	59	many	many	many	many	many	unknown

[a] For comets with periods shorter than the lifetime of SOHO (Marsden, Kracht, and P/2007 R5), the number of comets observed is greater than the number of unique comets. That is, some of these comets have apparently been observed on more than one apparition, but for these purposes, each apparition has been counted as a distinct comet.

[b] 1 $R_\odot$=0.0046524 AU

[c] The orbital arcs for most comets observed by SOHO are too short to determine an elliptical orbit and so are published with an eccentricity of 1.0. It is only through linking multiple apparitions that eccentricity and period are derived. The eccentricities and periods of Kreutz comets are for those observed from the ground.

Table 1.1: An overview of the orbital properties of the comets discovered by SOHO as of May 2008. The elements cited are averages of all members in a given family.

In this paper we reduce and analyze the comets observed by SOHO from 1996–2005. In the remainder of this chapter we discuss the reasons for studying sungrazing comets. In Chapter 2 we discuss the photometric reductions of comets observed by SOHO. In Chapter 3 we discuss the most famous group of sungrazing comets, the Kreutz group. In Chapter 4 we discuss the Marsden and Kracht groups, two groups of near-Sun comets which appear to be related to each other. Finally, in Chapter 5 we summarize our results and discuss the future of sungrazing comet observations. The Meyer group of sungrazing comets and P/2007 R5 are not investigated here, but will be revisited when considering the future of sungrazing comet observations.

1.2 The Importance of Studying Sungrazing Comets

Comets are believed to be the most accessible pristine remnants of the formation of the solar system[5]. Their compositions reflect the primordial abundances in the solar system. The study of comets has implications for the origin of life on Earth (comets are frequently considered as a source for water and possibly even for life itself) and is closely tied to other fields of astronomy such as interstellar dust, protostars, and exoplanets. This work studies sungrazing comets which are the product of repeated fragmentation, and broadens our understanding of how comets behave from birth to death.

1.2.1 Sungrazers: Probing the Extremes of the Solar System

As the evolution of the solar system is currently envisioned, the comets seen today were formed approximately 4–40 AU from the Sun, and were scattered outward by the planets (see e.g. Dones *et al.* (2004) and references therein). Those that were not ejected from the solar system were effectively in "cold storage", revolving around the Sun on long, slow orbits in the regions now known as the Kuiper Belt or the Oort Cloud until being perturbed into the inner solar system. Gravitational interactions with the planets trap some of these comets into orbits that are observable from the Earth. Most comets have highly eccentric orbits and only spend a short amount of time close to the Sun. When a comet approaches the Sun, the increasing temperature causes the volatile ices near its surface to sublime, with activity due to water

[5]Objects in the Kuiper Belt and the Oort Cloud are also considered to be nearly pristine but their perihelion distances are currently so large as to make them difficult (or impossible) to study and collectively they are as yet unvisited.

beginning around 3 AU. Gas escapes from the nucleus at high velocities, entraining dust with it. The comet brightens with decreasing heliocentric distance due to the increasing production rate of the volatiles, the increasing amount of dust in the coma which reflects the solar flux, and emission from excited species in the coma. Despite all this activity near the surface, the thermal wave typically only heats the outermost few meters of the nucleus, and the interior remains cold, preserving its primordial composition.

Many different techniques have been employed to directly and indirectly measure the compositions of comets including narrowband imaging, spectroscopy, space-based observations, and in situ measurements. Most of what is known of the composition of comets was obtained for comets observed close to the Earth, at heliocentric distances near 1 AU. Comets observable from the ground rarely reach distances smaller than 0.5 AU, and when they do they are often difficult to observe due to their small solar elongations.

Since the first space-based coronagraphs were launched in the 1970s, it has become possible to observe comets which pass very close to the Sun. SOHO has observed more than 1400 near-Sun comets since 1996, the vast majority of which are members of the Kreutz family of sungrazing comets. Thanks to these discoveries, we now know that the near-Sun environment is rich with small (probably smaller than 50 meters in radius) comets. These comets provide access to a region of the solar system in which no other small bodies have been observed. They probe regions of temperature encountered nowhere else in the solar system, and are subject to higher stresses (thermal and tidal) than any comets except those with rare close approaches to a planet (e.g. D/1993 F2 = 1994 X = Shoemaker-Levy 9). By studying sungrazing comets we can learn about the least volatile components of cometary nuclei and infer properties of their interiors.

1.2.2 Sungrazers: An Abundant Collection of Fragmented Comets

In the last two decades, fragmented comets D/1993 F2 Shoemaker-Levy 9 (SL9), C/1999 S4 LINEAR, and 73P/Schwassmann-Wachmann 3 (SW3) have garnered widespread attention. While rarely as spectacular as these examples, comet splitting is reasonably common. Noting the statistics of split periodic comets over the last ∼200 years, Boehnhardt (2004) estimated a rate of 3% per century. Chen and Jewitt (1994) estimated a rate of ∼1 fragmentation event per century per comet from a sample of 49 comets, while Weissman (1980) estimated a splitting rate of 1% for short period comets (also 10% for dynamically new comets and 4% for older long period comets).

Fragmentation can be explained by a number of mechanisms, perhaps the most obvious being tidal splitting due to the differential gravity applied across the comet nucleus. In theory, tidal splitting can happen near any massive body, but there is only evidence of it happening near Jupiter (e.g. SL9) and the Sun (e.g. C/1965 S1 Ikeya-Seki). Tidal splitting can also weaken the nucleus leading to its eventual fragmentation via other mechanisms. These include thermal stress induced by the propagation of a heat wave, buildup of internal gas pressure caused by excitation of volatiles trapped below the surface, and rotation of the nucleus faster than its internal strength can sustain. Comets may also split due to collisions, although these are unlikely in the current solar system (Boehnhardt (2004) and references therein).

Fragmentation can manifest itself in several ways: Two or more large fragments may be produced, such as the more than 50 fragments seen in SW3. This can result in a family (or group) of comets which usually share the same orbit but are

always linked dynamically. The comet may disintegrate into many small fragments which disappear over days to weeks as did C/1999 S4 LINEAR and/or can lead to meteor showers on Earth like the remnants of 3D/Biela. Finally, one or more small pieces may be dislodged which, while too small or short-lived to be seen directly, can cause unexpected features in the coma such as rapid brightening (this is a plausible explanation for the outburst of 17P/Holmes in October 2007 during which it brightened from magnitude ∼17 to magnitude ∼3 in about 42 hours) or striae in the dust tail (as seen in C/1995 O1 Hale-Bopp). It is evident from the above scenarios that fragmentation is a significant contributor to the end-state of comets: the shedding of mass accelerates the diminution of the nucleus. Repeated fragmentation can cause comets to become too small to be seen.

Fragmented comets are interesting to study because they provide a window into the interior composition and structure of comet nuclei. If it is assumed that the cometesimals from the primordial solar system are preserved in the interiors of comets, then disruption of nuclei gives an idea of the size distribution of the cometesimals in the area where they formed assuming that the fragmentation is back into the original cometesimals. Dynamical integrations and the chemical composition of these fragments provide additional clues to determine the parent comet's formation region which, in turn, constrains models of the early solar system. Comparison of the compositions of fragments with each other can yield information about the homogeneity or heterogeneity of the parent comet. Furthermore, combining shape and rotation periods can give lower limits on the bulk density of nuclei and, when comparing multiple fragments, possibly the bulk density of the parent comet. The rate of disappearance of fragments can give information on the size and composition of these fragments. Finally, determination of the separation velocity between fragments or the velocity of the leading edge of an outburst combined with estimates of

the mass involved can yield the total energy involved in the outburst.

Despite the prevalence of comet fragmentation, only one event is well understood: the disruption of SL9 (Asphaug and Benz 1996). More often, the result of the splitting is not seen until well after the event. Many of the comets which appear to have split have long periods and will not be seen again for 70–10^4 years (e.g. likely split pairs C/1988 F1 (Levy) and C/1988 J1 (Shoemaker-Holt), C/1988 A1 (Liller) and C/1996 Q1 (Tabur), C/2002 C1 (Ikeya-Zhang) and C/1661 C1, C/2002 A1 (LINEAR) and C/2002 A2 (LINEAR), and C/2002 Q2 (LINEAR) and C/2002 Q3 (LINEAR)). Furthermore, split fragments often do not persist and it is difficult to study them in comparison to one another. Only a handful of families (i.e. containing more than two surviving comets) are known: the Kreutz, Marsden, Kracht, and Meyer sungrazing groups, 73P/Schwassmann-Wachmann 3, and the (nameless) group of 42P/Neujmin 3, 53P/Van Biesbroeck, and possibly 14P/Wolf and 121P/Shoemaker-Holt 2 (Carusi *et al.* (1985); Tancredi *et al.* (2000)).

The Kreutz, Marsden, and Kracht sungrazing families are particularly promising systems of fragmented comets due to their large populations, frequency of observability, and linkages to other well observed comets. More than 1200 Kreutz comets are known, and on average one is seen in the SOHO field of view every few days. 32 Marsden and 31 Kracht comets have been seen, with arrivals on average every few months, and 7–8 comets in each group have been observed twice. The Kreutz comets seen by SOHO are the very small relatives of some of the most spectacular comets seen in the last 200 years (e.g. C/1965 S1 Ikeya-Seki and C/1882 R1). The Marsden and Kracht comets have been dynamically linked to the Machholz complex, a group which is believed to have split from a single progenitor prior to 950 CE and also includes 96P/Machholz 1, the Daytime Arietids, and the Southern δ Aquarids (Ohtsuka *et al.* 2003; Sekanina and Chodas 2005). While the data from

individual Kreutz, Marsden, or Kracht comets are sparse, in the aggregate they provide a meaningful sample size with which to study fragmented populations.

Chapter 2

Photometric Reductions

2.1 Overview of SOHO/LASCO

NASA's SOlar and Heliospheric Observatory (SOHO) satellite was launched in December 1995 and began taking data in January 1996. It is in a halo orbit around the Earth-Sun Lagrange point L1 (the Lagrange point on the line between the Earth and the Sun located approximately 0.01 AU from the Earth, which orbits the Sun with the same period as the Earth). SOHO contains a suite of instruments designed to continuously observe the Sun and the near-solar environment at varying wavelengths. These include the Coronal Diagnostic Spectrometer (CDS), Charge, ELement, and Isotope Analysis System (CELIAS), COmprehensive Suprathermal and Energetic Particle Analyzer (COSTEP), Extreme ultraviolet Imaging Telescope (EIT), Energetic and Relativistic Nuclei and Electron experiment (ERNE), Global Oscillations at Low Frequencies (GOLF), Large Angle and Spectrometric Coronagraph (LASCO), Michelson Doppler Imager (MDI), Solar Ultraviolet Measurements of Emitted Radiation (SUMER), Solar Wind Anisotropies (SWAN), Ultraviolet Coronagraph Spectrometer (UVCS), and Variability of Solar Irradiance and Gravity Oscillations (VIRGO) (Domingo *et al.* 1995).

Comets have been observed by three of the instruments on board SOHO: SWAN, UVCS, and LASCO. SWAN observes solar Lyman alpha photons (121.6 nm) and typically observes the whole sky three times per week[1]. It has observed several comets seen from the ground including C/1995 O1 (Hale-Bopp), C/1996 B2 (Hyakutake), 46P/Wirtanen, and C/1999 S4 (LINEAR), and at least eight comets seen only by SOHO (Bertaux *et al.* 1999; Combi *et al.* 2005, 2000; Mäkinen *et al.* 2001, 2000, 2001). UVCS makes high spectral and spatial resolution measurements in the ultraviolet from 2–10 $R_\odot$[2]. It has observed seven Kreutz comets (C/1996 Y1, C/1999 K1, C/1999 S1, C/2000 C6, C/2000 D1, C/2001 C2, C/2002 S2), one non-group sungrazer seen only by SOHO (C/1997 H2), 2P/Encke, and C/2002 X5 Kudo-Fujikawa (Bemporad *et al.* 2007, 2005; Povich *et al.* 2003; Raymond *et al.* 1998, 2002; Uzzo *et al.* 2001). By far the most prolific instrument on SOHO for observing comets has been LASCO, which has discovered more than 1400 comets since 1996 and has observed a few other comets including 2P/Encke and 96P/Machholz 1 (Biesecker *et al.* 2002; Grynko *et al.* 2004; Lamy *et al.* 2003). Up to date lists of all comets discovered by LASCO can be found on the "SOHO Comets" website maintained by NRL[3]. This paper deals with the comets observed by LASCO, which is explained in more detail below.

[1]Further information about the SWAN instrument can be found on the SWAN websites http://www.ias.u-psud.fr/swan/ and http://www.fmi.fi/research_space/space_7.html.

[2]Further information about the UVCS instrument can be found on the UVCS website http://cfa-www.harvard.edu/uvcs/.

[3]http://ares.nrl.navy.mil/sungrazer/index.php?p=introduction

Telescope	Field of View ($R_\odot$)	Occulter Type	Spectral Bandpass	Pixel Size (arcsec)	Brightness Range($B_\odot$)
C1	1.1–3.0	Internal	Fabry-Perot	5.6	2×10^{-5} – 2×10^{-8}
C2	2.0–6.0	External	Broadband	11.9	2×10^{-7} – 5×10^{-10}
C3	3.7–30	External	Broadband	56.0	3×10^{-9} – 5×10^{-11}

Table 2.1: Specifications for the C1, C2, and C3 telescopes. Reproduced from Table I in Brueckner *et al.* (1995).

2.1.1 LASCO

LASCO contains three coronagraphs, C1, C2, and C3, which have nested fields-of-view ranging from 1.1–30 $R_\odot$ on the plane of the sky. The innermost coronagraph, C1, has an annular field of view ranging from 1.1–3.0 $R_\odot$. It is internally occulted, and has a narrow passband Fabry-Perot interferometer tuned to hot coronal emission lines. C1 has not been used regularly since 1998 June 24, thus telemetry since then has been re-allocated to the C2 and C3 coronagraphs. No comets have been seen in C1, nor was it designed to observe them. Therefore, it is omitted from further discussion.

The outer two coronagraphs, C2 and C3 have annular fields of view from 2.0–6.0 $R_\odot$ and 3.7–30 $R_\odot$, respectively. C2 was deliberately designed to overlap both C1 and C3. Both C2 and C3 are externally occulted broadband imaging telescopes. Each telescope has a filter wheel, a polarizer wheel, a shutter, and a 1024×1024 pixel CCD. The pixel scale is 11.9 arcsec pixel^{-1} for C2 and 56 arcsec pixel^{-1} for C3. The specifications for C1, C2, and C3 are summarized in Table 2.1, and the C2 and C3 filters, bandpasses, and typical imaging modes are given in Table 2.2.

Filter	Telescope(s)	Bandpass (nm)	Typical Image Size (pixels)	Typical Exposure Time (sec)	Typical Frequency
Blue	C2 and C3	420–520	512×512	150 or 300	1 per day
Orange	C2	540–640	1024×1024	25	2–3 per hour
Orange	C3	540–640	512×512	90 or 300	1 per day
Light Red	C2	620–780	—	—	—[a]
Deep Red	C2 and C3	730–835	512×512	25 or 60	1 per day
Hα	C2 and C3	2.0 nm at 656.3 nm	1024×1024	300	—[b]
Infrared	C3	860–1050	512×512	180	1 per day
Clear	C3	400–850	1024×1024	19	2–3 per hour
3 Polarizers at 0°, ±60°	C2 and C3	400–850	512×512	100 (C2) 300 (C3)	1 sequence per day[c]

[a] The light red filter is listed in Table VI of Brueckner *et al.* (1995) however there are no reduced level-0.5 images available and it appears that this filter has never been used.
[b] The Hα filter is used very rarely.
[c] The polarizer sequence typically involves four half resolution (512×512) orange filter images: one exposure in each of the three alignments (0°, +60°, and −60°) and one with no polarization.

Table 2.2: Filters and polarizers for C2 and C3. Exposure times, image sizes, and frequency of images have varied throughout the lifetime of SOHO, and in many cases are different before and after the interruption in 1998. The values listed here should be considered as a guide only. The vast majority of images are full resolution (1024×1024) C2 orange or C3 clear images.

2.1.2 LASCO Observing Sequences

A small group of synoptic programs occupy most of the observing day. Originally, the white light synoptic program obtained one image each from C1 and C2 every 30 minutes, and an image from C3 every hour, with most images having a reduced field of view (most frequently 1024×768). However, since the mission interruption (discussed in Section 2.1.3), C1 has not been used regularly and its telemetry has been reallocated. Thus, since late 1998, typically three full-resolution (1024×1024) C2 orange and two full-resolution C3 clear images are taken per hour. Additionally, a polarization sequence using C2 and C3 is taken 1–2 times per day. A color sequence

is taken with C2 and C3 sporadically (sometimes as frequently as once per day, often as infrequently as once per week), usually at half resolution (2×2 pixels binned so the full image is 512×512). The synoptic programs utilize approximately 85% of the available daily telemetry[4]. The remaining available telemetry can be devoted to special observations.

2.1.3 SOHO Mission Interruptions

SOHO has operated nearly continuously since launching in late 1995. It suffered a major interruption from 1998 June 25 until 1998 October 22, when it lost pointing and went into an uncontrolled spin. Smaller unplanned interruptions have occurred intermittently, such as a 6 week interruption from December 1998 until February 1999. Pre-planned interruptions for routine maintenance, calibration, and satellite control have also occurred, and will continue to occur throughout the mission. Since the malfunction of the high-gain antenna in mid-2003, SOHO has needed to be rolled 180° every three months to keep the solar panels continuously pointing at the Sun. During these "keyhole" maneuvers which last approximately three weeks, some of the instruments are shut down. For a few days on either side of the roll maneuver, this frees up enough bandwidth and memory to increase the cadence of the C2 camera to five full resolution images per hour. This increased C2 cadence has led to slightly higher rates of comet discoveries during these periods. See Section 3.5.1 for a further discussion of discovery rates.

[4]http://lasco-www.nrl.navy.mil/index.php?p=content/handbook/hndbk

2.2 Calibrating Images

The SOHO/LASCO images we use for photometric reductions are "level-0.5" images which are publicly available via the SOHO website[5]. Level-0.5 images have been processed from the original data stream from the spacecraft (level-0) into fits files and oriented so that solar north is at the top of the image, however there is still a slight roll angle of each telescope from true solar north (typically much less than 1°). These images have units of DN (digital number or counts). An additional data product level, level-1, which is calibrated to units of solar brightness, is generated by the SOHO team using processing similar to those discussed here (Morrill *et al.* 2006). Our reductions were done in IDL using many of the Solarsoft IDL routines[6].

Beginning with a level-0.5 image we first subtract the offset bias. The offset bias is a positive voltage applied to the CCD to ensure that it does not read a negative voltage. It is calculated by the SOHO team for each image, and is typically 300–400 DN. The C3 offset bias has been increasing gradually throughout the mission, as seen in Figure 4 of Morrill *et al.* (2006).

Next, we multiply the exposure time given in the FITS header by an exposure correction factor which is calculated for each image by the SOHO team. The exposure correction factor is the ratio of the true exposure time to the exposure time recorded in the header for a given image, typically very close to 1. We then divide the bias subtracted image by the true length of exposure to convert it to a flux (DN $\sec^{-1}$).

Then we multiply the bias subtracted, normalized image by the vignetting func-

[5]http://sohowww.nascom.nasa.gov/data/realtime-images.html

[6]Solarsoft is a data reduction and analysis package for solar physics, notably SOHO. It can be downloaded at http://sohowww.nascom.nasa.gov/solarsoft/.

tion. This corrects for the reduction in light received at the CCD due to the optics of the telescope (namely the occulting disk and its support arm). The optical transmission varies radially, from zero at the center (behind the occulting disk) to nearly 1 at the edges. Superposed on this, the arm supporting the occulting disk (the "pylon") extends at a 45° angle from the southeast corner in unrolled images (the northwest corner in rolled images) to the center[7]. The vignetting varies between C2 and C3 and is shown in Figure 2.1. C2 suffers more vignetting across the image, while the majority of C3 is not vignetted. The effect along the occulting arm is stronger in C3 than in C2. The vignetting in C3 changed slightly due to a shift in the optics during the mission interrupt in 1998. Thus, three different vignetting functions are used when calibrating images: C2, C3 pre-interrupt, and C3 post-interrupt. For further discussion see Brueckner *et al.* (1995) and Morrill *et al.* (2006).

At this point the processed images are similar to level-1 images except that level-1 images have also had missing blocks of data replaced by extrapolation, have had stray light subtracted, have had a correction for geometric distortion applied, and have been multiplied by a distortion corrected mask containing the occulter, pylon, and the outer edge. This additional processing allows level-1 images to be used "without need of further correction" (Morrill *et al.* 2006). Of these additional corrections, only stray light is of importance for our photometry and it is removed by the background subtraction so we use our reduced level-0.5 images rather than the level-1 images.

We construct a background image from four images, two prior to the image of interest, and two after the image of interest, each processed to DN $\sec^{-1}$ as above. The images used in the background calculation are chosen to be as close in time

[7]Since mid-2003 the SOHO spacecraft has been rolled by 180° approximately every three months. See Section 2.1.3 for more information.

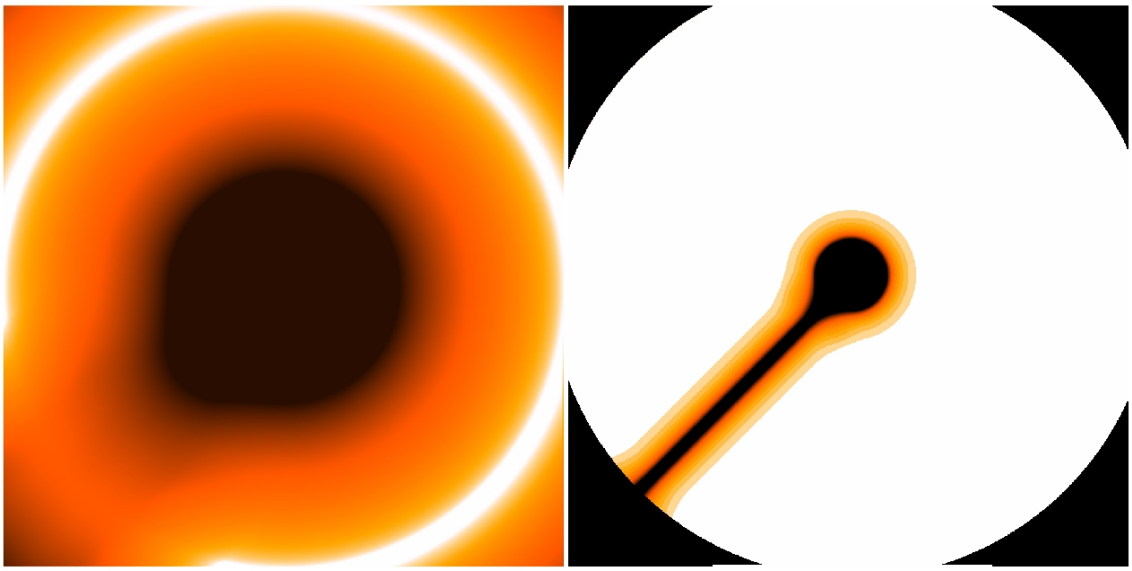

Figure 2.1: Vignetting function for C2 (left) and post-interrupt C3 (right). Both images are displayed logarithmically, however the color stretches are slightly different to accentuate the range of vignetting in each. White is no vignetting while black is completely vignetted. Orange is a continuum between the two. The effect of the occulting arm can be seen as an increase in vignetting along a diagonal line extending from the bottom left corner to the middle. The occulting disk is in the center of the image. The C3 pre-interrupt vignetting function looks nearly identical to the post-interrupt vignetting function and is not shown here.

to the image of interest as possible without contamination from either the comet, background stars, or anomalies such as cosmic rays or missing blocks of data (occasionally blocks of data are lost during downlinking from the spacecraft). We construct a background image using only images with the same telescope configuration (detector, filter, polarizer, summing on the chip, and telescope orientation). Occasionally fewer than four images are available for the background calculation, in which case the maximum number available is used. In general, images which were taken more than 24 hours apart are not used, as transient solar activity causes the background levels to vary over these timescales. We create the background image by taking the median value at each pixel. When an even number of background images is used, the median is the mean of the middle two values (the /EVEN keyword is

used in the IDL MEDIAN routine). We then subtract the background image from the processed image of interest yielding the final processed image which has units of DN $\sec^{-1}$.

Equations 2.1 and 2.2 summarize the processing.

$$processed\ image = \left(\frac{raw\ image - bias}{exposure\ time \times exposure\ factor} \right) \times vignetting \quad (2.1)$$

$$final\ image = processed\ image - median\ of\ neighboring\ processed\ images \quad (2.2)$$

2.3 Aperture Photometry

We calculated aperture photometry from processed images created as described in Section 2.2 using IDL. We used the MPFIT2DPEAK routine[8] to calculate a circular gaussian and find the optocenter of the comet. In the rare cases where the centroid routine did not converge on the comet (typically due to a bright star or cosmic ray nearby) it was forced to the whole-pixel comet position as determined by eye. Using the center specified by the centroiding routine, we then used the APER routine[9] to calculate the fluxes inside circular apertures of varying radii.

[8]MPFIT2DPEAK is part of a library of IDL routines made publicly available by Craig Markwardt at http://cow.physics.wisc.edu/∼craigm/idl/mpfittut.html.

[9]APER is an IDL routine which calculates concentric aperture photometry. It is based on the IRAF routine DAOPHOT and is publicly available from the Goddard IDL Astronomy User's Library (http://idlastro.gsfc.nasa.gov/).

2.3.1 Aperture Size

We selected the aperture size to encompass the coma while minimizing the contamination from stars and cosmic rays. To determine the appropriate aperture size, we calculated photometry for a range of circular apertures for 87 stars in C2 and 196 stars in C3. These stars were selected by randomly choosing twelve images (one image per month) in both C2 and C3 which contained a comet and selecting all the stars in the image which were used in the astrometric determination of the comet[10]. The stars cover a range of brightnesses and locations on the CCD. The mean full width half maximum (FWHM) was 1.31±0.21 pixels for stars in C2 and 1.08±0.18 pixels for stars in C3. For both C2 and C3, the FWHM was slightly larger for brighter stars and for stars at larger radial distances from the center of the CCD. By an aperture radius of 3.5 pixels in C2 and 3.0 pixels in C3, the median background flux was below 0.03 DN sec^{-1} $pixel^{-1}$.[11] Therefore at a minimum, comet apertures must be be 3.5 pixels in radius in C2 and 3.0 pixels in radius in C3.

To determine the proper aperture size for standardizing the comet magnitudes, a similar study was done for all comet images. The fraction of light enclosed within a given radius aperture was relatively constant for all ranges of brightness with two exceptions. The very brightest comets in C2 and C3 (∼2% of the sample), having

[10]Astrometry of SOHO observed comets was performed by D. Biesecker, C. St. Cyr, D. Hammer, K. McGleam and K. Battams and can be downloaded from http://ares.nrl.navy.mil/sungrazer/index.php?p=TXTS/iau_expl

[11]It is impossible to remove the background perfectly due to the transient fluctuations in the near-sun brightness, background stars (which move between images and therefore aren't subtracted out), cosmic rays, CCD detector inconsistencies, etc... Thus we consider 0.03 DN sec^{-1} $pixel^{-1}$ to be the inherent uncertainty in the background calibration. This is consistent with the remaining background flux for large apertures around faint comets.

more than 1000 DN sec^{-1} $pixel^{-1}$ in a 1 pixel radius aperture, saturate the detector and bleed into adjacent pixels. As a result, the peak is not properly recorded and the fraction of light enclosed within a given radius is not accurate. Second, the faintest comets seen in C3 (∼28% of all C3 images), having fewer than 10 DN sec^{-1} $pixel^{-1}$ in a 1 pixel radius aperture also have a lower percentage of their total counts enclosed in a given aperture. This is because the counts for the comet are so low that they are quickly dominated by the background fluctuations such as nearby stars and cosmic rays. This is not seen for similarly faint comets in C2 because they are generally brighter (despite having the same central pixel flux, the faintest C2 comets have twice the integrated flux as the faintest C3 comets). This difference between the faintest C2 and C3 comets may be due to the differing resolutions of the telescopes. The resolution of C2 is nearly five times better than the resolution of C3, so a 1 pixel radius aperture encompasses nearly 25 times as much area at the comet in C3 as compared to C2. Since the coma brightness decreases $\propto \rho^{-1}$ where ρ is the distance from the nucleus, the signal from a faint comet in C3 will be swamped by the background noise in many fewer pixels than a faint comet in C2.

For comparison across all comets, a circular aperture of radius 6 pixels (4.4 $arcmin^2$) was selected for C2 and 4 pixels (43.8 $arcmin^2$) was selected for C3[12]. The 6 pixel radius aperture for C2 encloses ∼94% of the counts in the 10 pixel radius aperture for most comets while the 4 pixel radius aperture for C3 encloses ∼96% of the counts in the 10 pixel radius aperture for most comets (∼85% for the faintest comets). The flux in the annulus from N-1 to N (where N is the aperture radius) for these apertures is 0.07 DN sec^{-1} $pixel^{-1}$ for the faintest comets in both C2 and C3. Moving to the next larger aperture decreases the flux in the new annulus to

[12]These radii are for full resolution 1024×1024 images. Half resolution 512×512 images use apertures with half the radius.

0.05 DN sec^{-1} $pixel^{-1}$ for the faintest comets in both C2 and C3. Given that the limiting background uncertainty is 0.03 DN sec^{-1} $pixel^{-1}$, moving to larger apertures adds more noise than signal, and increases the likelihood of contamination due to background stars or cosmic rays.

2.3.2 Conversion to Visual Magnitudes

We converted the flux (DN sec^{-1}) to visual magnitude by

$$m = ZP - 2.5log(flux) \tag{2.3}$$

where m is the visual magnitude, ZP is the zero point conversions calculated by the SOHO team (Llebaria *et al.* 2006; Thernisien 2003) and provided in Table 2.3, and flux is the integrated flux in DN sec^{-1}. The zero points were calculated using hundreds of stars which pass through the field of view annually. The zero points have changed slightly as the detector sensitivity has decreased over the life of the mission (by $\sim$0.4% per year in C3 and by $\sim$0.7% per year in C2 (Llebaria *et al.* 2006; Thernisien *et al.* 2006)). We use the global zero point calculated from 1996–2004 for C2 and from 1996–2003 for C3, and include an uncertainty due to the changing zero point of $\pm$0.05 mag in the error estimate.

2.3.3 Normalization of the Magnitude

In order to compare the lightcurves of comets directly, it is necessary to correct for the effects of the changing geometry. Traditionally, comet magnitudes are normalized to r=Δ=1 AU using the equation

$$m_0 = m_1 - 2.5nlog(r) - 2.5klog(\Delta) - \Phi(\theta) \tag{2.4}$$

where m_0 is the "absolute" magnitude normalized to r=Δ=1 AU, m_1 is the observed magnitude at the distances r and Δ, r is the heliocentric distance, n is the index of

Telescope	Filter	Zero Point	Reference
C2	Orange	11.867[a]	Llebaria *et al.* (2006)
C3	Blue	8.246[b]	Thernisien (2003)
C3	Orange	9.472[b]	Thernisien (2003)
C3	Clear	11.160[b]	Thernisien (2003)
C3	Deep Red	9.546[b]	Thernisien (2003)
C3	IR	8.217[b]	Thernisien (2003)

[a]This is the average zero point in a 7×7 pixel square aperture from 1996–2004. Yearly zero points which vary by ∼0.01 mag year^{-1} and zero points for square apertures of 3×3, 5×5, and 7×7 pixels are given in Table 2 of Llebaria *et al.* (2006). The average zero point given here was used in our photometric reductions.

[b]These are the average C3 zero points over 1996–2003. The C3 clear zero point changed by ∼0.003 mag/year over this time. No information on aperture size or the yearly changes for the other filters are available at this time.

Table 2.3: Photometric zero points for C2 and C3

the brightening as a function of r, Δ is the geocentric distance (in this case Δ is the spacecraft distance), k is the index of the brightening as a function of Δ which is assumed to be 2, and $\Phi(\theta)$ is the phase dependent magnitude correction.

Since the focus of our study of the lightcurves (discussed in Section 3.4) is to derive the dependence of the brightness on the heliocentric distance, the apparent magnitude is corrected for Δ and phase angle, but not for r. Comet fluxes are corrected for Δ by normalizing to 1 AU from the spacecraft. SOHO is in a halo orbit around the Earth-Sun Lagrange point L1. The correction for Δ assumes that SOHO is always at L1 and does not correct for the minor deviations from L1 caused by its orbit. These deviations are less than 1% of the comet–spacecraft distance and their effect on the magnitude is much less than the uncertainty from the photometric reductions (discussed in Section 2.3.4). Therefore they have been ignored.

The correction for phase angle is much less straight forward and potentially has a much larger effect on the interpretations of the light curves. Phase angle, θ, is

defined as the Sun-comet-observer angle. Most comets observed from the ground are at relatively modest phase angles and the geometry change during a series of observations is typically minimal. As a result, phase angle is often ignored for comets observed near 1 AU, and when included, the correction is typically a simple linear correction of 0.03–0.04 mag degree^{-1} (Jewitt 1991).

Due to their highly eccentric orbits, small perihelion distances, and high velocities, sungrazing comets observed close to perihelion can undergo dramatic changes in phase angle over very short timescales. The phase angle of many Kreutz comets changes by 20–30° and the phase angle of the Marsden group comet C/1999 U2 changed by nearly 120° over 37 hours! Furthermore, many sungrazing comets are seen at large phase angles, some in excess of 150°. Only a few non-sungrazing comets have been observed at large phase angles. These include 1P/Halley, C/1927 X1 (Skjellerup-Maristany), C/1975 V1 (West), C/1980 Y1 (Bradfield), 96P/Machholz 1 (in 2002), C/2004 F4 (Bradfield), and C/2006 P1 (McNaught), all of which showed large increases in brightness (Gehrz and Ney 1992; Grynko *et al.* 2004; Marcus 2007b,c; Marcus and Seargent 1986; Ney 1982; Ney and Merrill 1976). Thus, it is necessary to correct the apparent magnitudes for the changing phase angle before attempting to understand the heliocentric brightness dependence.

Kolokolova *et al.* (2004) combined observations of a number of comets over a wide range of phase angles and produced a plot (their Figure 1) for the phase dependence of cometary albedo due to scattering off of dust in the coma. This shows a strong forward-scattering (scattering off of dust in the coma in roughly the same direction that photons were traveling) surge at phase angles greater than 100°, a relatively flat region at intermediate phase angles, and a slight back-scattering (scattering off of dust in the coma in the direction opposite the initial direction of motion of the photons) peak at phase angles smaller than 30°.

Marcus (2007b) undertook a more rigorous examination of the phase dependence of coma brightness due to dust, deriving a "compound Henyey-Greenstein" (HG) model of the phase function which combines Henyey-Greenstein functions for forward- and backscattering. Similar in shape to the Kolokolova *et al.* (2004) figure, this model can be adjusted for varying coma dust-to-gas light ratios, and accurately predicted the surge in brightness of C/2006 P1 (McNaught) at large phase angle (Marcus 2007a,c). The full form of the compound HG model is given in Equation 1 of Marcus (2007c):

$$\phi(\theta) = \frac{\delta_{90}}{1+\delta_{90}} \left[k \left(\frac{1+g_f^2}{1+g_f^2-2g_f cos(180-\theta)} \right)^{\frac{3}{2}} + (1-k) \left(\frac{1+g_b^2}{1+g_b^2-2g_b cos(180-\theta)} \right)^{\frac{3}{2}} + \frac{1}{\delta_{90}} \right] \tag{2.5}$$

where $\phi(\theta)$ is the scattering function which can be converted to a magnitude by $\Phi(\theta)$=2.5log[$\phi(\theta)$], θ is the phase angle, δ_{90} is the dust-to-gas light ratio of the coma at $\theta = 90°$, k is the partitioning coefficient between forward- and back-scattering ($0 \leq k \leq 1$), and g_f and g_b are the forward- and back-scattering asymmetry factors ($0 \leq g_f < 1$ and $-1 < g_b \leq 0$). Marcus (2007b) fit the data using g_f=0.9, g_b=–0.6, k=0.95, and δ_{90}=1 for a "usual" comet or δ_{90}=10 for a "dusty" comet. The function is normalized to 0 magnitude correction at a phase angle of 90°. We plot the phase function for dust-to-gas ratios of 1, 0.52, and 0.16 in Figure 2.2. For further derivation of the compound HG function and its parameters, see Equations 4–8 and 11–17 in Marcus (2007b) and references therein.

The scattering off dust is strongly dependent on the phase angle but the emission from gas in the coma is isotropic. As will be discussed in Section 3.4.3, the Kreutz comets appear ∼1 magnitude brighter in the orange than in the clear filter which is attributed to sodium emission. The contribution of the isotropic sodium emission to the flux must therefore be accounted for in order to properly apply the scattering correction. In Section 3.6, we estimate the flux of sodium emission necessary to

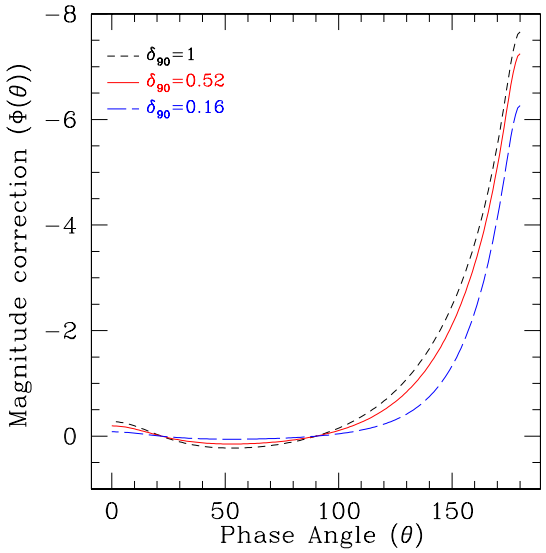

Figure 2.2: Marcus (2007b) phase function as given by Equation 2.5. Three dust-to-gas light ratios (δ_{90}) are plotted: 1 (black dashed line), 0.52 (red solid line), and 0.16 (blue long-dashed line).

cause the comets to appear ∼1 magnitude brighter in the orange than in the clear filter. The ratio of the flux due to the solar continuum (ie. scattering off the dust in the coma) to the flux due to the sodium emission (ie. gas) is $\delta_{90} = 0.52$ for the C3 clear filter and $\delta_{90} = 0.16$ for the C2 orange and C3 orange filters. These values of δ_{90} result in a smaller correction due to phase angle than was found by Marcus (2007b) for typical comets but are necessary to account for the strong contribution of sodium to the apparent brightness of the Kreutz comets. The other parameters were left unchanged, as they proved robust for the sample of six comets fit by Marcus (2007b,c). With these parameters, we use Equation 2.5 to correct the apparent visual magnitude to a phase angle of 90°.

2.3.4 Estimating the Error

The error in the flux is calculated using counting statistics for the electrons received on the CCD. Converting from electrons to DN and dividing by the exposure time, the error in DN sec^{-1} within a given aperture is approximated as

$$\sigma_{\frac{counts}{s},\ comet} = \sqrt{\frac{G}{exptime}\left(\frac{counts}{s}_{raw} + \frac{1}{N}\frac{counts}{s}_{background}\right)} \tag{2.6}$$

where G is the gain in DN $\mathrm{electrons}^{-1}$, *exptime* is the exposure time (in seconds), $\frac{counts}{s}_{raw}$ is the integrated counts sec^{-1} in the aperture of the pre-background subtracted image of interest (processed to DN sec^{-1}), N is the number of images used to calculate the median, and $\frac{counts}{s}_{background}$ is the integrated counts sec^{-1} in the aperture of the background image[13]. The gain, G, of C3 was found to be $\frac{1}{13}$ (13 electrons per DN) by Morrill *et al.* (2006). The gain of C2 was estimated to be 15–20 electrons per DN ($G = \frac{1}{15} - \frac{1}{20}$) prior to launch by Brueckner *et al.* (1995). No observationally derived gain for C2 has been published since then, and since the C3 gain was also estimated at 15–20 electrons per DN prior to launch, we have elected to use the measured gain of 13 electrons per DN by Morrill *et al.* (2006) for both telescopes.

The total error (in magnitudes) is then a combination of the errors from the various components which went into the magnitude calculation added in quadrature:

$$\sigma_{mag,\ total} = \sqrt{(\sigma_{mag,\ counts})^2 + (\sigma_{mag,\ \Delta})^2 + (\sigma_{mag,\ phase})^2 + (\sigma_{mag,\ ZP})^2}. \tag{2.7}$$

Here $\sigma_{mag,\ counts}$ is the statistical error of the electrons on the detector, $\sigma_{mag,\ \Delta}$ is the uncertainty in the comet–spacecraft distance (we estimate the uncertainty in the

[13]Note that this is an approximation since we used a median background to mitigate anomalous points (rather than an average background). Given the much larger systematic uncertainties this should have little effect on the error estimate.

position due to the cometary orbital elements and the spacecraft's position relative to L1 is ∼1%, thus $\sigma_{mag,\ \Delta}$ ∼$1.086\sqrt{\frac{\sigma_\Delta}{\Delta}}$ ∼$1.086\sqrt{0.01}$, $\sigma_{mag,\ phase}$ is the estimated error in the magnitude due to the uncertainty in the phase function (we estimate the uncertainty in the phase correction to be ∼10% of the magnitude correction, thus $\sigma_{mag,\ phase}$ ∼$0.1\times\Phi(\theta)$, and $\sigma_{mag,\ ZP}$ is the error in the magnitude due to the uncertainty in the zero point scale (estimated to be ∼0.05 mag to account for the decreasing sensitivity of the detectors).

Several other possible sources of error have been ignored for these calculations since they are much smaller than the above errors. These include:

- The bias has increased steadily throughout the mission although the cause is not understood (Morrill *et al.* 2006). The rate of increase is slow (∼8 DN year^{-1}) thus the uncertainty in the bias at any given time is very small.

- The dark count is effectively zero for C3 (Morrill *et al.* 2006) and there is no reason to believe it should differ for C2.

- The exposure time correction is very small (∼1–3$\times10^{-3}$) and is calculated in two ways (Llebaria and Thernisien 2001; Morrill *et al.* 2006) which differ by only 10^{-3} to 10^{-4}.

- The error due to the vignetting function is unknown but presumed to be very small as it has been robustly determined both in the lab prior to launch (Brueckner *et al.* 1995) and from data collected over 10 years in flight Morrill *et al.* (2006).

- Morrill *et al.* (2006) found a very weak fixed pattern noise in the C3 CCD, however they find it is insignificant relative to the other sources of noise.

- Morrill *et al.* (2006) found a very small number of hot and cold pixels in C3.

Hot pixels occur at a rate of ∼0.15% and typically have an excess of ∼2 DN. Since background images are subtracted from the same pixel position, most of the effects of hot pixels should be removed in the background subtraction. Cold pixels having sensitivity <10% of the average are potentially more problematic but are exceedingly rare (∼0.008%). The photometric sample reported here contains ∼20,000 images. It is thus possible that the photometry of a handful of images have been affected by cold pixels. No attempt has been made to correct for this, however, anomalous points in the lightcurves of individual comets have been removed manually.

- The read noise in C3 was found to be ∼5–7 electrons (Morrill *et al.* 2006). With the gain of 13 electrons DN^{-1}, this is an uncertainty of less than 1 DN and can safely be ignored.

- (Morrill *et al.* 2006) found a very low level of stray light. Since the level is proportional to the exposure time and has the same pattern for different filters and exposure times, it is removed during background subtraction. Any remaining uncertainty due to stray light is minuscule.

Chapter 3

Kreutz Comets

3.1 Overview

As discussed in Section 1, the Kreutz group was recognized by Kirkwood (1880) and Kreutz (1888, 1891, 1901) on the basis of the similar orbits of several comets from the 1600s and 1800s. As additional group members were observed in 1943, 1963, 1965, and 1970, Marsden (1967), Hasegawa (1966), Kresák (1966), Sekanina (1967a,b), and others updated and expanded the analysis of the Kreutz group. The discovery of 16 fainter Kreutz comets from 1979–1989 (and three more in archival images since then) by the space-based coronagraphs SMM and Solwind (MacQueen and St. Cyr 1991; Marsden 1989; Michels *et al.* 1982; Sheeley *et al.* 1982) and the hundreds of Kreutz comets discovered by SOHO (Biesecker *et al.* 2002; Raymond *et al.* 1998; Uzzo *et al.* 2001) has led to renewed interest in the Kreutz group.

Much of this work has focused on the orbital dynamics of the largest members of the group. It has been well established that the two most prominent comets, C/1965 S1 Ikeya-Seki and C/1882 R1 split from each other very close to perihelion around the year 1100 CE (e.g. Marsden (1967), Sekanina and Chodas (2002a)) and were quite possibly observed as the magnificent comet of 1106 (X/1106 C1).

While the fragmentation history of the remaining ground observed comets is not well understood, it is likely that they split from one or more parent fragments at some time prior to the 1500s, and that all of these parent fragments (including the parent of C/1882 R1 and C/1965 S1) split from a single progenitor within the last 2500 years (Sekanina and Chodas 2002b, 2004, 2007). The most recent of these models (Sekanina and Chodas 2007) envisions the Kreutz group to be much more populous than previously suggested, incorporating more than 20 poorly observed near-Sun comets recovered from the historical records by Hasegawa and Nakano (2001), Strom (2002), and England (2002), and potentially linking the progenitor with comets observed in 214 BCE, 423 CE, and/or 467 CE.

The Solwind, SMM, and SOHO discovered comets are not sufficiently well observed to permit investigation of the dynamical history of individual comets. Instead, it has been demonstrated through statistical arguments (Sekanina 2000a, 2002a,b) that these comets are likely products of runaway fragmentation throughout their orbits. In this model, the small coronagraphically discovered comets all split from their parent fragments since the previous perihelion passage. These fragmentation events occurred both before and after aphelion, at distances small and large. Splitting is likely to have continued in the newly produced fragments with increasing time between subsequent events. Thus, the comets which are observed today are likely separated by several generations of fragmentation events from their source comet (the comet of which they were a part on the preceding perihelion passage). This widespread and repeated fragmentation results in a nearly steady stream of arrivals which have very different orbital elements and in most cases appear unrelated to each other.

Comet D/1993 F2 Shoemaker-Levy 9 (SL9) is frequently cited as an analog for the Kreutz group. However, unlike the fragmentation of SL9 (which has been ex-

plained by disruption due to tidal forces on its close approach to Jupiter in 1992 (Asphaug and Benz 1996)), additional processes are required to explain the cascading fragmentation evident in the SOHO observed Kreutz comets. Presumably the parent comet was weakened by tidal forces and the intense solar radiation incurred during its previous perihelion passage. These forces may have caused the comet to fragment at or very near perihelion (both C/1882 R1 and C/1965 S1 were observed to split into discrete fragments soon after perihelion) or they may have simply weakened the comet by causing cracks and fissures throughout the nucleus. Eventually stresses on the weakened nucleus such as due to rotation, outgassing, or the thermal wave propagating to deeper pockets of volatiles would cause a fragmentation event. This may have resulted in one or two massive fragments and a distribution of smaller fragments. Subsequent splitting events due to the same processes would likely occur less often, but would result in a size distribution consisting of ever smaller fragments. The velocities imparted on the fragments (relative to the parent comet's orbit) and non-gravitational forces would cause a wide variety of orbital periods and elements, depending on the location, orientation, and magnitude of the fragmentation event.

3.2 Orbital Elements

A comet's orbit can be defined by six coordinates called the orbital elements. The most commonly used are the time of perihelion passage (T), the perihelion distance (q), the eccentricity (e), the inclination (i), the argument of perihelion (ω), and the longitude of the ascending node (Ω). The time of perihelion passage is the time when the comet is closest to the Sun (perihelion). The comet's distance from the Sun at perihelion is the perihelion distance. The eccentricity defines the shape of the orbit. e=0 is a circle, 0< e <1 is an ellipse, e=1 is a parabola, and e >1 is a hyperbola. The

inclination is the angle between the plane of the orbit and the ecliptic. The longitude of the ascending node is the angle (in the plane of the ecliptic) between the vernal equinox and the point where the comet's orbit crosses the ecliptic going northward (called the ascending node). The argument of perihelion is the angle, measured in the plane of the comet's orbit, between the ascending node and the perihelion point. See Figure 6.9 in Danby (1992) for an illustration of these elements.

To understand the Kreutz family, it is instructive to discuss the unusual properties of its orbit. First, due to the high eccentricity (>0.9999 for all members observed well enough to calculate an elliptical orbit) and high inclination ($i \sim 143°$), Kreutz comets can never pass closer than ∼3 AU from Jupiter. The osculating orbital elements at the time of perihelion are affected by the position of Jupiter (and to a smaller extent the other planets). Depending on where Jupiter is in its orbit, two comets which originated in the same orbit but reach perihelion at different times can have arguments of perihelion and longitudes of the ascending node which differ by upwards of 10°. Furthermore, Jupiter can perturb the orbit enough to make the perihelion distance smaller than 1 $R_\odot$! See Section III of Marsden (1989) for further discussion of the perturbations of Jupiter as well as the original orbital elements referred to the barycenter of the solar system.

Another property of the orbit which bears discussion is the effect of fragmentation at various points throughout the orbit. Sekanina (1977, 1978, 1982) has developed a framework for modeling split comets using radial, transverse, and normal separation velocities, with maximum separation velocities typically less than ∼5 m s^{-1} relative to the parent body. The application of these velocities of separation at varying times in the orbit has very different consequences. Fragmentation near perihelion has almost no effect on q, ω, Ω, and i but can cause the fragments to next reach perihelion centuries apart. Fragmentation on the way to aphelion can change q, ω,

Ω, and i by small amounts and cause them to next reach perihelion years to decades apart. Fragmentation at or near aphelion can change q, ω, Ω, and i dramatically but has very little effect on the time of next perihelion. The effects of fragmentation on q, ω, Ω, and i are roughly symmetric around aphelion, however the change in the time of next perihelion passage is small (days to weeks) if the fragmentation occurs after aphelion. Examples of these perturbations can be found in Table 8 of Sekanina (2002b) and they can be derived analytically using the equations for isolated impulses in Danby (1992) (Equation 11.5.13).

Typical orbital elements for the Kreutz family are given in Table 1.1, and Figure 3.1 plots the argument of perihelion versus the inclination (left panel) and the longitude of the ascending node versus the perihelion distance (right panel) for all known Kreutz orbits[1]. The remaining two orbital elements, time of perihelion and eccentricity are not plotted as they have very little utility for understanding the Kreutz comets observed by SOHO. The orbital arcs of all but the brightest ground observed Kreutz comets are far too short to calculate an eccentricity (and hence a period), thus all of the SOHO, SMM, and Solwind elements have only parabolic fits ($e = 1.0$).

While no estimates have been published for the uncertainty in the orbital elements of the SOHO observed comets, they are assumed to be large due to the poor angular resolution (11.9 arcsec pixel^{-1} in C2 and 56 arcsec pixel^{-1} in C3), short orbital arcs (most comets are observed for only a few hours and the brightest are seen for less than 2 days), and the lack of observations after perihelion (no Kreutz comets

[1]The concentration of orbits with q just larger than 1 $R_\odot$ is misleading. In many poorly observed SOHO comets, the observations could be fit equally well by orbits inside or just slightly outside the solar radius, and solutions which did not impact the Sun were chosen. Thus, it is likely that the distribution of q actually extends gradually to distances smaller than 1 $R_\odot$ (Marsden 2001, private communication, as referenced by Sekanina (2002b)).

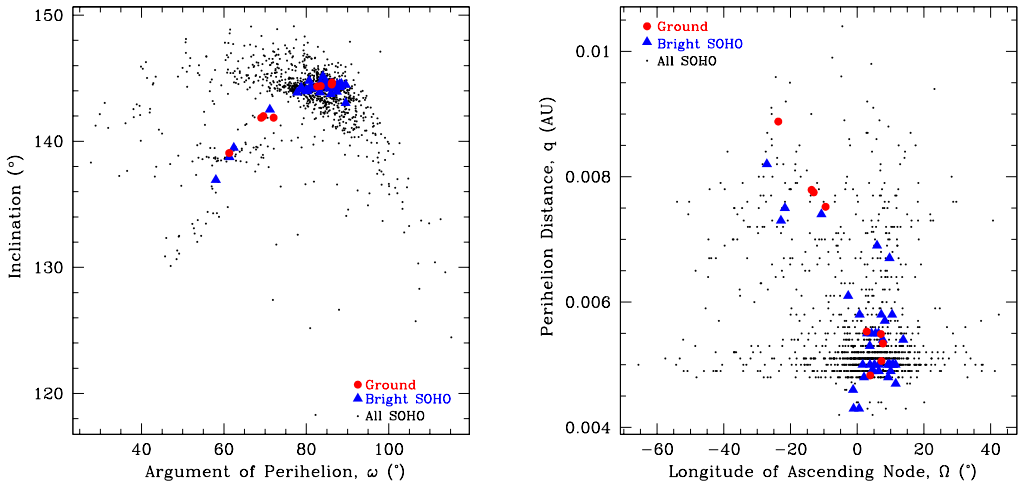

Figure 3.1: Orbital elements of the Kreutz group. The left panel plots the argument of perihelion (ω) against the inclination. The right panel plots the longitude of the ascending node (Ω) against the perihelion distance (q). The red circles are the comets observed from the ground (none since 1970). The blue triangles are the brightest SOHO observed comets (1996–2005). The black crosses are all SOHO observed comets discovered as of May 2008. The orbital elements for the ground observed comets were compiled from the references given in Table A.1. The orbital elements for the SOHO comets were compiled from Minor Planet Electronic Circulars (MPECs) and International Astronomical Union Circulars (IAUCs) and in the interest of space, these references are excluded.

observed by SOHO have been seen after perihelion). Marsden (private communication) has commented on the occasional need to ignore points when fitting orbits, and orbits for comets which were only observed in C3 are particularly problematic. With the recent detection of Kreutz comets by STEREO, improved orbits for 13 comets have now been published utilizing the observations from both STEREO spacecraft (Marsden and Battams 2008a,b; Marsden and Baldwin 2008). Six of these have been published with an additional significant digit, suggesting much more confidence in the solutions. To estimate the uncertainty in typical orbital elements obtained from SOHO images, we calculated the root mean square difference of the original orbital elements relative to the improved orbital elements. This yields the following uncertainties: $\sigma_T = \pm 0.019$ days, $\sigma_q = \pm 0.0012$ AU, $\sigma_\omega = \pm 7.4°$, $\sigma_\Omega = \pm 7.1°$, and $\sigma_i =$

$\pm 1.4^\circ$. It is likely these values will change as additional orbits are recalculated, but for the purposes of this paper they provide a reasonable estimate of the uncertainty of typical Kreutz orbits derived from SOHO observations.

There is significant scatter in the elements shown in Figure 3.1, however the brightest (and hence best observed) comets are clustered along a line through the middle of the scatter (the red circles and blue triangles). The scatter in orbital elements could be interpreted as either an artifact of the orbital calculation – comets which are fainter have fewer observations and their fits are poorly constrained resulting in large scatter – or as genuine and evidence of evolutionary differences. Two evolutionary effects could be at work: dynamical scattering and non-gravitational forces. It is difficult to speculate on the effects of non-gravitational forces given the uncertainty of the orbits. Since the comets seen by SOHO are believed to be products of cascading fragmentation throughout their orbits, it stands to reason that the most massive fragments have remained in orbits most closely resembling those of their progenitor. When fragmentation occurs, the separation velocity imparted on the smaller fragment causes its orbital elements to be scattered away from the orbits of the most massive fragments. A series of progressively smaller fragmentations (in random orientations at differing places in the orbit) would behave like a random-walk, moving some fraction of comets much farther away from the main cluster than would be expected from a single fragmentation event.

Hasegawa (1966), Kresák (1966), and Marsden (1967) noted the clustering of the orbital elements of the ground observed comets. Using the terminology of Marsden (1989) (illustrated in their Figure 7), subgroup I is centered around $q = 0.0055$ AU, $\omega = 85^\circ$, $\Omega = 5^\circ$, $i = 144.5^\circ$ and consists of C/1843 D1, C/1880 C1, and C/1963 R1, subgroup II is centered around $q = 0.008$ AU, $\omega = 69^\circ$, $\Omega = -14^\circ$, $i = 142^\circ$ and consists of C/1882 R1, C/1945 X1, and C/1965 S1, and subgroup IIa consists

of C/1970 K1 which has $q = 0.00888$ AU, $\omega = 61°$, $\Omega = –24°$, $i = 139°$. The vast majority of SOHO observed comets (as well as all but two of the SMM/Solwind comets) appear to be members of subgroup I. While there are several dozen comets with orbits close to subgroup II and a few close to subgroup IIa, there is no evidence of a large population of small comets as seen around subgroup I.

This is at first surprising since C/1882 R1 and C/1965 S1 were such spectacular comets, and one might expect them to have had much ongoing fragmentation resulting in a large debris cloud. Furthermore, it could be expected that the comets reaching perihelion today are related in nearly equal fractions to the comets of 1963, 1965, and 1970 which represent subgroups I, II, and IIa, respectively. Why then are they clustered around subgroup I? Sekanina and Chodas (2007) suggest that the center of mass of the Kreutz system is closest to the subgroup I orbit. Since fragmentation near perihelion can change the orbital period of Kreutz comets by decades with little effect on the other orbital elements, they argue that the fragments being seen today are actually the leading edge of a debris cloud around an as-yet undiscovered large fragment which will arrive in the next few decades rather than the trailing edge of debris from the comets observed in the 1960s. They further interpret the rising discovery rate of SOHO comets from 2001–2005 as supporting evidence of this coming cluster. We have more rigorously investigated the apparent increase in the discovery rate, and conclude that the actual rate of Kreutz comets reaching perihelion has increased, even after correcting for the improved observing circumstances (see Section 3.5.4). Furthermore, we cannot posit a reasonable explanation for the paucity of subgroup II (or IIa) comets seen by SOHO. Thus, we agree with the suggestion that the large number of subgroup I comets may be indicative of another coming large fragment belonging to subgroup I.

3.3 Temporal Clustering

It has long been noticed that Kreutz comets arrive close together in time. Clustered arrivals occurred from 1668–1702 (four comets), 1880–1887 (four comets), and 1963–1970 (three comets). The only other suspected Kreutz comets seen from the ground since the mid-1600s were seen in 1843 and 1945. Based on previous clustering, Marsden made a tongue-in-cheek prediction in 1966 that another comet might arrive in 1970 and was proved correct with the arrival of the last ground-observed Kreutz comet, C/1970 K1 (Marsden 1989)!

Clustering has also been evident in the coronagraphic discoveries. While one or both of SMM and Solwind were operational nearly continuously from 1979–1989, the perihelion times of the 19 Kreutz comets discovered by these two satellites were hardly uniform. Four comets were discovered from June–November 1981, two from July–September 1983, two from July–August 1984, two in October 1987 (12 days apart!), and eight from June 1988–September 1989. The only other comet observed during this time was the first comet discovered, in 1979, which was followed by a gap of some 17 months. MacQueen and St. Cyr (1991) noted the "highly episodic" arrivals of the SMM comets and calculated a probability of just $\sim$0.01% that the distribution of detections by SMM was drawn from a random sample. It should be noted that three of the 19 comets observed during this period were discovered much later (Kracht and Marsden 2005a,c) and were not included in the analysis by MacQueen and St. Cyr (1991), however their inclusion does not affect the conclusions which were based on the clustering from 1987–1989.

The sheer number of Kreutz comets discovered by SOHO makes it difficult to identify clustering on an individual basis, however clustering can be tested for statistically. Both panels in Figure 3.2 show a histogram (black hashes) of the separation

between the arrival times of all Kreutz comets observed from 2004–2007, where the separation time for each comet is the time (in days) between the perihelion of a given comet and its closest neighbor (either before or after the comet in question). This distribution peaks strongly in the smallest bin, for separations less than 0.2 days.

To test whether this represents an excess of close arrivals (i.e. clustering), we generated data sets where the time of perihelion is chosen randomly from the range 2004–2007 (this time period is shown in Section 3.5.1 to be the most complete and uniform period of observations by SOHO). Since there is a strong seasonal dependence on the monthly discovery rate (Figure 3.15), we allocated the discoveries on a monthly basis at the same frequency as the true discoveries. Thus, since 33 total comets were seen in January 2004, January 2005, January 2006, and January 2007, an average of 8.25 perihelion times were generated in January for each of the four years. We then simulated 1000 data sets and averaged the results, which are plotted as the heavy red line in the left panel of Figure 3.2. We found that there is an overabundance of actual comets which arrive less than 0.2 days apart. From the 1000 generated data sets, we found an average of 96 ± 12 comets which arrived less than 0.2 days apart with a maximum of 131 (138 were actually observed).

Next, we constructed a series of models to simulate the data by assuming some fraction of the comets arrive in clusters. We generated random data sets with monthly discoveries allocated at the discovery rate of SOHO, defining a fraction of them to be in clusters. For each generated perihelion time, a second random number was chosen. If it was within the fraction of clusters, the new perihelion was defined to be in a cluster with the previous comet, and its perihelion time was drawn from within a smaller range of times which were considered to be clustered. We varied the fraction of comets which are in clusters as well as the maximum separation

for a comet to be considered a cluster. Each model was simulated 100 times. We found that a model with ∼8% of comets in clusters and a maximum separation for a defined cluster of 0.2 days best fit the data, reducing the least squares error by a factor of 4. This curve is plotted in the right panel of Figure 3.2.

While it is clear from the statistical evidence that a sizable percentage of SOHO comets arrive in close clusters, it is difficult to identify these pairs and even harder to determine when they broke up. This is illustrated by the pair C/1998 K10 and C/1998 K11 which arrived 0.18 days apart. Both were among the five brightest comets observed by SOHO, were seen in more than 50 images spanning over 40 hours (making their orbital elements among the best constrained of all SOHO comets), and exhibited similarly shaped lightcurves (although both saturated the detectors making it impossible to determine the precise shapes). These two comets meet all the qualifications of having split from each other quite recently, however their elements still differ by $\Delta q = 0.0008$ AU, $\Delta\omega = 3.66°$, $\Delta\Omega = 5.89°$, and $\Delta i = 0.53°$. Because they were simultaneously in 12 images, Sekanina (2000a) was able to apply his standard model for split comets which indicated C/1998 K10 and K11 split from each other ∼53 years before perihelion at a distance of ∼67 AU. However, a fragmentation event at that distance with most of the assumed 5 m s^{-1} separation velocity in the radial direction could have resulted in a $\Delta T \approx 10$ days. Although the differences in the orbital elements are within the estimated error bars (Section 3.2), with a separation of 10 days between the arrivals they might not have been recognized as a pair. Furthermore, Sekanina's split comet model requires that comets be observed simultaneously (which they would not be if arriving 10 days apart). Thus, for most separation velocities in this scenario, the comets would not be easily identified as being recently split.

The problem of identifying recently fragmented comets and thus constructing

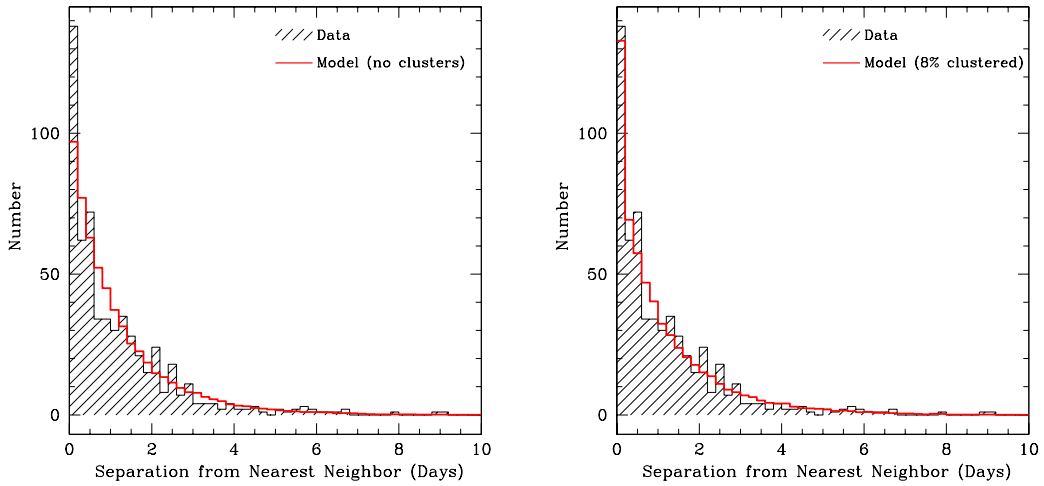

Figure 3.2: Histograms of the separation between Kreutz comet times of perihelion from 2004–2007. In both panels the hashed (black) histogram is the actual distribution of separation times. The heavy (red) line in the left panel is the distribution of separation times that would be expected if the comet arrivals were spread out randomly over the time period. The heavy (red) line in the right panel is the distribution of separation times for the best fit model which has 8% of Kreutz comets arriving in clusters (with a separation less than 0.2 days) and all other comets arriving at random times.

a fragmentation tree is further confused by the high frequency of arrivals. The comets observed by SOHO are understood to be products of cascading fragmentation throughout the orbit. Even very recent fragmentations occurring within the last 30 years can cause differences in arrival times of a week or more. It becomes virtually impossible to identify these as pairs since 5–10 comets can arrive during a 10 day window. Given the uncertainty in the orbital elements and the fact that nearly all of these comets are descended from the same subgroup (albeit with perhaps 3–5 intermediate fragmentations), it seems impossible to derive a unique fragmentation history of a given SOHO comet.

3.4 Lightcurves

Prior to SOHO, most Kreutz comets had only been seen after perihelion (most ground observed comets) or inside of 10 $R_\odot$ (the SMM and Solwind comets). A surprising trait of the Kreutz comets observed by SOHO is the shape of their lightcurves, first discussed in Biesecker *et al.* (2002) and illustrated in Figure 3.3. Typical Kreutz comets brighten steadily as they approach the Sun, begin to flatten out at $\sim$16 $R_\odot$, reach a peak in brightness prior to perihelion at a distance of 11–13 $R_\odot$, then fade as they continue to approach the Sun. Occasionally the fading flattens out or they brighten again at distances inside of $\sim$8 $R_\odot$ before disappearing. No Kreutz comet observed by SOHO has ever been seen after perihelion. Due to the seasonal geometric effects (discussed in Section 3.5.2), data gaps, and/or the sensitivity of the detectors, most comets are not observed well enough to exhibit all of these features. However, nearly every comet displays some component of this general shape, and none are in contradiction to it.

In this section we discuss the lightcurves of the 924 comets which reached perihelion from January 1996–January 2006 for which we have calculated photometry. The photometry was calculated as described in Section 2.2, and has been normalized to unit SOHO-centric distance and corrected for phase angle unless otherwise noted.

3.4.1 Peak Distance and the "Universal Curves"

Biesecker *et al.* (2002) studied the first 141 Kreutz comets observed by SOHO from 1996–1998. Of these, 17 were determined to reach a peak brightness in C3 without saturating the detector (the peaks are not well observed in C2 so these were excluded). The peak distances of these 17 were found to be bimodal, with 11 comets reaching peak brightness at a slightly larger heliocentric distance than the remaining

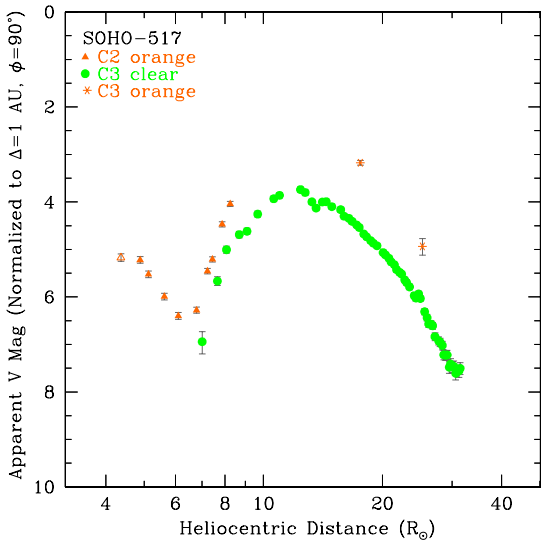

Figure 3.3: Lightcurve of C/2002 S2 (SOHO-517) which is representative of the typical Kreutz lightcurve shape. The orange triangles are C2 orange filter images, green circles are C3 clear filter images, and orange asterisks are C3 orange filter images. The open points are images which had vignetting greater than 4.0.

6. When curves were fit to these groups, the 11 member Universal Curve 1 (UC1) peaked at 12.3 $R_\odot$ while the 6 member Universal Curve 2 (UC2) peaked at 11.2 $R_\odot$. Furthermore, UC2 brightened and faded more rapidly than did UC1. With our much larger sample size, we are equipped to more rigorously test the bimodality of peak distance and the existence of the universal curves.

We have calculated the photometry of the 924 Kreutz comets which were discovered in the SOHO field of view by January 2006. We were able to determine a peak in the lightcurve for 79 of these, 65 in C3 and 14 in C2. Peaks were determined by a combination of fitting a quadratic to the data and by selecting the single brightest photometric values. Six comets were observed to peak in C3 but saturated the detector so they have been omitted: SOHO-54 (C/1998 K10), 55 (C/1998 K11), 111 (C/2000 H2), 347 (C/2001 R2), 367 (C/2001 U9), and 614 (C/2003 K7)[2]. We omit-

[2]We include SOHO numbers in this discussion for comparison with the nomenclature of Biesecker *et al.* (2002). These are simply the order in which the comets were discovered. IAU

ted eight comets which were included in the Biesecker *et al.* (2002) sample: SOHO-10 (C/1997 K1), 13 (C/1997 L4), 17 (C/1996 H1), 22 (C/1996 O2), 23 (C/1996 O4), 29 (C/1997 R3), 30 (C/1997 S1), and 37 (C/1998 A1). These are among several dozen comets for which it is likely that the peaks were observed, however the data near peak is sparse and/or noisy and we opted to exclude them. The lightcurves of the 71 comets which peaked in C3 (including those that saturated the detector) are plotted in Figures B.1–B.9 in the Appendix.

A histogram of the heliocentric distance of peak brightness for the comets observed to peak in C3 is shown in Figure 3.4. The histogram has a maximum at 12.25 $R_\odot$ and a shoulder at 11.25 $R_\odot$. These features are consistent with the bimodality seen by Biesecker *et al.* (2002) (peaks at 11.2 and 12.3 $R_\odot$). However, unlike the Biesecker *et al.* (2002) sample, we see a broad range of peak distances from 10.5–14 $R_\odot$. Thus, while the sample retains the preference for peaking in brightness near 11 or 12 $R_\odot$, there is a continuum of peak distances centered around 12 $R_\odot$. We note that it is difficult to determine the exact peak distance of most light curves as they often have a broad, flat peak over a distance of 1–2 $R_\odot$. Thus we estimate the uncertainty in peak distance could be as large as 0.5 $R_\odot$.

The geometry of the orbit makes it rare to see Kreutz comets at heliocentric distances larger than 10 $R_\odot$ in C2. Since we require there to be a clear trend of both brightening and fading around the peak, it becomes increasingly more difficult to observe a peak in C2 the larger the heliocentric distance of the peak. As a result, little can be inferred from the peak distances for the comets observed to peak in C2. The 14 comets observed to peak in C2 had peak distances between 10.6 and 11.9 $R_\odot$. The lack of observed peaks beyond 12 $R_\odot$ should not be considered real, but instead is a product of the viewing geometry.

---

designations are used elsewhere.

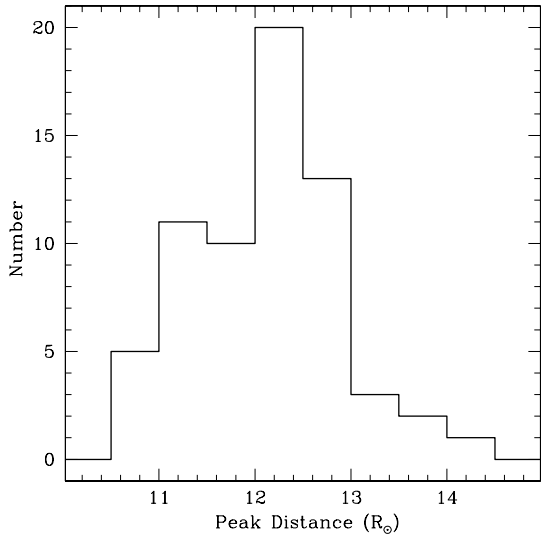

Figure 3.4: Histogram of the heliocentric distance of peak brightness for comets observed to peak in C3.

The opposite effect may occur to a lesser extent in C3. While the C3 field of view extends to 3.7 $R_\odot$ in the plane of the sky, the photometry becomes increasingly unreliable at small distances as the vignetting and sky background increase and transient solar activity becomes more common. In principle comets should be observable until well after their peak in C3, however it is possible that some peaks are not recognizable due to the increasing difficulty of observing comets at small elongations. This is more likely to occur for fainter comets and comets which reach a peak at smaller heliocentric distances.

We next investigated whether the universal curves were evident in our larger sample. Rather than looking strictly at the distance of peak brightness, we considered the shape of each comet's lightcurve. We found that the lightcurves could be loosely divided into three shapes, and that these shapes generally correspond to the distance of peak brightness in the same manner as the universal curves of Biesecker *et al.* (2002) (Figure 3.5). We group them together to illustrate trends across the range of peak distances, not as canonical curves. The choice of three groups is some-

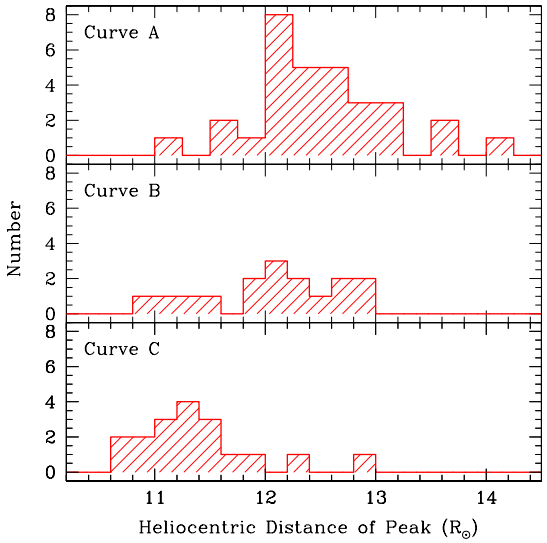

Figure 3.5: Histogram of the heliocentric distance of peak brightness for the three characteristic shapes of brightening. The top panel is curve A, the middle panel is curve B, and the bottom panel is curve C.

what arbitrary. In principal 4 or 5 groups could be identified, however the number of comets in each group would become problematic for statistics. We constructed composite curves for each group by offsetting all the comets in a given group to peak at the same magnitude (peak magnitude = 1) and taking the median magnitude of all the observations in a given heliocentric distance range. The curves are plotted in Figure 3.6 and have been offset so they all peak at 12 $R_\odot$. To avoid confusion with the nomenclature of Biesecker *et al.* (2002), we designate these groups A–C from largest peak distance to smallest.

Curve A is similar to UC1. It contains 31 comets with a median peak distance of 12.3 $R_\odot$. Curve B contains 16 comets with a median distance of 12.1 $R_\odot$. Curve C is similar to UC2, containing 18 comets with a median peak distance of 11.3 $R_\odot$. Shifting the three curves in magnitude and log(r) so that they overlap at their peak brightness, curve C brightens most steeply while curve A has the shallowest slope of brightening. At distances larger than ∼24 $R_\odot$, all three curves have similar slopes.

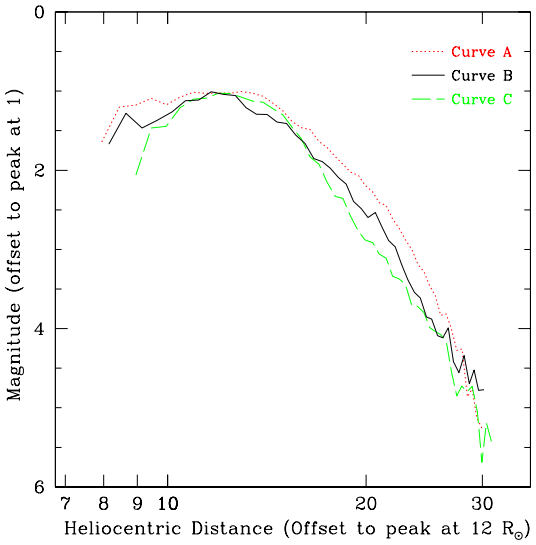

Figure 3.6: Plots of the three characteristic curves normalized so that they all peak at a magnitude of 1 and a heliocentric distance of 12 $R_{\odot}$. Curve A is the dotted red line, curve B is the solid black line, and curve C is the dashed green line.

The slopes of fading are harder to distinguish than the brightening due to fewer observations over a smaller region and generally noisier data, however curve A fades the most rapidly, followed by curve B, with curve C fading the most gradually.

We searched for trends that might correlate with the characteristic shape of these curves. There were no trends between orbital elements (q, Ω, ω, or i) or peak brightness and the curves. Furthermore, there are members of all three curves in both subgroups discussed in Section 3.2, suggesting that the lightcurve behavior is not dependent on the major fragment from which each comet is descended. The curves do not show a seasonal dependence, although the number of comets observed to peak in C3 (regardless of the curve to which they belong) shows a seasonal dependence consistent with the overall detection rate in C3 (see Section 3.5.2).

Interestingly, 15 of the 16 comets in curve B have been discovered since mid-2002 (Figure 3.7). Prior to 2003, nearly all the comets observed to peak in C3 were members of curves A or C, however since then all but five comets have been in

curves A or B. It is possible that this is diagnostic of a varying composition of the swarm of Kreutz comets as a function of position angle in the orbit. That is, there may be some clustering of composition on the timescale of years, and the comets with composition causing them to brighten similarly to curve B only began reaching perihelion en masse in 2003.

An alternative explanation is that the increase in comets which brighten similarly to curve B is a result of improved detection circumstances for SOHO. As discussed in Section 3.5.1, there have been numerous changes to the way in which SOHO observes since 2000 (and particularly since mid-2003), resulting in more C3 images being taken per hour. This increased cadence makes it more likely that comets will be well observed and therefore easier to identify the peak in the lightcurve, the criteria for being included in this study. It is possible that the flux of comets identified as belonging to curve B has remained constant throughout the mission, however our ability to recognize them as such has improved. For this reason we hesitate to ascribe the increase in curve B comets to compositional differences as a function of position in the orbit.

3.4.2 Brightening and Fading

Due to the geometry of the Kreutz orbit and periodic gaps in the imaging sequences, most comets are only observed over a portion of the typical brighten-then-fade curve. While this limits the number of comets for which the distance of turnover can be determined, there are many more partial lightcurves available to give information about the brightening and fading behavior. We considered slopes (slope = x where brightness $\sim$ r^{-x}) over three ranges: brightening at heliocentric distances larger than 24 $R_\odot$, brightening from 24–16 $R_\odot$, and fading from 10–7 $R_\odot$. We considered two regions for the brightening slope because there appears to be a break in the

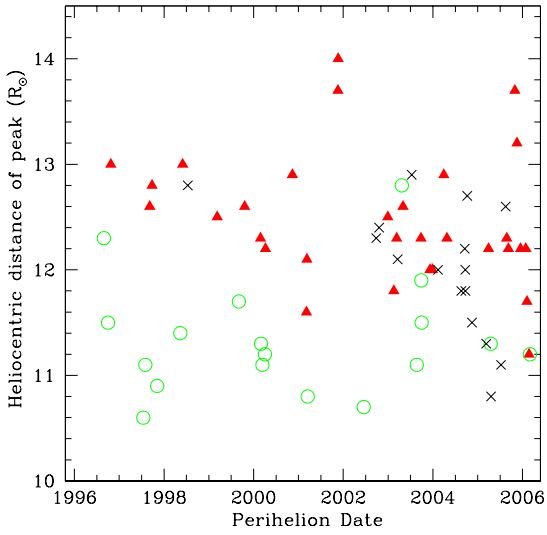

Figure 3.7: Perihelion date versus heliocentric distance of the peak magnitude for the comets observed to peak in C3. The red triangles are in curve A, black crosses are in curve B, and green circles are in curve C.

slope for many comets between 20–27 $R_\odot$. We calculated fading slopes for both C2 orange and C3 clear images, however we only calculated brightening slopes for C3 clear images as no comets were observed in C2 beyond 16 $R_\odot$ and no comets were observed well enough in C3 orange to calculate a slope. We did not calculate any slopes between 10–16 $R_\odot$ because this is the region where lightcurves turn over. We also did not calculate any slopes at distances smaller than 7 $R_\odot$ because the data are sparse and noisy, however the few comets which were well observed in this region tend to show a second brightening or a flattening out. We calculated slopes for all comets with at least five images within the specified ranges which could be reasonably well fit by a power law. This frequently excluded the faintest comets (typically fainter than magnitude $\sim$7) where the uncertainty in the magnitude was comparable to the extent of the brightening or fading. Histograms of the brightening (left panel) and fading (right panel) are plotted in Figure 3.8.

We calculated the slope in log(brightness) versus log(r) beyond 24 $R_\odot$ for 67

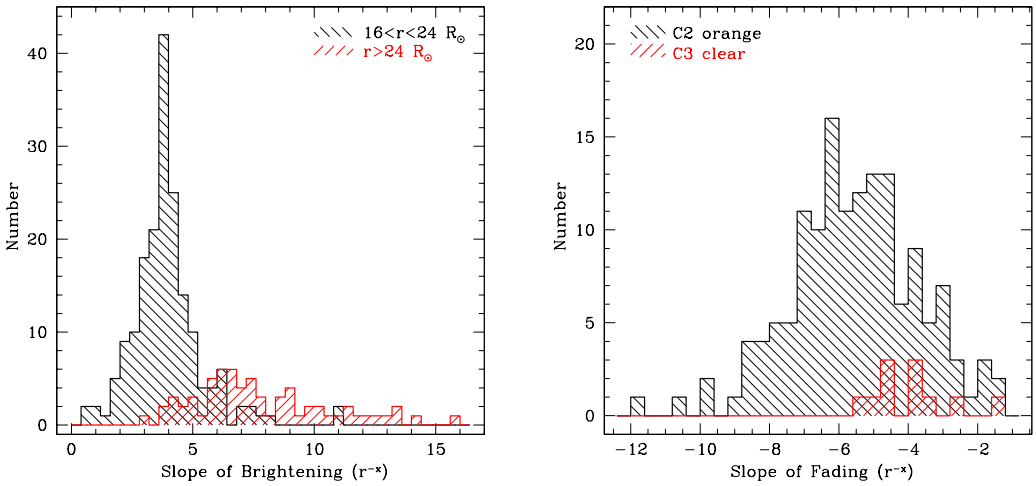

Figure 3.8: Histograms of the slope of the brightening (left panel) and fading (right panel) of Kreutz comets. The slopes of brightening are calculated for two regions in the C3 clear filter: distances larger than 24 $R_\odot$ (red hatching at +45°) and from 24–16 $R_\odot$ (black hatching at −45°). The slopes of fading are calculated from 10–7 $R_\odot$ for the C3 clear filter (red hatching at +45°) and the C2 orange filter (black hatching at −45°). All distances are prior to perihelion.

comets, finding that they brightened with a median slope of 7.3 (with a semi-interquartile range[3], SIQR, of 2.0). 181 comets had calculable slopes from 24–16 $R_\odot$ with a median slope of 3.8 (SIQR=0.7). Among comets observed to fade from 10–7 $R_\odot$, 145 were observed in the C2 orange filter with a median slope of −5.5 (SIQR=1.2) and 11 were observed in the C3 clear filter with a median slope of −3.9 (SIQR=0.7).

The change in the slope of brightening which occurs around 24 $R_\odot$ is striking. While there is significant spread in the slopes beyond 24 $R_\odot$, the slope is unmistakably steeper than the slope from 24–16 $R_\odot$. The spread in slopes beyond 24 $R_\odot$ is likely due to fewer images, higher noise, and the distance of the break in the slope varying from comet to comet and not always occurring at 24 $R_\odot$. It is unlikely

[3]Semi-interquartile range is a measure of volatility. It is half the distance between the 25^{th} and 75^{th} percentiles.

that the steeper slope is a product of poor photometry caused by faint comets because there are comparable numbers of equally faint observations in the 24–16 $R_\odot$ range without a corresponding tail of steep slopes. Assuming the change in slope is real, it may be tied to an ongoing physical process of the nucleus which is typically exhausted around 24 $R_\odot$. We will consider possible scenarios in Section 3.6.

It is interesting to note that the brightening and fading in the C3 clear filter appears to be symmetric inside of 24 $R_\odot$ with the caveat that the sample of C3 clear fading is very small (14 comets). Combined with the fact that the fading in the C2 orange filter is steeper than the brightening or fading in the C3 clear filter (inside of 24 $R_\odot$), this confirms the heliocentric color dependence discussed in the next section.

3.4.3 Orange – Clear Magnitude Difference

While the shapes of the lightcurves in the orange and clear filters tend to be similar, the comets generally appear brighter in the C2 and C3 orange filters than in the C3 clear filter. There are relatively few overlapping orange and clear observations due to the geometry (comets are rarely observed simultaneously in C2 and C3) and the scarcity of C3 orange images. Furthermore, those that do overlap tend to be noisy due to the proximity to the C3 occulter for comets observed simultaneously in C2 and C3 and the very faint magnitudes of most comets observed beyond 20 $R_\odot$. Only a handful of comets have more than three overlapping orange and clear images, making it difficult to draw conclusions from the color behavior of individual comets. Instead, we consider the orange – clear magnitude difference in the aggregate.

Figure 3.9 shows the orange – clear magnitude difference as a function of heliocentric distance. Images that were brighter in the orange than in the clear are negative. Orange filter images with clear filter images taken both before and after

were included. A cubic spline was fit to the clear filter images and the interpolated magnitudes were subtracted from the orange filter magnitudes. Saturated images were excluded. Error bars were calculated by adding the orange and clear error bars in quadrature, and the clear error bars were estimated as the weighted average of the two nearest clear error bars. All C3 orange filter images were half-resolution 512×512 images while all C3 clear and C2 orange filter images were full-resolution. C3 orange filter images were typically taken as part of a polarizer sequence (no polarizer, 0°, +60°, and −60°). We include only the C3 orange filter images without polarization.

While there is substantial scatter in Figure 3.9, the trend is for comets to brighten slightly (or remain constant) in the orange relative to the clear until a distance of 15–20 $R_\odot$, then fade in the orange relative to the clear interior to this. In general, the comets are brighter in the orange than the clear except for a handful of images taken at distances smaller than 8 $R_\odot$ and a dozen or so points when the comet was only marginally observed leaving C3 beyond 10 $R_\odot$. The anomalous points beyond 10 $R_\odot$ are likely due to C3 clear magnitudes which were artificially inflated by an uneven removal of transient solar activity. A quadratic fit weighted by the error bars (red line) suggests the peak in the orange relative to the clear occurs at ∼19 $R_\odot$. (Biesecker *et al.* 2002) found a similar color dependence using only C3 orange and clear images for 11 comets observed from 1996–1998.

This orange – clear behavior is consistent with the observation that comets fade faster in C2 orange images than in C3 clear images (Section 3.4.2). Furthermore, it is evident in the lightcurves of the few comets observed extensively in both orange and clear filters. Figure 3.10 shows two of the best observed. In the left panel (C/2001 U7 = SOHO-365) the orange – clear difference is largest when the comet is first visible in C2 (at ∼10.5 $R_\odot$) and decreases as the heliocentric distance decreases. In the

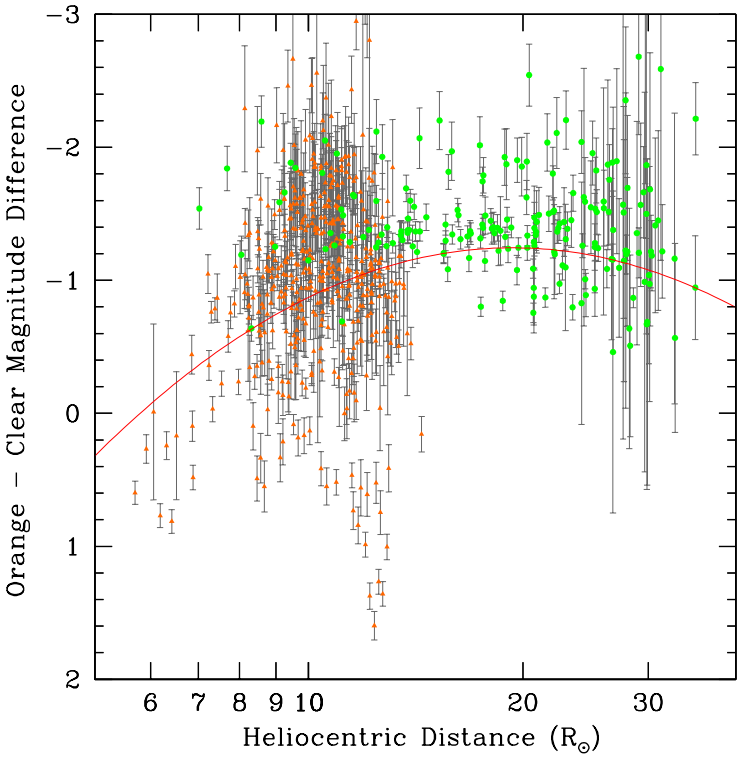

Figure 3.9: Orange – clear magnitude difference as a function of heliocentric distance. Negative values are brighter in the orange than the clear. The green circles are C3 orange – C3 clear magnitudes and the orange triangles are C2 orange – C3 clear magnitudes. The red line is the best fit quadratic to the data, which peaks at 18.6 $R_\odot$.

right panel (C/2001 R2 = SOHO-347) the orange – clear difference peaks between 15–20 $R_\odot$ (the detector was saturated from 10–15 $R_\odot$ making these magnitudes unreliable) and is slightly smaller at distances larger than 20 $R_\odot$ and smaller than 10 $R_\odot$.

3.4.4 Size Distribution

The observed magnitudes can be converted to an estimate of the size of the nucleus. We assume that the brightness is due entirely to the surface area of dust grains in the coma which are reflecting sunlight. For simplicity we assume the coma is made of spherical dust grains 0.5 μm in radius having albedo 0.04 (the size distribution of

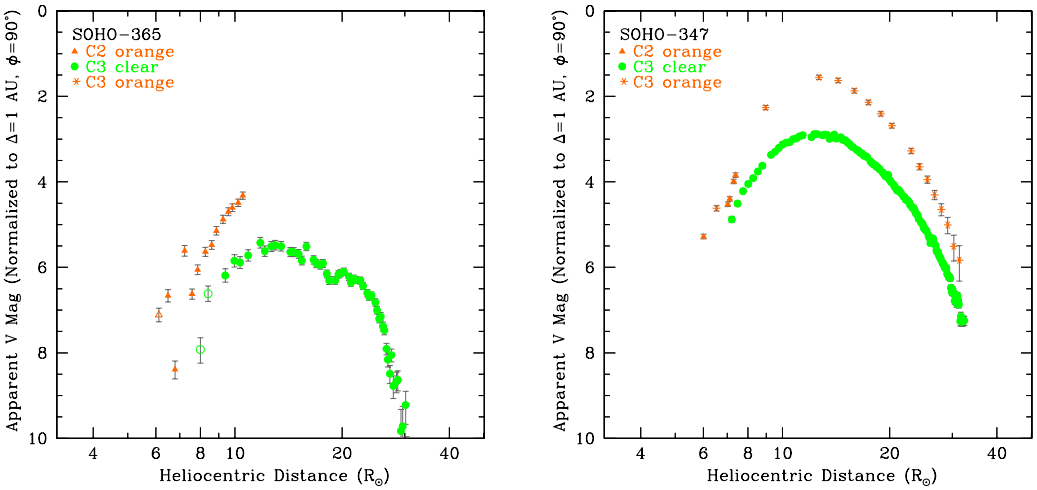

Figure 3.10: Lightcurves of Kreutz comets with overlapping orange and clear images. The left panel is C/2001 U7 (SOHO-365) and the right panel is C/2001 R2 (SOHO-347). The orange triangles are C2 orange images, the green circles are C3 clear images, and the orange asterisks are C3 orange images. Open points signify images which have significant vignetting (greater than 4.0). Note that C/2001 R2 saturated the C3 detector at its peak, making the brightest points unreliable.

dust in the ejecta relative to the ambient coma of 9P/Tempel 1 peaked at 1-μm in diameter (Lisse *et al.* 2006) and the albedo of the nucleus of 9P/Tempel 1 was 0.04 (A'Hearn *et al.* 2005)). We then determine the effective radius a sphere of these particles would have been if it disintegrated completely to produce the observed brightness of the comet. If we assume the nucleus has totally disrupted to produce the dust in the coma, we find sizes ranging from 2–50 meters in radius. This is a lower limit to the size of the nucleus since if any nucleus remains at this time then the total size is larger than the size estimated from the brightness.

In this manner, we can estimate the size distribution of the Kreutz comets seen by SOHO. Ideally we wish to calculate the size at the peak in brightness, however because our sample is small and the peak is generally only well determined for bright comets, the size distribution calculated from comets observed to peak is inconclusive

(Figure 3.11, left panel)[4]. Therefore, we approximate the size distribution by using all comets which were observed between 10–15 $R_\odot$ in the C3 clear filter (Figure 3.11, right panel). While this does not necessarily include the peak brightness for all comets, most are observed very close to peak, so the distribution should be relatively accurate, although somewhat flatter than the true distribution. We do not include C3 orange filter observations because very few comets were observed in this filter and their inclusion would skew the results towards too many large comets since the comets are brighter in the orange filter, implying a larger nucleus. We do not include C2 observations because most are only observed inside 12 $R_\odot$ and many are too far past their peak brightness, skewing the results toward too many small comets. We fit a line to the data in log(number) vs. log(radius) space, with the slope being the power law exponent. This results in a cumulative size distribution $N(>R) \propto R^{-2.2}$ from 5–35 meters in radius. The turnover for sizes smaller than $\sim$5 meters is likely artificial due to incompleteness and the seasonal dependence of the limiting magnitude. The lack of comets larger than 30 meters may be real and indicative of a turnover in the distribution or it may simply be small number statistics.

3.4.5 The Effect of Normalizing the Photometry

As discussed in Section 2.2 we normalized fluxes to unit SOHO-centric distance and applied a correction for the phase angle. Since these corrections have a seasonal effect on the lightcurves, they alter individual lightcurves differently. The largest effect is generally to the intrinsic magnitude, as comets observed at very large phase

[4]Here we included the six comets which saturated the detector for completeness. While their sizes may be slightly underestimated, their exclusion implies a misleadingly small upper end of the size distribution.

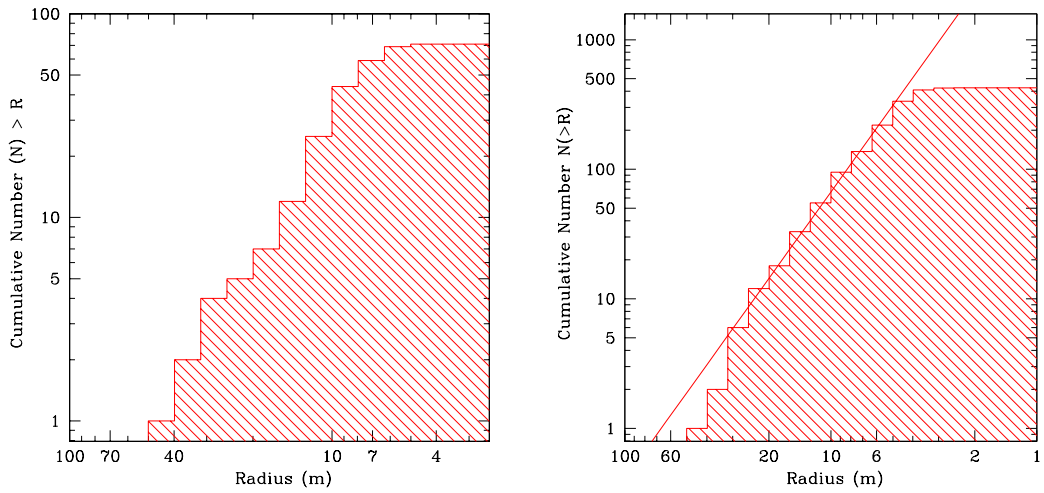

Figure 3.11: Cumulative size distribution of the comets with a discernible lightcurve peak in the C3 clear filter (left panel) and the cumulative size distribution based on the brightest point of all comets observed in the C3 clear filter between 10–15 $R_\odot$ (right panel). Both plots include the six comets which were omitted from the earlier discussion of peak distances because they saturated the detector (Section 3.4.1). These represent six of the seven points with sizes greater than 20 meters. The line in the right panel is a logarithmic fit from 5–35 meters in radius having a slope (log(number) vs. log(radius)) of −2.2.

angles (greater than 150°) can appear two or more magnitudes brighter than comets observed at intermediate phase angles (30–100°). This in turn affects the apparent size distribution of the family. The changing phase angle from image to image can also affect the shape of the lightcurve, altering the slope of brightening and fading and the distance of the peak of the lightcurve.

The first effect of the photometric normalization is on the distance of peak brightness. In Figure 3.12 we plot a histogram of the distances of peak brightness in C3 based on the raw magnitudes (left panel) and for the corrected magnitudes (right panel, replicated from Figure 3.4). In both cases the data peak at 12.25 $R_\odot$ and have a shoulder at 11.25 $R_\odot$, but the corrections spread the distribution out. Only 9 of the 65 comets reached a peak in brightness at a distance larger than 12.5 $R_\odot$ in the uncorrected sample, while 19 did in the corrected sample. The number of comets

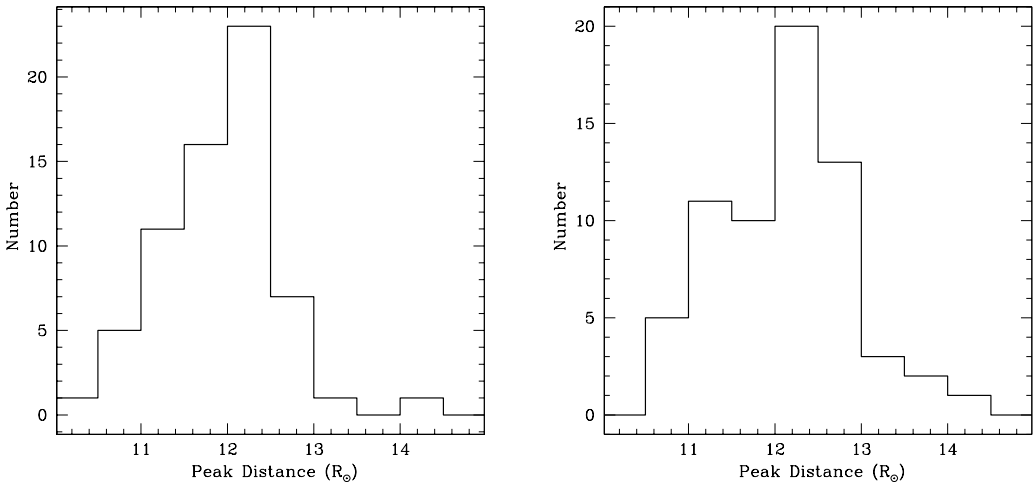

Figure 3.12: Histograms of the heliocentric distance of peak brightness for comets observed to peak in C3 for the uncorrected data (left panel) and the corrected data (right panel, which is identical to Figure 3.4).

with peak distances smaller than 11.5 $R_\odot$ was unchanged. Thus, normalizing the photometry reveals that the distribution of peak distances is much wider and less steeply peaked than would be inferred from the uncorrected sample.

The photometric normalization affects the shape of the lightcurve of some individual comets strongly. Figure 3.13 shows the uncorrected (black crosses) and corrected (all other points) lightcurves of C/2005 S1 (SOHO-1024). When first visible in C3, its phase angle was 98° resulting in a minimal change in magnitude. The phase angle steadily increased, reaching 128° when last visible in C3 and 143° when last visible in C2, resulting in increasingly larger corrections to the magnitude. As a result, after correcting for phase it appeared to brighten less steeply, fade more steeply, and reach a peak in brightness at a larger heliocentric distance.

While the effect of photometric normalization on individual lightcurves can be significant, the overall effect on lightcurve shapes is mitigated by the fact that there are roughly equal numbers of comets made to appear brighter or fainter These effects are summarized in Table 3.1. The median peak distance is slightly larger and the

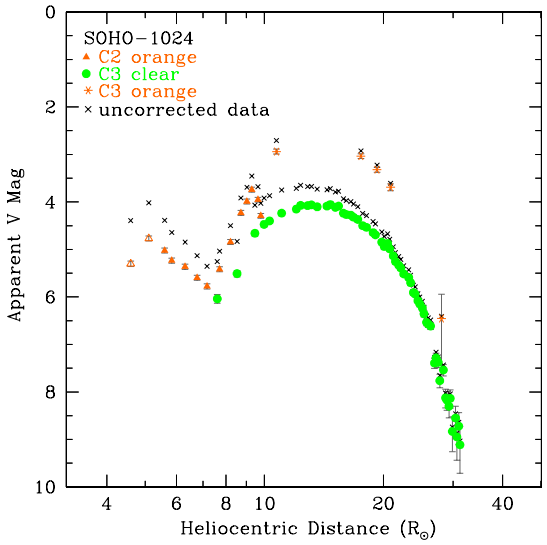

Figure 3.13: Lightcurve of C/2005 S1 (SOHO-1024) with and without photometric correction. The uncorrected data are plotted as black crosses. The corrected data are plotted as orange triangles (C2 orange filter), green circles (C3 clear filter), and orange asterisks (C3 orange filter). Open points are images with vignetting greater than 4.0.

Parameter	Raw data (median ± SIQR)	Corrected data (median ± SIQR)
Peak Distance ($R_\odot$)	11.9 ± 0.45	12.2 ± 0.55
Slope of C2 orange fading from 10–7 $R_\odot$	−5.1 ± 0.9	−5.5 ± 1.2
Slope of C3 clear fading from 10–7 $R_\odot$	−3.9 ± 0.9	−3.9 ± 0.7
Slope of C3 clear brightening from 24–16 $R_\odot$	+3.9 ± 0.6	+3.8 ± 0.7
Slope of C3 clear brightening beyond 24 $R_\odot$	+8.0 ± 1.9	+7.3 ± 2.0
Slope of size distribution	−2.22	−2.22
Median orange – clear magnitude difference	−1.03 ± 0.30	−1.19 ± 0.34

Table 3.1: The effects on the lightcurve properties of normalizing the photometry to a unit SOHO-centric distance and correcting for phase angle.

spread in peak distances is greater. The slope of the brightening in C3 beyond 24 $R_\odot$ is somewhat more shallow. The slopes of the brightening from 24–16 $R_\odot$ and fading in C3 are nearly unchanged and still symmetric. The slope of fading in C2 becomes slightly steeper. The spreads in the slopes of brightening and fading are essentially unchanged.

Since differing δ_{90} values were used for calibrating the clear (δ_{90}=0.52) and orange (δ_{90}=0.16) filter images, the orange – clear magnitude differences are affected even though they are interpolated from clear filter images at the same time (and thus phase angle) as the corresponding orange filter images. The change is equal to the difference between the δ_{90}=0.52 and δ_{90}=0.16 lines in Figure 2.2. For phase angles (θ) smaller than $\sim$100° the change is less than $\pm$0.1 magnitude. For θ>100° the correction is larger in the clear filter than the orange, hence the orange – clear color difference increases, with an increase of $\sim$0.5 magnitude for θ>130°. About half of the orange – clear points have a phase induced magnitude change less than than $\pm$0.1 magnitude, however, due to the asymmetry of the phase correction, the average correction to the orange – clear magnitude was $-$0.17 magnitude. Thus, as a result of the phase correction the orange – clear magnitude difference is larger than in the uncorrected data, meaning a larger fraction of the light is due to sodium than would be inferred from the uncorrected data.

The limiting magnitude of both C2 and C3 is approximately 8. In practice, C2 is more sensitive to comets in the range 7–8 magnitudes than C3 because of its smaller pixel scale and better signal to noise, making detections easier. As a result, the dataset is relatively complete for comets brighter than apparent magnitude 7 in C3 and apparent magnitude 8 in C2. The correction for phase (Figure 3.14) reveals that the distribution of intrinsic magnitudes is not as clear cut. A significant number of comets intrinsically too faint to be seen by SOHO are made bright enough to be visible due to phase effects (the excess of comets at magnitudes fainter than 8 in the red histograms with hatching at +45°). Roughly equal numbers of comets experience phase related brightening and fading, however due to the asymmetric effect of scattering (when corrected to a scattering angle of 90°), comets may appear $\sim$2 magnitudes brighter but only $\sim$0.1 magnitude fainter. Thus the magnitude

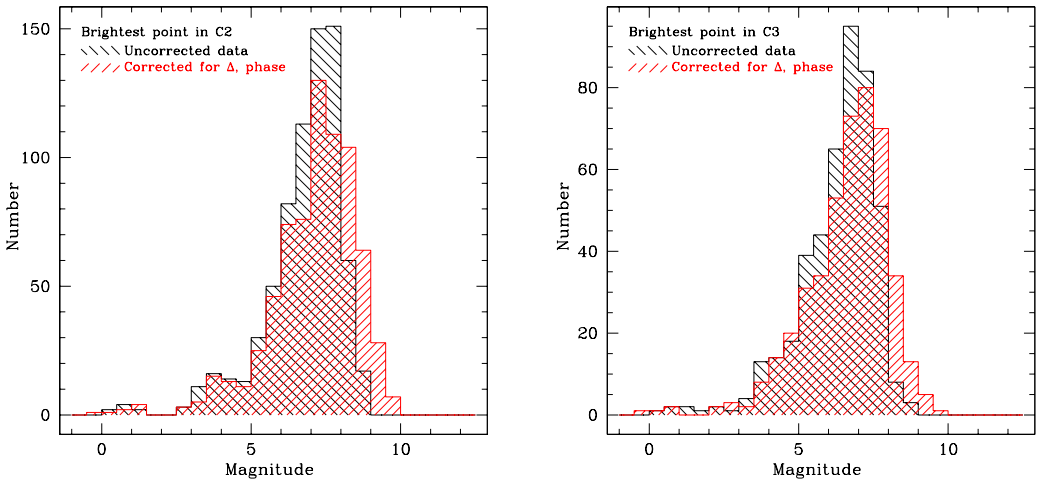

Figure 3.14: Histogram of brightest magnitude for comets observed in C2 (left panel) and C3 (right panel). The uncorrected size distribution has black hatching going at −45° and the data corrected for phase angle and SOHO-centric distance has red hatching at +45°.

distribution should be nearly complete down to a corrected magnitude of ∼8 in C2 and ∼7 in C3. The turnover in the distribution for magnitudes fainter than this is a product of the sensitivity of the detectors and the effects of the phase angle. The substantial numbers of magnitude 9–10 comets despite the limited annual times when these comets are visible confirms that there are ever larger numbers of comets at fainter magnitudes.

Despite the significant changes to the magnitude distribution due to the phase correction, the slope of the size distribution is unchanged. For all comets seen in the C3 clear filter from 10–15 $R_\odot$, both the uncorrected and corrected datasets yield a slope of −2.22 for nuclei of radius 5–35 meters. For comets brighter than the completeness limit for C3 (magnitude 7 which corresponds to a 4.9 meter radius), the phase angle affects the same proportion of comets of all sizes.

Year	C2	C3	Total
1996	7	26	27
1997	53	31	69
1998	66	17	70
1999	53	33	71
2000	70	32	79
2001	76	33	84
2002	91	39	106
2003	98	65	131
2004	105	84	146
2005	117	87	145
2006	112	70	141
2007	125	80	150
Total	973	597	1219

Table 3.2: Yearly SOHO Kreutz discoveries by telescope from 1996–2007. Note that many comets are seen in both C2 and C3. Therefore the combined total is less than the sum of the individual telescopes.

3.5 Population

3.5.1 Yearly Detection Rate

Over SOHO's first twelve years, 1996–2007, 1219 Kreutz family comets were discovered in its images (Table 3.2). The discovery rate has increased throughout the mission due to a number of factors. First, the telemetry bandwidth allocated to C2 and C3 increased from 1996 to 2000, resulting in more full resolution images per day. While an average of only 6 full resolution images were taken per day by both C2 and C3 in 1996, the rate had increased to about 60 per day in C2 and 40 per day in C3 by 2000, and has remained relatively constant ever since.

The duty cycle, or the fraction of time SOHO takes images, also increased from 1996–2000. Following the definition of Biesecker *et al.* (2002), we define a gap in excess of four hours between full resolution images in a given telescope to be

Year	C2 Duty Cycle	C3 Duty Cycle
1996	0.727	0.742
1997	0.947	0.946
1998	0.597	0.598
1999	0.787	0.787
2000	0.944	0.943
2001	0.945	0.944
2002	0.957	0.956
2003	0.917	0.916
2004	0.891	0.884
2005	0.965	0.962
2006	0.894	0.891
2007	0.924	0.917
Total	0.875	0.874

Table 3.3: Yearly SOHO duty cycle by telescope from 1996–2007. The duty cycle calculation is described in the text.

significant, with the time exceeding four hours considered to be lost time. All of the excess time is then summed for a whole year, divided by the total hours in a year, and subtracted from 1. A year with no missed time would have a duty cycle of 1.0 while a year with no full-resolution images would be defined to have a duty cycle of 0. Due to the lower bandwidth allocated to C2 and C3 as well as several significant hardware failures endured by the spacecraft, the duty cycle for both C2 and C3 from 1996–1999 only exceeded 0.80 once and was as low as 0.60. Since 2000 however, the yearly duty cycle in both telescopes has remained above 0.88. The duty cycle by year and telescope is given in Table 3.3.

The "SOHO/LASCO Comet Observations website"[5] became commonly used as a means of reporting comet discoveries in late 2000[6]. This site allows amateur comet

[5]http://ares.nrl.navy.mil/sungrazer/

[6]Publicly available reporting of amateur discoveries began in late 2000 however the SOHO team had been working privately with amateurs for several years prior to this (Biesecker, private communication 2008).

hunters to download images in near real time in several formats to search for new comets. Since mid-2000 nearly every Kreutz comet has been discovered in near real time. In addition to searching the real time images, many users have systematically combed the archives for earlier comets, and it is believed that very few Kreutz comets have escaped detection.

Beginning in mid-2003, SOHO has been rolled by 180° approximately every three months due to the malfunction of the high-gain antenna (discussed in Section 2.1.3). The roll periods cause an increase in detections in C3 due to the rotation of the occulting arm out of the path of Kreutz comets. This allows fainter comets to be discovered during the roll periods than would be seen if they arrived when the telescope was not rolled (discussed further in Section 3.5.2 below). Furthermore, there is an increase in the telemetry devoted to C2 for a few days on either side of each roll maneuver which causes a slight increase in the C2 detection rate by allowing fainter comets to be discovered (since they only have to remain above the threshold for a shorter amount of time to be detected). Taking all of the above factors into account, the period from 2004–2007 has the most complete temporal coverage and the most uniform month-to-month selection effects. Thus we consider this time frame to be representative of the true detection rate of SOHO.

3.5.2 Seasonal Variability

There is a distinct seasonal variation in the observation rates of Kreutz comets (Figure 3.15). Observations of comets in C2 (these comets may or may not be seen in C3) peak strongly from April to June and again from October to December each year, while C3 observation rates (these comets may or may not be observed in C2) are more constant, but dip strongly in April and weakly from March to June and November to December. Since many comets are seen in both C2 and C3 and since

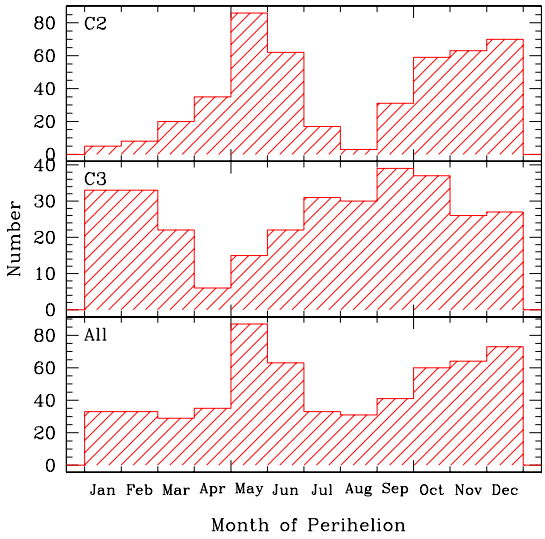

Figure 3.15: Histogram of the month of perihelion for Kreutz comets observed by SOHO from 2004–2007. The top panel shows comets observed in C2. The middle panel shows comets observed in C3. The bottom panel shows all comets observed, regardless of telescope. Note that the the total number of comets observed is less than the sum of the comets observed in C2 and C3 because many comets are seen in both telescopes. The period displayed (2004–2007) was chosen because it represents the most complete and uniform period of the dataset as discussed in Section 3.5.1.

C2 is more prolific than C3, the combined discovery rate is relatively flat with peaks that mirror the peaks in C2. This seasonal variability is due to the combination of two factors: the geometry of the Sun-SOHO-Kreutz orbit and the brightness behavior of Kreutz comets at small heliocentric distances. We discuss these effects below.

Kreutz comets approach the Sun from the south (the bottom of unrolled SOHO images when north is up and east is to the left). Figure 3.16 shows the track of a typical Kreutz comet through the SOHO field of view on the 15^{th} of each month. From January through May, they approach from the bottom left. In June the track begins to pass to the other side of the field of view and comets move nearly straight up from the bottom middle. From July through November they move diagonally up from the bottom right. Finally in December the track begins to swing back to the

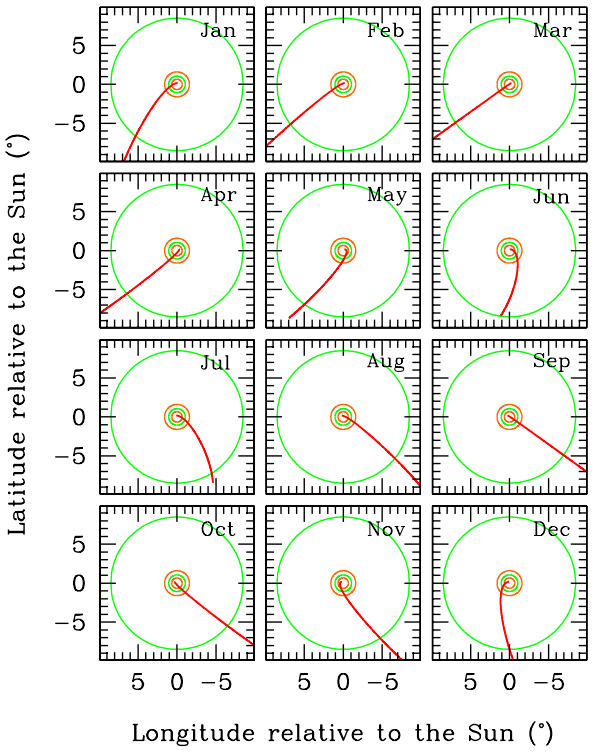

Figure 3.16: Monthly track across the SOHO coronagraphs for typical Kreutz comets. The track is for a comet which reaches perihelion on the 15^{th} day of the month specified in the upper right corner of each plot. The heavy red line is the orbit prior to perihelion. The post-perihelion track is not plotted since no Kreutz comets have been seen by SOHO after perihelion. The green (C3) and orange (C2) circles denote the outer and inner radii of the SOHO coronagraphs.

left and comets move nearly straight up from the bottom middle.

The occulting arms on C2 and C3 extend from the bottom left corner to the middle at roughly a 45° angle in unrolled images and from the top right in rolled images (see Figure 2.1). Thus, comets which arrive from January to early May frequently cross the occulting arm in unrolled images. This reduces the counts recorded, sometimes completely obscuring the comet and preventing detections. This has a minimal effect in C2, but is strong in C3 where the vignetting is more severe, and results in a lower discovery rate during these months.

This effect has been mitigated since mid-2003 by the 180° rolls necessary every ∼3

months since the malfunction of the high-gain antenna (discussed in Section 2.1.3). When the telescope is rolled, the occulting arm extends from the northwest and does not cross the Kreutz track. This has improved the discovery rate during times when the track is usually obstructed by the occulting arm. These include: 2003 December 31–2004 March 29, 2004 December 23–2005 March 21, 2005 December 16–2006 March 13, and 2006 December 6–2007 March 5. This effect can be seen in the C3 discoveries in January to April in Figure 3.15. During this time, SOHO has always been rolled in January and February, has been rolled about half the time in March, and has never been rolled in April. The discoveries in C3 mimic this pattern: 33 comets were observed in C3 in January, 33 in February, 22 in March, and only 6 in April.

A second effect of the geometry is on the elongation at which the Kreutz comets reach peak brightness. As discussed in Section 3.4, Kreutz comets brighten at a nearly constant rate as they approach the Sun, reach a peak in brightness between 10–13 $R_\odot$, and fade rapidly at smaller heliocentric distances. None of the SOHO-observed Kreutz comets has been observed to survive perihelion. The elongation as a function of heliocentric distance is plotted in Figure 3.17.

The SOHO-Sun line is approximately in the plane of the Kreutz orbit from April to June and October to December. During these months, comets approach the Sun from behind (April to June) or in front (October to December) and reach their peak brightness at a smaller solar elongation. During these months, typical Kreutz comets are at a heliocentric distance of 8.5–12 $R_\odot$ when they enter the C2 field of view, making them visible in C2 at or soon after their peak brightness. From January to March and July to September, the SOHO-Sun line is roughly perpendicular to the plane of the Kreutz orbit. During these months, typical Kreutz comets are at a heliocentric distance of 6–7 $R_\odot$ when they enter the C2 field of view. Thus, they

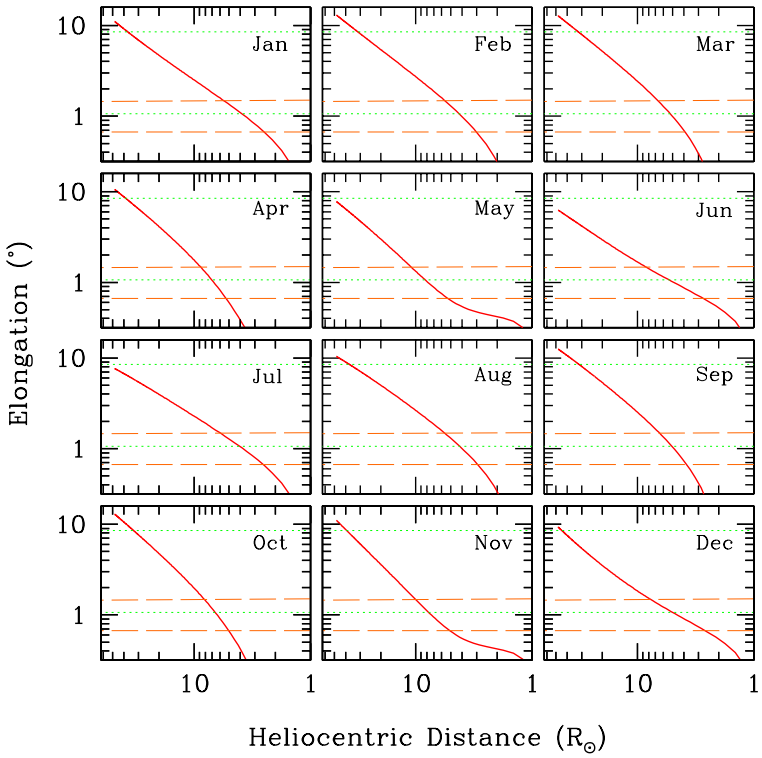

Figure 3.17: Solar elongation as a function of heliocentric distance for typical Kreutz comets. The orbit is for a comet which reaches perihelion on the 15^{th} day of the month specified in the upper right corner of each plot. The heavy red line is the last 3 days of the orbit prior to perihelion. The post-perihelion track is not plotted since no Kreutz comets have been seen by SOHO after perihelion. The dotted green and dashed orange horizontal lines denote the outer (upper) and inner (lower) radii of the C3 and C2 coronagraphs respectively.

do not appear in C2 until well after peak brightness, and fewer comets are visible. The heliocentric distance at which comets leave C2 has no effect on discovery rates, as only the very brightest comets are still seen leaving C2.

This plane-of-sky geometry has a small but opposite effect on comet detections in C3. The maximum heliocentric distance at which comets leave C3 varies from 3.5–8.5 $R_\odot$ throughout the year, meaning the peak brightness is always within the C3 field of view. However, the signal to noise and vignetting are worse closer to the occulting disk, so there is a preference for geometries in which the comet peaks at a larger elongation. Thus, the detection rate is slightly higher from January to March

and July to September when the apparent heliocentric distance of the peak in the lightcurve is largest. Only the very brightest comets are seen near the outer edges of C3, so the varying distance at which comets enter the field of view does not affect the discovery rate.

Another effect of the geometry is the changing phase angle at which SOHO observes the comets at a given heliocentric distance. As discussed in Section 2.3.3, Kolokolova *et al.* (2004) and Marcus (2007b) found that the scattering of sunlight off of dust in the coma causes comets to brighten strongly due to forward-scattering at phase angles greater than 100° and to brighten slightly due to backscattering at phase angles smaller than 30°. The brightness at intermediate phase angles is relatively unchanged. Figure 3.18 shows the phase angle of Kreutz comets as a function of elongation on the 15^{th} of each month.

Comets which reach perihelion from September to January have phase angles greater than 100° for most or all of the time they are within the C3 field of view. Forward-scattering causes these comets to appear brighter than identical comets which reach perihelion from February to August, when they are at moderate phase (∼30°–100°) and experience no brightness enhancement due to phase. Thus, C3 detection rates are enhanced from September to January. Similarly, C2 detection rates are enhanced from August to December when comets are forward-scattering in the field of view. The brightening (and thus the increased detection rate) is strongly dependent on phase angle. A comet at phase angle ∼120° would appear brighter by ∼0.5 magnitude relative to a comet at 90° phase while a comet at ∼150° would appear brighter by ∼2.0 magnitudes relative to a comet at 90° phase (Marcus 2007b). The magnitude correction as a function of phase angle can be seen in Figure 2.2.

A final effect of the geometry is that the comets are closer to the spacecraft from September to March than they are from April to August. At the extremes, comets

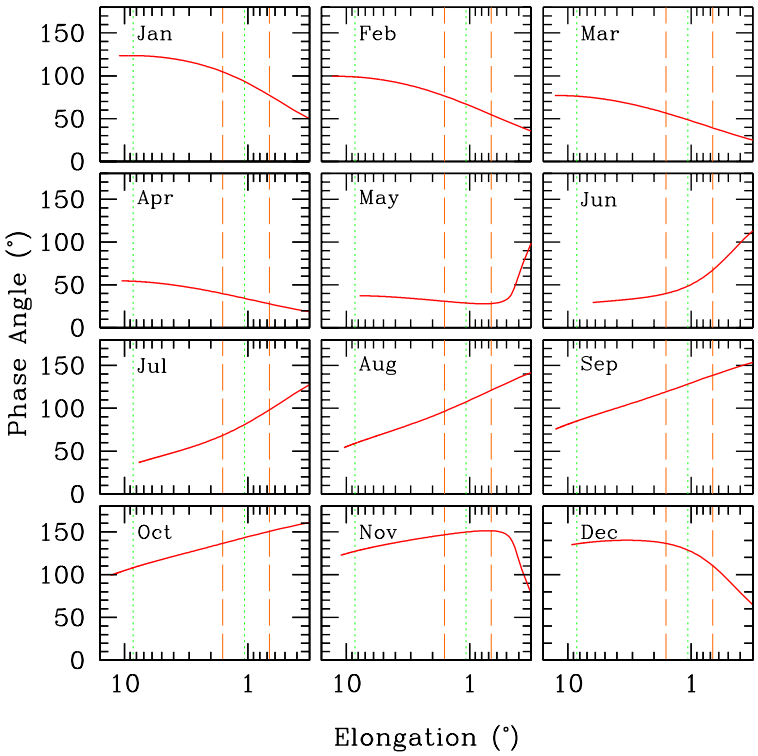

Figure 3.18: Monthly phase angle as a function of elongation for typical Kreutz comets. The phase angle is for a comet which reaches perihelion on the 15^{th} day of the month specified in the upper left corner of each plot. The heavy red line is the phase angle prior to perihelion. The post-perihelion track is not plotted since no Kreutz comets have been seen by SOHO after perihelion. The dotted green and dashed orange vertical lines denote the outer (left) and inner (right) radii of the C3 and C2 coronagraphs respectively.

which reach perihelion in November and December (when the SOHO-Sun line is nearly in the plane of the Kreutz orbit and comets approach from the near side of the Sun) are ∼10% closer than comets which reach perihelion in May and June (when the SOHO-Sun line is nearly in the plane of the Kreutz orbit and comets approach from the far side of the Sun). As a result, a comet which arrives in November or December would appear ∼0.2 magnitudes brighter than an identical comet which arrives in May or June. Thus, slightly more comets are detectable from September to March than from April to August. We summarize the seasonal effects in Table 3.4.

Effect	When	C2 Discovery Rate	C3 Discovery Rate
Occulting arm	Jan–May	small decrease	large decrease
Telescope roll	every 3 months	small increase when rolled in Jan–May	large increase when rolled in Jan–May
SOHO-Sun line nearly in plane of Kreutz orbit	Apr–Jun & Oct–Dec	large increase	slight decrease
SOHO-Sun line nearly perpendicular to plane of Kreutz orbit	Jan–Mar & Jul–Sep	large decrease	slight increase
Phase angle	Sep–Jan	no change	increase
Phase angle	Aug–Dec	increase	no change
SOHO-comet dist <1 AU	Sep–Mar	slight increase	slight increase
SOHO-comet dist >1 AU	Apr–Aug	slight decrease	slight decrease

Table 3.4: Summary of seasonal effects on detection rate.

3.5.3 True Arrival Rate

As discussed above, 2004–2007 is representative of the true detection rate of SOHO because during this period SOHO was continuously operational and the image cadence, duty cycle, and roll periods were nearly identical. Furthermore, amateur comet hunting was already well established on the Sungrazer website, and virtually all the comets were found in near real time (as opposed to pre-2000 discoveries which have been largely discovered in archival images, making it more difficult to be sure that all the images have been searched as thoroughly).

We use the four years 2004–2007, corrected for the duty cycle, as the true monthly discovery rates of SOHO (Table 3.5). There is no reason to think the true flux varies from month to month, so we estimate the actual flux of Kreutz comets to be the average of the highest monthly detection rate (22.9 comets month^{-1}, in May). Therefore, we estimate the flux of Kreutz comets brighter than the threshold for observation by SOHO as ∼0.74 comets day^{-1}, or ∼270 comets year^{-1}. This is

significantly higher than the rate of 14 month^{-1} found by Bzowski and Królikowska (2005) using data from 1997–2002 and the lower limit of 60 year^{-1} found by Biesecker *et al.* (2002), but is reflective of the improved discovery circumstances and the apparent overall increase in comet flux (discussed in the next section))since then.

This rate is still only a lower limit as the spacecraft distance and phase angle effects discussed in Section 3.5.2 are sub-optimal during May. In principal, these effects could combine to improve the detection threshold by another 0.7 magnitudes (0.2 magnitudes due to the spacecraft distance and 0.5 magnitudes due to the phase angle). Since the size distribution of the Kreutz family heavily favors small comets, an ideal scenario where the viewing geometry and detector sensitivity are all aligned could yield ∼60% more comet detections (all at the faint end).

3.5.4 Quantifying the Change in Comet Flux

While the number of Kreutz comets discovered by SOHO has increased since the beginning of the mission, we must correct for all of the changing detection biases before concluding that the flux has truly increased. First, we estimated the number of comets which were discovered due to a higher image cadence. From 1997–1998, an average of 42 C2 orange images and 25 C3 clear images were taken per day (the rates were lower in 1996 and most were not full resolution 1024×1024). We used this as a baseline and randomly removed images from the dataset of the comets discovered from 1999-2005 at a rate proportional to the average excess number of images in a given telescope per day for that year. For example, the rate of C2 orange images in 2001 was 63.3 day^{-1}, or 21.3 day^{-1} more than in 1997–1998. Thus, we removed $\frac{21.3}{63.3}$=33.6% of the 2001 C2 orange images from our dataset. We created 10 such simulated datasets and compared the numbers of comets observed at different magnitudes, the length of observation, and the number of images in

Month	C2 Raw	C2 Duty Cycle	C2 Adjusted	C3 Raw	C3 Duty Cycle	C3 Adjusted	C2+C3 Adjusted Total
January	5	0.966	5.2	33	0.944	35.0	35.0
February	8	0.923	8.7	33	0.922	35.8	35.8
March	20	0.871	23.0	22	0.863	25.5	33.5
April	35	0.897	39.0	6	0.911	6.6	39.0
May	86	0.951	90.4	15	0.951	15.8	91.5
June	62	0.911	68.1	22	0.903	24.4	69.2
July	17	1.0	17.0	31	0.998	31.1	33.1
August	3	0.913	3.3	30	0.912	32.9	34.0
September	31	0.802	38.7	39	0.794	49.2	51.7
October	59	0.970	60.8	37	0.969	38.2	61.8
November	63	0.926	68.0	26	0.923	28.2	69.1
December	70	0.872	80.3	27	0.871	31.0	83.7
Total	459	0.919	502.5	321	0.914	353.7	637.4

Table 3.5: Monthly SOHO Kreutz discoveries by telescope from 2004–2007 adjusted for duty cycle. Many comets are seen in both C2 and C3. Therefore the combined total is less than the sum of the individual telescopes. Note that summing the monthly adjusted totals results in a slightly different number than calculating an adjusted total directly using the raw total and the aggregate duty cycle.

which the comet was observed. This allowed us to estimate the number of comets which would not have been discovered from 1997–1998 either because they did not reach the brightness threshold or because they were not observed in enough images due to the lower image cadence.

Next, we estimated the number of comets which have been discovered due to the roll of the telescope (starting in mid-2003) which would not have been discovered prior to then. Since 2004 the telescope has been rolled from January to March, times when the occulting arm would obscure comets if the telescope was not rolled. Since the raw number of comets discovered has increased as the mission has progressed, we took the ratio of the average number of detections from April to December in 2004–

2007 relative to the average number of detections from April to December in 1999-2003 (the image cadence has been relatively stable since 1999 so we exclude the 1996–1998 data). We then multiplied this ratio by the average number of detections from January to March in 1999–2003, to estimate the number of comets we would have expected in January–March 2004–2007 based on the baseline increase in detections. Finally, we subtracted the expected number from the actual number detected to estimate the increase due to the telescope roll.

A final bias we attempted to correct for was the human element. In our calculation of the photometry of more than 900 comets, it subjectively appears that more comets of dubious quality have been discovered as the mission has progressed. This could be due to either changes in the SOHO team members confirming comet discoveries and reporting them to the IAU or an improvement in the ability of the amateurs discovering comets. Doug Biesecker was the primary SOHO team member who verified comet discoveries and reported them to the IAU through mid–2002, while Karl Battams has been the primary person in that position since then. The difference in personal bias in what constitutes a comet discovery could result in the increase in questionable comets. However, the number of SOHO "X-comets"[7], objects which show properties consistent with being a comet but lack sufficient evidence for a confirmation, have remained relatively constant at $\sim$5 comets year^{-1}. This suggests that the threshold for accepting an object as a comet has remained relatively constant throughout the mission, independent of the individual making the confirmations. The amateurs discovering comets have unquestionably become more skilled at picking faint comets out of the noise. It is unclear how thoroughly the archival data has been searched at these levels, and the increase in dubious detections may simply reflect that the data have been searched more thoroughly

[7]http://ares.nrl.navy.mil/sungrazer/index.php?p=xcomets

in recent years. Regardless of the cause, the number of comets whose brightest raw magnitude was fainter than 8 increased sharply 2002–2003 and has remained high since. To quantify the increase, we averaged the number of comets year^{-1} fainter than magnitude 8 discovered from 1997–2001 (again ignoring 1996 due to its poor discovery circumstances). This was multiplied by the ratio of the number of comets brighter than magnitude 8 discovered from 2002–2005 relative to 1997–2001 to estimate the number of comets fainter than magnitude 8 that would be expected in 2002–2005 based on the overall increase in comet detections. Finally, we subtracted the expected number from the actual number of observed comets fainter than magnitude 8 from 2002–2005 to yield an estimate of the human bias.

Combining all of these effects, and dividing by the duty cycle for each year, we estimated the normalized number of detections for each year (Table 3.6). We included estimates for 2006 and 2007, where the increase due to the cadence was the average from 2004–2005, the increase due to the roll was calculated in the manner discussed above, and the increase due to human bias was the average from 2002–2005[8]. From 1997–2002 a corrected average of 83.5±8.4 comets year^{-1} were discovered while from 2003–2007 125.1±7.6 comets year^{-1} were discovered. Even after correcting for the varying circumstances throughout the mission, the jump in

[8]We have slightly altered the detection statistics for 1998 and 1999 from those given in Tables 3.2 and 3.3. We have estimated the number of detections for July–October 1998 (SOHO was not operational from 1998 June 24 until 1998 October 22) as the average of the detection rates from July–October 1997 and 1999, and for January 1999 (SOHO was not operational from 1998 December 21 until 1999 February 2) as the average of the detection rate from January 1998 and 2000. Furthermore, the duty cycles listed for 1998 and 1999 are the duty cycles when the telescope was operational rather than the duty cycle for the whole year. Making these corrections decreases the estimates for 1998 and 1999 since the times when the spacecraft was inoperational are times when there are historically few comets discovered.

Year	Actual Number	Extra Due to Increased Cadence	Extra Due to Roll	Extra Due to Human Bias	Net Number	Duty Cycle	Corrected Number
1996	27	0	0	0	27.0	0.735	36.7
1997	69	0	0	0	69.0	0.946	72.9
1998	92	0	0	0	92.0	0.928	99.1
1999	74	1.6	0	0	72.4	0.862	84.0
2000	79	8.9	0	0	70.1	0.944	74.3
2001	84	9.7	0	0	74.3	0.944	78.7
2002	106	16.5	0	6.2	83.3	0.957	87.0
2003	131	12.7	0	4.2	114.1	0.917	124.4
2004	146	11.3	12.6	8.2	113.8	0.888	128.2
2005	145	19.0	11.6	5.2	109.1	0.964	113.2
2006	141	15.2	7.6	6.0	112.2	0.893	125.7
2007	150	15.2	5.6	6.0	123.2	0.920	133.9

Table 3.6: Detection rates corrected for the varying detection biases. Column 1 is the year. Column 2 is the actual number of comets discovered, except that 1998 and 1999 have been extrapolated to fill in data gaps (see footnote in text for more information). Column 3 is the estimated number of comets that were discovered due to the higher image cadence than in 1996–1998. Column 4 is the estimated number of comets that were discovered due to the roll of the telescope. Column 5 is the estimated number of comets that were accepted as comets due to changing human bias. Column 6 is the net number of discoveries after subtracting the increases (columns 3–5). Column 7 is the duty cycle (see footnote in the text regarding 1998 and 1999), and Column 8 is the corrected number of detections after correcting the net number for the duty cycle.

discoveries remains evident.

The jump in discoveries is not restricted to the faintest comets. The number of comets year^{-1} brighter than magnitude 6 increased from an average of 18.1±3.1 from 1997–2002 to 32.6±4.9 from 2003–2005, in increase of 80%. Comets 6^{th} magnitude and brighter are typically observed for at least 24 hours and should have been easily discovered throughout the mission. The changing discovery circumstances should have little to no effect on the rate of discovery of these bright comets.

Sekanina and Chodas (2007) noted the increase in raw discoveries and suggested

it may be "an early warning of another cluster of bright sungrazers approaching the Sun in coming decades." Our much more rigorous analysis of the detection statistics supports this finding. Coupled with the appearance in mid-2002 of comets with a rather intermediate lightcurve shape and peak distance (Section 3.4.1), their suggestion of "a nonuniform distribution of mini-comets along the filament" is plausible.

3.6 Discussion

3.6.1 Size Distribution

The sizes of coronagraphically observed Kreutz comets have consistently been estimated to be a few meters to tens of meters. MacQueen and St. Cyr (1991) estimated the brightest SMM comets to be ∼16 meters in radius prior to the onset of sublimation. Ly-α fluxes recorded by UVCS have yielded estimates of the diameters of three comets at distances from 3–7 $R_\odot$: 6.7 meters for C/1996 Y1 at 6.8 $R_\odot$ (Raymond *et al.* 1998), 5.0–6.7 meters for C/2000 C6 at 6.36–5.71 $R_\odot$ (Uzzo *et al.* 2001), and 7.8 meters (with an unresolved 5.4 meter companion) for C/2001 C2 at 4.98 $R_\odot$ (Bemporad *et al.* 2005). Sekanina (2003) estimated initial diameters ranging from 17–200 meters by modeling 27 lightcurves with varying effective latent energies of erosion (analogous to sublimation heat). Iseli *et al.* (2002) used the fact that no Kreutz comets have been seen by SOHO after perihelion to derive an upper limit for the radius of 63 meters if it was composed entirely of water ice and destroyed by sublimation alone.

Despite a number of simplifying assumptions, our estimate of the size distribution, ranging from 2–50 meters in radius (Section 3.4.4), is consistent with these values. Before proceeding with an estimate of the total mass of the system, we consider the validity of these assumptions. First, we assumed that the brightness is

due entirely to the reflection of sunlight off dust grains in the coma. In actuality, the brightness is a combination of scattering and emission. The scattering component consists of scattering from the coma and the nucleus. A bare nucleus (i.e. no coma) 50 meters in radius should have an apparent magnitude of ∼18 at 12 $R_\odot$. Since the faintest comets are approximately magnitude 9, we can safely ignore scattering off the nucleus in comparison with scattering off the coma.

The emission consists of the bands typically observed in comets at larger heliocentric distances (e.g. C_2, NH_2, etc...), ions not seen at larger distances, and elements seen in the spectra of sungrazers ([O I], Na I, K I, Ca II, Cr I, Mn I, Fe I, Ni I, Cu I, and CN were reported in C/1965 S1 Ikeya-Seki by Preston (1967) and Slaughter (1969)). Of the emission lines seen in Ikeya-Seki, only [O I] (6300 Å) and Na I (5890 and 5896 Å) fall within the orange filter bandpass (5400–6400 Å). Since sodium is much brighter than the forbidden oxygen line, it is the most likely source for the excess brightness in the orange filter relative to the clear filter (Section 3.4.3).

To test this, we estimated the increase in the sodium line relative to the solar continuum required to cause the orange filter to increase by ∼1 magnitude relative to the clear filter. We calculated the flux due to the scattering of the solar continuum by dust in each detector/filter combination (C3 clear, C3 orange, C2 orange) by multiplying the solar flux at each wavelength[9] by the transmission of the filter at that wavelength[10] and the quantum efficiency of the detector at that wavelength[11]. We then simulated the flux of sodium emission by adding a rectangle of width 10 Å centered at 5895 Å (to encompass both sodium D-lines) and of a variable height.

[9]We used the 1985 Wehrli Standard Extraterrestrial Solar Irradiance Spectrum from http://rredc.nrel.gov/solar/spectra/am0/wehrli1985.new.html.

[10]http://lasco-www.nrl.navy.mil/index.php?p=content/filter/filter

[11]http://lasco-www.nrl.navy.mil/content/tech/QE/c3_qe.txt

The apparent magnitude was ∼1 magnitude brighter in the orange filters relative to the clear filter for a height of sodium emission ∼600 times stronger than the solar continuum at 5895 Å. The integrated flux due to the sodium emission was ∼1.9 times more than the integrated flux due to the solar continuum in the clear filter and 6.4 times more in the orange filter.

To convert this to an estimated mass of sodium, we then estimated that the contribution from the sodium emission was $\frac{1.9}{2.9}$ of the total flux received by SOHO from the comet (in the C3 clear filter). Next we divided the total flux of the comet by the g-factor for sodium[12], and converted this to a mass of sodium. For a 5^{th} magnitude comet this yields a mass of ∼1000 kg. The photoionization lifetime of sodium at 12 $R_\odot$ is ∼9 minutes. Therefore a production rate of ∼2 kg s^{-1} is required to sustain the brightness. In this manner we integrated the sodium production for the lightcurve of C/2005 S1, which was observed in C3 from 31.2–7.6 $R_\odot$ over 33 hours and reached a peak magnitude of ∼4.5 at 14 $R_\odot$. During this time it produced 1.7×10^8 g of sodium. This is large compared to the estimated mass of C/2005 S1 (4×10^9 g using the estimated size and a density of 0.35 g cm^{-3}), however if the nucleus is a factor of two larger, the sodium would represent less than 1% of the mass. Given the assumptions in our size estimate, this begins to be plausible.

It is likely that emission from other atoms or molecules besides sodium contributes to the overall brightness, however the ∼1 magnitude orange – clear difference indicates that emission in the orange filter bandpass is by far the dominant emission in the visible range. It is also possible that as yet unidentified refractory

[12]The g-factor is the emission rate per molecule. We estimated it to be 5.5×10^{-11} erg s^{-1} $atom^{-1}$ at 1 AU from Figure 2 in Watanabe *et al.* (2003) and scaled it by r^{-2} to 12 $R_\odot$. Note that the radial velocity of a typical Kreutz comet at this distance is ∼230 km s^{-1}, which is well beyond the dip in the g-factor due to the Swings effect.

silicates are responsible for emission in the orange filter bandpass. While we cannot rule out this possibility, the observation of strong sodium emission at small heliocentric distances in Ikeya-Seki and C/2006 P1 McNaught (Snodgrass *et al.* (2007) and Voulgaris private communication 2007) indicate that sodium emission should be extremely bright at the distances observed by SOHO, and the estimated mass of sodium to produce this is plausible. Therefore the contributions from other emission sources are likely small compared with sodium emission.

An alternative explanation of the orange – clear magnitude difference is improper photometric normalization. The photometric zero points were calculated using thousands of images of dozens of F, G, and K stars repeated annually over the life of the mission (Llebaria *et al.* (2006); Thernisien *et al.* (2006), Thernisien private communication 2003). We consider these to be reliably well determined and conclude that the orange – clear magnitude difference is a real effect diagnostic of differences in the flux from that of the solar continuum.

If we assume the comet is made entirely of water ice and scale the water production rate from 10^{18} molecules s^{-1} cm^{-2} at 1 AU by a factor of r^{-2}, a comet which is $\sim$50 meters in radius when it enters the SOHO field of view will decrease in radius by 16 cm $hour^{-1}$ at 30 $R_\odot$, 36 cm $hour^{-1}$ at 20 $R_\odot$, and 143 cm $hour^{-1}$ at 10 $R_\odot$ (assuming a density of 0.35 g cm^{-3}). If we further assume the comet has a rotation period of 1 day, a thermal inertia of 50 W K^{-1} m^{-2} $s^{0.5}$ (the upper limit for the thermal inertia of 9P/Tempel 1 (Groussin *et al.* 2007)), and heat capacity C_p=2.05 J g^{-1} K^{-1}, its skin depth would be $\sim$1 cm. Even if the heat capacity is lower and the rotation period longer, the skin depth would not be more than 3–5 cm for reasonable values. Thus, the rate of erosion in the SOHO field of view is much larger than the skin depth. As a result, no volatile depleted mantle can form and the erosion exposes fresh ices which were buried below the surface until very

recently.

As an analog, we use the ejecta released by the Deep Impact experiment which excavated nearly pristine ice below the surface of 9P/Tempel 1, resulting in a size distribution that was smaller than the ambient pre-impact coma and rich in water ice (e.g. Fernández *et al.* (2007); Knight *et al.* (2007); Schulz *et al.* (2006); Sunshine *et al.* (2007)). Lisse *et al.* (2006) found that the Deep Impact ejecta were dominated by 0.1–10 μm particles, with a peak in the size distribution at 1 μm. Our size estimate assumed that the coma was optically thin and consisted of uniform spheres of radius 0.5 μm and albedo 0.04. While acknowledging that modeling the coma with a distribution of particles of size 0.1–10 μm might improve the size estimate, the uncertainties inherent in this estimate make an overly specific size distribution superfluous. Equivalent nuclear radii constructed entirely from spheres of radius 0.1 μm or 10 μm differ from the 0.5 μm equivalent nuclear radius by a factor $\sim$2–3 (smaller particles have a larger surface area to volume and a smaller equivalent nucleus and vice versa).

Our final assumption is that the comet has disintegrated completely into dust at the distance of peak brightness (10–14 $R_\odot$). This is very likely not the case as UVCS observations indicate the presence of a nucleus in all three comets observed by it at distances inside 7 $R_\odot$, although the nuclei are believed to have fragmented or sublimated completely by $\sim$3 $R_\odot$ (Bemporad *et al.* 2005; Raymond *et al.* 1998; Uzzo *et al.* 2001). If the nucleus has not been completely destroyed at the distance of peak brightness, then the total size of the nucleus plus coma is larger than that inferred from the brightness. However, the low albedo of comets is believed to be due to organics, but at the heliocentric distances observed by SOHO much of the organics are likely gone. Thus the albedo of the dust may be higher than the 0.04 assumed and the comet may be smaller than that inferred from our estimates.

Based on the uncertainties in all of the assumptions, we estimate that the nuclear sizes are likely good to within a factor of two. Thus the actual size range may be 1–100 meters in radius.

3.6.2 Total Mass

To estimate the total mass of the Kreutz system, we need to correct the size distribution for the comets which were unobserved due to data gaps. From 1996–2005, the collective duty cycle for C3 with the clear filter was 0.868 (Table 3.3). We do not need to correct for the seasonal effects because our size distribution was calculated using only the comets which were large enough to have been observed regardless of the geometry. Over 10 years, we observed 219 comets bigger than 5 meters. Assuming a continuous distribution of comets throughout the orbit, this represent 0.868 of the total observable. For an 800 year orbit, this yields ∼20,000 comets larger than 5 meters in radius in the orbit. The cumulative size distribution is

$$N(> R) \approx 869 \times R^{-2.2} \tag{3.1}$$

where N(>R) is the number of comets year^{-1} larger than radius R (in meters) which reach perihelion. This is plotted in Figure 3.11. Assuming the density is 0.35 g cm^{-3}, this converts to a cumulative mass distribution of

$$N(> m) \approx 2.1 \times 10^{7} m^{-0.73} \tag{3.2}$$

where N(>m) is the number of comets year^{-1} larger than mass m (in grams) which reach perihelion. Note that Equations 3.1 and 3.2 predict the true number of comets in the system, and are slightly larger than the actual number observed by SOHO due to gaps in the data.

Extending Equation 3.1 to radii larger than 3.6 meters (which correspond to comets ∼8^{th} magnitude or about the nominal limiting magnitude of C3), we should

have observed 267 comets between 3.6–5 meters in radius, but only saw 162. Even after correcting for the duty cycle, ∼30% of the expected comets in this range were unobserved. This is largely due to the viewing geometry, but is also due to the limited amount of time over which comets attain their peak brightness. A comet is required to be in at least 5 images to be confirmed by the SOHO team[13]. An average of 2–3 C3 clear images are taken per hour. Thus the comet must be above the minimum threshold for ∼2 hours to be discoverable. Near the lightcurve peak, the comet will travel ∼2 $R_\odot$ in 2 hours. So, for comets near the limiting magnitude, if the brightness peaks steeply the comet will not be detected, but if it has a broad peak it may be detected. Many of the faintest detections appear this way–they have no discernible slope, just 5 or so points barely above the limiting magnitude.

There are also fewer comets larger than 30 meters than expected. We would expect five such comets in 10 years and two were seen. While this may be real and an indication that there is a break in the power law around 30 meters, the statistics are very low. Until the baseline of observations is increased, we cannot conclude that there are signicantly fewer comets than expected larger than 30 meters.

Sekanina (2002b) compiled observations of the ground observed Kreutz comets and calculated their lightcurve parameters. Only C/1965 S1 Ikeya-Seki was observed at r<50 $R_\odot$ (except for a single observation of C/1843 D1), however, we can extrapolate each comet's brightness using the lightcurve parameters. Setting r=12 $R_\odot$ and Δ=1 AU for each ground observed comet, we can compare the brightness at the distance of lightcurve peak for the SOHO observed sungrazers[14]. If we then make

[13]Occasionally comets with fewer than 5 images have been confirmed. All of these clearly show cometary activity and were only in fewer than 5 images because the rate of C2 images was low.

[14]The magnitudes for the 19^{th} century comets are generally for the nuclear condensation, while for the 20^{th} century comets, integrated magnitudes are given. The SOHO photometry uses a fixed aperture which more closely resembles the nuclear condensation. The integrated magnitudes imply

a crude assumption that the brightness is proportional to the square of the radius, we can derive an estimate for the nuclear size. Setting the size of an 8^{th} magnitude comet at 4 meters in radius (for Δ=1 AU, r=12 $R_{\odot}$), we estimate the nuclear radii as follows: C/1843 D1≈8 km, C/1880 C1≈1.1 km, C/1882 R1≈30 km, C/1945 X1≈0.6 km, C/1963 R1≈14 km, C/1965 S1≈4.3 km, and C/1970 K1≈1.1 km. No nuclear condensation was seen for C/1887 B1, and Sekanina (2002b) believed it to be much smaller, calling it a "transition object" between the bright ground observed ones and the faint SOHO observed ones. Sekanina (2003) estimated the radius needed to survive until perihelion to be 250–350 meters, and the radius needed to survive until a subsequent perihelion passage to be ∼500 meters. Since no nuclear condensation was seen for C/1887 B1, it is likely that its nucleus disappeared near perihelion so we assume it was ∼350 meters in radius.

Assuming the distribution of comets seen by SOHO is constant throughout an 800 year orbit and setting N(>R)=1, we would expect the largest comet to have a radius of ∼500 meters. Thus, C/1887 R1 was one of the largest fragments in the distribution, and C/1945 X1 is consistent with the distribution if it is the largest comet in the orbit (we expect ∼0.3 comets 800 meters and larger). The size distribution cannot explain the six comets larger than 1.1 km (we would expect ∼0.1 such comets)[15]. Even if our rough estimates of the nuclear sizes are an order of magnitude too large, we are still left with 3–4 comets larger than than the expected maximum size. Thus we conclude that there is a break in the size distribution which occurs by 500–1000 meters in radius (and possibly as small as 30 meters) and that

brighter comets than the nuclear condensation, but for this order of magnitude calculation it is sufficient to assume they are equivalent.

[15]If the near sun comets observed since the 16^{th} century and considered as possible Kreutz comets by Sekanina and Chodas (2007) are included, 23 additional massive comets are in the group and the size distribution fails miserably for large comets.

the fragmentation of the Kreutz progenitor was relatively recent. With enough time, repeated splitting should cause the entire population to be described by a continuous power law. Alternatively, the distribution may not be uniform around the orbit, and the distribution seen by SOHO may not be representative of the distribution at other times.

Integrating over the size range 5–500 meters we find a total mass of the system of $\sim 4 \times 10^{14}$g for a bulk density of 0.35 g cm^{-3} (the bulk density of 9P/Tempel 1 determined by the Deep Impact mission (A'Hearn and Combi 2007)). We note that Sekanina (2003) found a more shallow size distribution and estimated the total mass to be $\sim 1 \times 10^{16}$–8×10^{17} g using only the photometry of the 26 brightest comets published by Biesecker *et al.* (2002). A total mass of $\sim 4 \times 10^{14}$ g is equivalent to a sphere of radius ∼650 m (for a density 0.35 g cm^{-3}). The total mass is dependent on the upper cutoff of the size distribution. If the maximum size is ∼50 meters (the largest comet observed so far by SOHO), the total mass in the system is only $\sim 5 \times 10^{13}$ g, corresponding to a sphere of radius ∼325 meters. Sekanina (2002b) concluded that C/1882 R1 was the largest Kreutz comet, estimating its effective mass at $\sim 10^{19}$ g. By extension from the sizes estimated from the lightcurves above, the masses of the six other most massive fragments range from $\sim 10^{15}$–10^{18} g. Therefore, the inferred total mass of the population of coronagraphically observed fragments is much smaller than the mass of any of the bright ground observed comets. This is further evidence that the splitting of the group was recent.

The slope of the cumulative size distribution, $N(>R) \propto R^{-\alpha}$, of the Kreutz comets ($\alpha$=2.2) is similar to the slope of the Jupiter family comets which is 1.73–1.91 (Lamy *et al.* 2004; Meech *et al.* 2004; Weissman and Lowry 2003) or 2.65–2.7 (Fernández *et al.* 1999; Tancredi *et al.* 2006). After accounting for the effects of fragmentation and sublimation, Lowry *et al.* (2008) estimate that the primordial slope was 1.83–

2.01. The two populations were produced by different mechanisms (splitting for the Kreutz comets versus collisions for the Jupiter family comets), but it is nonetheless interesting that the slopes are similar.

3.6.3 Rate of Brightening

Of the ground-observed Kreutz comets, only C/1965 S1 Ikeya-Seki was well observed prior to perihelion, while five were observed after perihelion: C/1843 D1, C/1882 R1, C/1963 R1, C/1965 S1, and C/1970 K1 (Sekanina 2002b). The fading rate for the ground observed Kreutz comets was between $\propto r^{-3.2}$ and $\propto r^{-4.5}$, which is similar to the brightening rate we derived from 16–24 $R_\odot$ for the comets observed by SOHO ($\propto r^{-3.8\pm0.7}$). Despite being observed at much larger heliocentric distances, the brightness behavior of the largest comets (all of which survived perihelion) is remarkably consistent with that of the smallest. From this we conclude that the brightening seen in the SOHO field of view from 16–24 $R_\odot$ is due to the typical processes which cause the Kreutz comets to brighten rather than processes which are unique to the smallest comets, such as catastrophic disruption.

The SOHO-observed Kreutz comets brighten at $\propto r^{-7.3\pm2.0}$ beyond $\sim$24 $R_\odot$. Only Ikeya-Seki was observed at distances within the SOHO field of view, although a single observation of the nucleus of C/1843 D1 in daylight was reported. Ikeya-Seki brightened near $\propto r^{-4}$ from 1.02–0.03 AU. Unfortunately, it was not observed from 50–20 $R_\odot$ prior to perihelion. After perihelion there were nine observations from 9–50 $R_\odot$, including three between 20–40 $R_\odot$. The lightcurve fluctuates about the $\propto r^{-4}$ line, but there is no obvious section which fades significantly steeper than this. If Ikeya-Seki experienced a significant period of brightening near $\sim r^{-7}$, it only occurred prior to perihelion. Thus we cannot determine when the $\propto r^{-7.3}$ brightening begins, but conclude it does not extend beyond 50 $R_\odot$.

Sekanina (2000b) examined the tail morphology of 9 comets observed from 1996–1998, finding that the production of dust peaked at 20–30 $R_\odot$ and had $\beta \leq 0.6$ (β is the ratio of the force due to solar radiation pressure and the force due to the Sun's gravity). The distances of peak production correspond to the approximate locations of the changes in slope from $\propto r^{-7.3}$ to $\propto r^{-3.8}$. We compared the lightcurves of the 9 comets in the Sekanina (2000b) study with their inferred distance of peak dust production. While 8 of the 9 comets in the sample exhibited a change of slope between 20–30 $R_\odot$, the distances did not correlate well. Four transitioned at a larger distance than the inferred peak production distance, three approximately agreed, one transitioned at a smaller distance, and one showed no change in slope (this comet was anomalous in the sample; Sekanina (2000b) inferred its dust production peaked at 230 $R_\odot$).

66 comets in our sample were observed well enough to calculate a slope beyond 24 $R_\odot$. The vast majority of these had well defined tails as is common for bright comets observed by SOHO. The exceptions were all faint, making it difficult to determine the presence of tails, but in general these comets also had less obvious changes in slope at 20–30 $R_\odot$. While a more thorough investigation of the tail parameters is beyond the scope of the current work, it is likely that the tail formation is a result of the same process which causes the comet to brighten steeply, and warrants further study.

We suggest that the steep rate of brightening (and apparently the accompanying tail formation event) is due to the onset of activity of a previously inactive species (presumably a refractory organic) which results in an explosive outburst. In this scenario, the increasing insolation causes a buildup of pressure below the surface. At some point (the exact distance varying from comet to comet) the pressure exceeds the strength of the regolith and an outburst blows off much of the outer layer. The

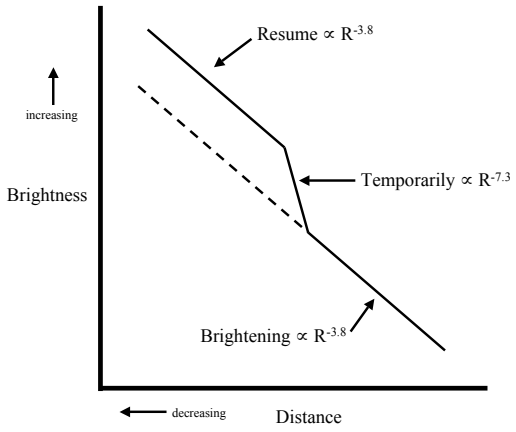

Figure 3.19: Illustration of the Kreutz brightening rate.

destruction of the regolith would deposit a large amount of small silicate dust grains into the coma, and the surface area of the coma would continue to increase for some time while the ejected dust fragmented further. As the process slows, the comet returns to its $\propto r^{-3.8}$ brightening, offset brighter if the active surface area has increased as a result of the outburst. Alternatively, the onset of activity may trigger the entire nucleus to become active rather than just a few regions. In either case, the steeper rate of brightening ($\propto r^{-7.3}$) can be seen as a δ-function superposed on top of the $\propto r^{-3.8}$ rate. The increased surface area will result in the $\propto r^{-3.8}$ rate resuming at an elevated level after the initial burst fades. This is illustrated in Figure 3.19.

To test the rate of brightening beyond the SOHO field of view, we surveyed regions of the sky statistically likely to contain Kreutz comets approximately 3–6 months prior to perihelion using the MOSAIC camera on the KPNO 4-m telescope. We searched the images by aligning three consecutive images and blinking them to look for moving objects. Later, as comets were discovered by SOHO which should have been in the field of view, we searched the images again to look for comets

near the expected positions. While as many as 12 comets may have been in the field of view, no comets were found, suggesting that they either brightened at a rate steeper than $\propto r^{-3.5}$ or that the orbital element uncertainties are larger than we had estimated.

3.6.4 Qualitative Explanation of the Lightcurve

Previous interpretations of the lightcurves of the Kreutz group have focused on the apparent bimodality of the peak in brightness noted by Biesecker *et al.* (2002). Sekanina (2003) has explained the differences as corresponding to comets having differing latent energies of erosion and in some cases additional fragments too small or too recently separated to be individually resolved. Kimura *et al.* (2002) attribute the two peaks as corresponding to fluffy aggregates of crystalline olivine (the peak at 11.2 $R_\odot$) and fluffy aggregates of amorphous olivine (the peak at 12.3 $R_\odot$). They further argue that the observed lightcurves are a superposition of two lightcurves: one due to olivine which peaks from 10–13 $R_\odot$ and one due to pyroxene which peaks inside 7 $R_\odot$, with the relative heights of the peaks at $\sim$12 $R_\odot$ and inside of 7 $R_\odot$ indicative of the abundance ratio of olivine to pyroxene.

Our photometric analysis (Section 3.4.1) shows that the distance of peak brightness is not bimodal, but is more nearly a gaussian centered at 12 $R_\odot$ and ranging from 10–14 $R_\odot$. Without the need to explain two distinct lightcurves, this can now be viewed as reflecting a spectrum of comets with similar compositions which behave slightly differently due to their unique fragmentation history, topography, rotation, etc... Rather than being confined to two narrow ranges, the peak distances actually vary over a fairly large region, representing a change of $\sim$30% in heliocentric distance between the largest and smallest peak distances.

In Section 3.4.1 we demonstrated that rather than the two "universal curves"

which were discriminated by distance of the peak, the lightcurves have a continuum of shapes. To illustrate this, we arranged them into three groups (A–C) based on their shapes of brightening and fading. Group A had the most gradual slope of brightening and fading and the largest peak heliocentric distance. Group B had intermediate slopes of brightening and fading and peak distance. Group C had the steepest slope of brightening and fading and the smallest peak distance. These features can be explained by a continuum of compositions between amorphous and crystalline olivines. Kimura *et al.* (2002) showed that amorphous olivines sublimate more slowly and at larger distances than crystalline olivines. Thus the comets in group A have higher ratios of amorphous olivines to crystalline olivines than the comets in group B, which in turn have higher ratios than group C.

There does not appear to be a correlation between size of the nucleus and the distance of peak brightness. We would expect a size dependence since bigger comets take longer to erode and therefore survive to a smaller heliocentric distance. However, as shown in Figure 3.20, if the erosion is dominated by water production, nuclei of nearly all sizes will survive until heliocentric distances smaller than the lightcurve peak at 10–14 $R_{\odot}$. The smallest nuclei will erode prior to the peak distances, but these do not produce enough dust to reach the threshold for detection and therefore do not appear in our database. Since the distance of the lightcurve turnover does not correlate with the size estimate, the destruction of the nucleus by erosion is not the primary cause of the lightcurve turnover.

As explored by previous authors (e.g. Biesecker *et al.* (2002); Kimura *et al.* (2002)), the lightcurve shape is an amalgamation of numerous processes which depend on the heliocentric distance. These include but are not limited to the production of water and other volatiles from the nucleus, emission of sodium and other heavy elements, the sublimation of olivine, pyroxene, and other silicates from the

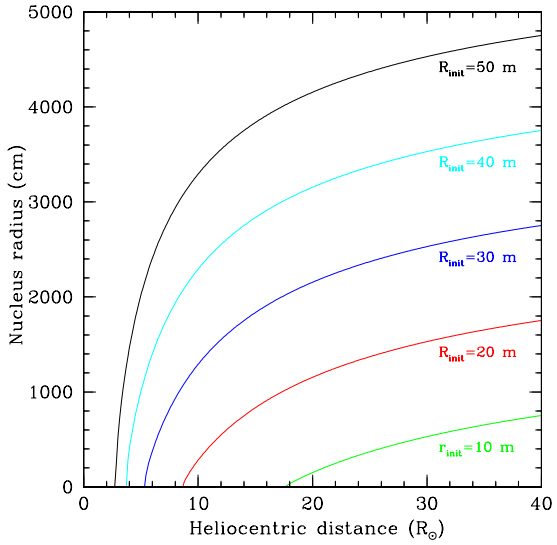

Figure 3.20: Decrease in size of a Kreutz nucleus due to water production. The initial sizes listed for each curve were the sizes 4 days prior to perihelion at a distance of ∼58 $R_\odot$. The comet follows the orbit of C/1963 R1 which is very close to the "subgroup I" orbit of most SOHO observed comets. The nucleus is assumed to be composed entirely of water, and the water production rate is scaled from 10^{18} molecules s^{-1} cm^{-2} at 1 AU by a factor r^{-2}.

coma and the nucleus, the photoionization lifetimes of particles in the coma, fragmentation, and tidal forces on the nucleus. Undoubtedly the unique evolutionary history of each comet contributes to its distinct shape, but we can explain the general shape as follows.

At large heliocentric distances, the comets behave like dynamically young comets, rich in ices and with a small dust size distribution due to frequent fragmentation exposing new surfaces, e.g. Sekanina (2000a, 2002a). Beyond 50 $R_\odot$ they likely brighten at a rate near $\propto r^{-4}$ as C/1965 S1 Ikeya-Seki did (Sekanina 2002b). Although it is unclear exactly where, at some point prior to entering the SOHO field of view most begin to brighten steeply, near $\propto r^{-7.3}$. This continues until ∼24 $R_\odot$ when the rate rapidly transitions to $\propto r^{-3.8}$.

Around 16 $R_\odot$ the lightcurve begins to turn over, reaching a peak between 10–13 $R_\odot$. The turnover in the lightcurve is likely due to the rate of sublimation of

dust grains in the coma exceeding the production rate of dust from the nucleus. Kimura *et al.* (2002) showed that sublimation of fluffy aggregates of amorphous and crystalline olivine occurs at 10–13 $R_\odot$. This will rapidly deplete the reflecting area of the coma. While the production rate (per cm^2) is increasing $\propto r^{-2}$, at some point the surface area of the nucleus becomes too small and the total production drops. The combination of a declining production rate and an increasing sublimation rate cause the lightcurve to turn over and fade rapidly. As shown in Figure 3.20, a comet made entirely of water ice with initial radius from 20–50 meters prior to entering the SOHO field of view will disappear entirely between 3–9 $R_\odot$.

Inside of $\sim$7 $R_\odot$, the comet will erode very rapidly. UVCS observations of three comets suggest that the nuclei disappear entirely by $\sim$3 $R_\odot$ (Bemporad *et al.* 2005; Raymond *et al.* 1998; Uzzo *et al.* 2001). Kimura *et al.* (2002) predict that the sublimation of crystalline and amorphous pyroxenes would cause a second peak at 4–6 $R_\odot$. The lightcurve data in this region are sparse, but are in general agreement with this as the lightcurves tend to level off or brighten again inside $\sim$7 $R_\odot$. See the lightcurves in Figures B.1–B.9 for representative behavior. An alternative explanation for this phenomenon is that fragments too small to be individually resolved and which have substantially higher erosion energies reach a peak in brightness in this region (Sekanina 2003). Since the range of peak distances indicates that the comets are relatively homogeneous, we find it unlikely that they would fragment into pieces with such disparate energies of erosion. Therefore we favor the final disruption of the nucleus and sublimation of pyroxene as the mechanism to cause this final brightening.

3.6.5 Lightcurve Behavior for the Comets Beyond the Sizes Seen By SOHO to Date

The scenario described above should hold true for comets in the size distribution observed by SOHO. Comets smaller than a few meters would be destroyed by erosion at larger distances than 10–14 $R_\odot$. These comets would never achieve the brightness necessary to be observed by SOHO, however if the size distribution holds, they should be numerous. While the nucleus of such a comet would have disrupted, the dust should continue along the orbit (subject to the effects of radiation pressure) and would exhibit the same series of brightness enhancements caused by the increasing temperature. Future coronagraphic missions with much greater sensitivity might observe these as headless comets similar to but much fainter than C/1887 B1 (Sekanina (2002b) and references therein).

Iseli *et al.* (2002) estimated that comets larger than 63 meters in radius would survive long enough past perihelion to be observed for some time by SOHO if they were composed entirely of water ice. Using an argument based on the energy of erosion, (Sekanina 2003) estimated that such a comet would need to be 250–350 meters in radius. The largest comet in our sample was below either of these estimates, and was not seen after perihelion. The lightcurve of a comet which survives past perihelion should brighten more steeply when it reaches distances where its refractory grains begin to sublime. Based on the interpretation of the features of the SOHO observed comet lightcurves, we would expect the brightening to become more steep near 10–14 $R_\odot$ and 4–6 $R_\odot$ due to the sublimation of olivine and pyroxene, respectively, however we would not expect it to peak in brightness until perihelion. The lightcurve would be roughly symmetric about perihelion (e.g. Hale-Bopp (Biver *et al.* 2002)), however, it would disappear rapidly once the nucleus eroded away. It

is possible that C/1887 B1 was such an object, being large enough to survive perihelion, but having no nucleus (or one so small that it is not outgassing appreciably), therefore appearing as a headless tail when first observed 0.46 AU after perihelion.

Sekanina (2003) calculated the minimum size for a sungrazer to survive perihelion and return on its next apparition is ∼0.5 km in radius. At least six comets this large have been seen (C/1843 D1, C/1880 C1, C/1882 R1, C/1963 R1, C/1965 S1, C/1970 K1)), although the only one observed both before and after perihelion is C/1965 S1 Ikeya-Seki, whose lightcurve is plotted in Figure 1 of Sekanina (2002b). Its pre- and post-perihelion lightcurves are nearly identical in slope. Interestingly, the point at ∼12 $R_\odot$ prior to perihelion is ∼0.5 magnitude brighter than the next point interior to it at ∼11 $R_\odot$, and the slope inside of ∼13 $R_\odot$ is steeper than the slope for the whole range of observations (0.03–1.63 AU). The bright point at 12 $R_\odot$ is consistent with the rapid sublimation of the olivine in the coma and the continuing steeper slope interior to that is consistent with the sublimation of olivine from newly released dust. There is a corresponding bright point at ∼12 $R_\odot$ in the post-perihelion lightcurve which is difficult to explain since we would not expect an increase in sublimation as the distance was increasing. Furthermore, the only point prior to it is slightly fainter than predicted from the average slope. While the lightcurves of the comets observed to survive perihelion demonstrate that the activity of Kreutz comets is nearly symmetric about perihelion, they were not observed well enough to conclusively support or refute the particulars of the composition inferred from the coronagraphic lightcurves.

Chapter 4

The Marsden and Kracht Groups

4.1 Overview

After the Kreutz group, the Marsden and Kracht groups are the next most studied groups of sungrazing comets. Average elements for each group are listed in Table 1.1. Unlike the Kreutz comets observed by SOHO, numerous Kracht and Marsden comets are observed to survive perihelion, and it is believed that a number have been seen on two apparitions. Their survival is likely tied to their perihelion distances (q≈8–12 $R_\odot$) which are nearly an order of magnitude larger than those of the Kreutz comets (q≈1–2 $R_\odot$). While the average orbital elements of these two groups differ by $\Delta i \sim 13^\circ$, $\Delta\omega \sim 35^\circ$, and $\Delta\Omega \sim 35^\circ$, dynamical integrations (Ohtsuka *et al.* 2003; Sekanina and Chodas 2005) indicate that these groups, along with 96P/Machholz 1, the Daytime Arietids, and the Southern δ Aquarids are related to each other as part of the larger Machholz Complex. The various components of the Machholz Complex appear to have split from their progenitor comet before 950 CE, and subsequent close approaches to Jupiter have caused the orbits to diverge. Well before the Marsden and Kracht groups of comets were discovered it had been noted that 96P/Machholz 1 was a future sungrazer, oscillating between a high inclination orbit with perihelion

distance near 1 AU to a low inclination sungrazing (or nearly sungrazing) orbit over roughly a 4000 year cycle (Bailey *et al.* 1992; Green *et al.* 1990; Rickman and Froeschle 1988). While the Marsden and Kracht groups currently have different orbits, we discuss them together in this section due to their probable common origin.

Like all sungrazing comets observed by SOHO, the Marsden and Kracht groups are only observed over a short orbital arc. The best observed are seen for less than 2 days, and the most poorly observed are seen for only a few hours. As a result, only parabolic orbits can be determined from a single apparition. When apparent linkages can be made from multiple apparitions a period and eccentricity can be calculated. The uncertainty in the orbital elements is large and since none of the Kracht or Marsden comets have been seen three times the apparent linkages are still tenuous.

As of May 2008, 32 Marsden comets and 31 Kracht comets have been discovered. However, these totals include all apparitions, and a number of these have likely been observed more than once. Accounting for the apparent linkages, at least 24 distinct Marsden comets and 23 distinct Kracht comets have been observed. The published linkages are listed in Table 4.1 and the orbital elements of all Marsden and Kracht comets are given in Tables A.3 and A.4, respectively. In this chapter we will revise some of these linkages based on the photometry and dynamical integrations, and will make predictions for future returns. To date, the Marsden and Kracht comets have only been observed by the C2 and C3 coronagraphs on SOHO, but they should be observable with STEREO and possibly from the ground as well, which will be discussed in Chapter 5.

First Apparition	Second Apparition	Period (yr)	Group	MPEC
1996 X3, X4, X5	2002 S4, S5, S7, or S11	5.78–5.81	Kracht	2006-C49
1999 J6	2004 V9	5.50	Marsden	2004-X73
1999 M3	2004 L10	4.95	Kracht	2004-X73
1999 N5	2005 E4	5.67	Marsden	2005-E87
1999 N5	2005 G2	5.76	Marsden	2005-H24
1999 N6	2004 J4 or J18	4.81–4.84	Kracht	2004-X73
1999 U2	2005 W5	6.10	Marsden	2005-Y27
2000 C3, C4, or C7	2005 W1	5.78	Marsden	2005-W7
2000 O3	2005 W4	5.32	Kracht	2005-X14
2002 Q8	2008 E4	5.52	Kracht	2008-F32
2002 R1	2008 A3	5.37	Marsden	2008-B61
2002 R4	2007 Y4	5.30	Marsden	2008-B49
2002 S11	2008 G6	5.53	Kracht	2008-L29

Table 4.1: Published linkages of Marsden and Kracht comets on two apparitions. The last column, MPEC, is the Minor Planet Electronic Circular on which the linkage is reported. In the interest of space, these are not included in the references. We will revise some of these linkages based on the photometry and dynamical integrations, and the revised linkages with predictions for future returns will be given in Table 4.2. Specifics of each of these potential linkages are given in Appendix C.

4.2 Clustering and Linkages

The arrivals of Marsden and Kracht comets are highly non-random. 21 of the 31 Kracht comets have arrived within 3 days of another Kracht comet, and all but five have arrived within 12 days of another Kracht comet. Similarly, 14 of the 32 Marsden comets have arrived within 3 days of another Marsden comet, and 22 of 32 arrived within 12 days of another Marsden comet. Furthermore, comets which arrive close together in time generally have orbits which are more closely related to each other than to the rest of the group. The temporal spacing and similarity of orbits suggest that many of the comets have split recently, most likely since their last perihelion passage.

Based on the similarities of their orbits, it has been suggested that seven Kracht comets and eight Marsden comets have been observed on two apparitions (see Table 4.1 and references therein). These linkages have a range of periods from 4.81–5.81 years for the Kracht comets and 5.30–6.10 years for the Marsden comets. Most Kracht and Marsden comets can be accounted for on previous perihelion passages by direct linkages or their membership in temporal clusters which suggest they were produced via fragmentation since the previous perihelion passage. Ten Kracht and five Marsden comets were apparently unobserved on their previous perihelion passage. Four Kracht and 12 Marsden comets were unobserved on their subsequent perihelion passage. Nearly all of these missed comets can be explained by data gaps or being too faint to be observed. We discuss each Marsden and Kracht comet individually in Appendix C.

We plot the orbital elements of the Kracht and Marsden comets in Figures 4.1 and 4.2, respectively. The shaded ellipses around each point are an estimate of the uncertainty in the elements based on the length of time each was observed[1]. The comets are color coded based on temporal clustering and likely linkages (the same colors and symbols are used for the same comets in both plots for each group). For example, the red triangles in the top left of the Kracht ω–Ω plot and the top right of the q–i plot are C/2000 O3 and C/2005 W4. Note that the scales of the corresponding plots are similar except that the Marsden inclination covers approximately twice as large a range as the Kracht. Two Marsden comets (C/2003 Q1 and C/2003 Q6) were omitted as they deviate significantly from the rest of the Marsden group

[1]The length of time the comet was observed may be longer than the length of time over which the orbit was computed. There is a known discrepancy between positions calculated from SOHO's C2 and C3 telescopes, and when available, C2 images are strongly preferred due to their smaller pixel size.

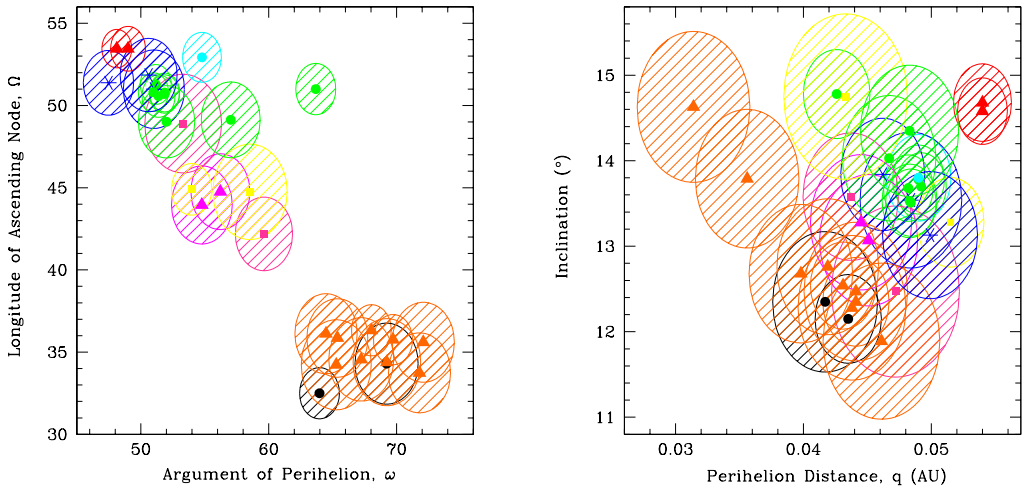

Figure 4.1: Orbital elements for the Kracht comets. The left panel is argument of perihelion (ω) versus longitude of the ascending node (Ω), the right panel is perihelion distance (q) versus inclination (i). The points are color coded to correspond with the temporal clusters and linked pairs as discussed in the text. The shaded regions are estimated error ellipses based on the length of time each comet was observed.

and their exclusion allows better resolution of the rest of the family. The scatter between the color coded subgroups is generally larger than the scatter within the subgroups. This suggests the members of a given subgroup are more closely related to each other than they are to members of different subgroups and is consistent with the conclusion that they are the results of recent fragmentation.

We suggest three explanations for the scatter within subgroups. First, the scatter may correspond to how recently the fragments split from each other. That is, the small scatter among the green circles in the Kracht plots relative to the orange triangles may indicate a more recent fragmentation (less time for the elements to evolve away from each other due to perturbations by the planets). Second, the scatter may be due to the location in the orbit where fragmentation occurred. In this case, orbits which are spread out in time but with all other elements (q, ω, Ω, i) being similar may have split near perihelion while orbits which arrive at similar times but with larger spreads in the other elements may have fragmented near aphelion.

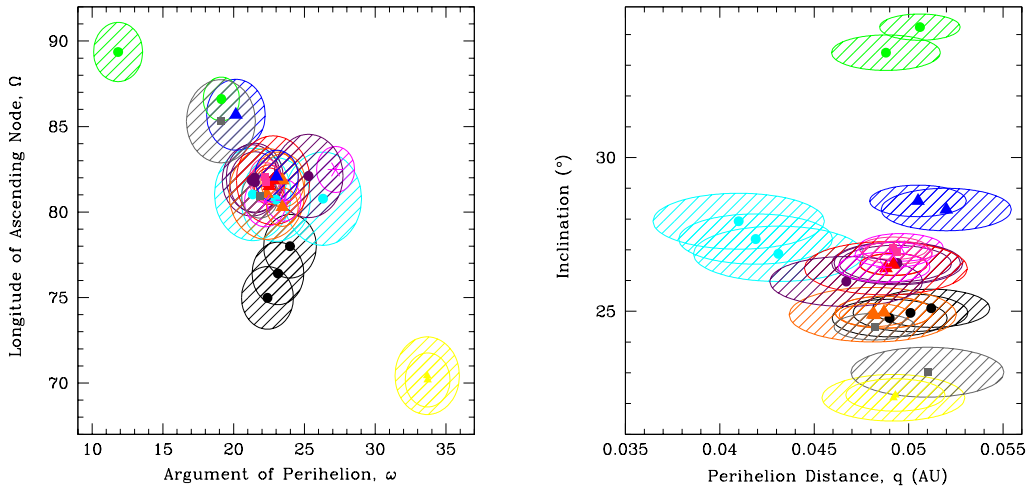

Figure 4.2: Same as Figure 4.1 but for the Marsden group. Two questionable members (2003 Q1 and 2003 Q6) deviate significantly from the rest of the Marsden group and have been omitted to allow better resolution of the family.

The location, orientation, and separation velocity necessary to cause these changes are similar to those for the Kreutz comets which are discussed in Section 3.2 and in Sekanina (2002b), however the magnitude of the changes are much smaller for the Kracht and Marsden groups. Finally, the scatter within the subgroups may be due to the quality of the orbital fits. In general, comets which were better observed are closer to the centers of the groups, and much of the scatter may be attributed to a paucity of observations.

Elliptical solutions have been published for six Kracht comets and 14 Marsden comets. The Tisserand parameters for these 20 comets support each linkage, differing by less than 0.002 for all pairs[2]. The Tisserand parameters range from 1.80–1.99

[2]The Tisserand parameter is a nearly conserved quantity during an interaction between a planet and a small body. It can be calculated for each planet but is most often used for Jupiter. The equation is

$$T_J = \frac{a_J}{a} + 2\left[(1-e^2)\frac{a}{a_J}\right]^{\frac{1}{2}} cos(i) \tag{4.1}$$

where T_J is the Tisserand parameter relative to Jupiter, a_J is the semi-major axis of Jupiter, and a, e, and i are the semi-major axis, eccentricity, and inclination of the small body, respectively.

bracketing the value of 96P/Machholz 1 (T_J=1.9422), and suggest that the Machholz complex was of Oort cloud origin (T_J<2), although they are close enough to 2 that a Jupiter Family Comet origin cannot be ruled out.

4.3 Dynamical Simulations

We chose to focus on the recent dynamical history of the Kracht group because a larger fraction of its members appear to be related than in the Marsden group, making it more promising for determining additional linkages. To test the fragmentation history, we conducted numerical simulations using the freely available HNBody integration package[3] (Rauch and Hamilton 2002). We used a Runge-Kutta integrator and simulated the solar system using the Sun, the eight planets, and Pluto. Comets were treated as "light weight particles" whose masses affected the orbits of the ten "heavy weight particles" but not each other. We used a heliocentric coordinate system and the particles were subject only to gravity. Each comet was started at perihelion using the orbital elements published by the IAU, and the epoch of the orbital elements was assumed to be the time of perihelion. The planets were integrated forward or backward from their positions given in the Astronomical Almanac for the Year 2000 (U. S. Naval Observatory and Royal Greenwich Observatory 1999) to the start time of the integration.

We tested the error introduced by the code by integrating a typical Kracht comet forward 100,000 days and then back to the initial start position. The test was repeated in reverse: integrating backwards 100,000 days and then forward to the start position. We varied the accuracy parameter (the fractional error allowed

Most asteroids have T_J>3, most Jupiter Family Comets have 2<T_J<3, and most Oort Cloud comets have T_J<2.

[3]http://janus.astro.umd.edu/HNBody/

per step) from 10^{-8} to 10^{-15}, and compared the comet's position at time T=0. Simulations with the accuracy parameter from 10^{-8}–10^{-10} produced unacceptably large errors (>0.01 AU). Simulations with accuracy parameters 10^{-11} and smaller produced satisfactory results with integration times increasing by ∼50% per order of magnitude improvement in the accuracy parameter. The errors improved rapidly until an accuracy parameter of 10^{-12} but negligibly for more accurate integrations. Thus, we selected an accuracy parameter of 10^{-12} which provided the best balance of speed and error minimization (the positions agreed to within 0.00013 AU).

4.3.1 Simulation 1: From the Present to the Past

We integrated the orbits of all the Kracht comets known as of mid-2007 backwards for 200 years. For comets with apparent linkages, we used the eccentricity derived from the linkage while for the comets without apparent linkages we varied the eccentricity for a fixed perihelion distance to correspond to orbital periods between 4.5 and 6.0 years. For each comet we generated 100 orbits with elements drawn randomly from within an estimated error range of Δq=±0.005 AU, $\Delta\omega$=±3°, $\Delta\Omega$=±3°, and Δi=±1° and Δe=±0.001 (T was not changed)[4].

We looked for instances where the orbital elements and positions of the comets were similar at the same time. We developed a simple metric to quantify the differences in orbits at each time step and sought solutions which minimized it to help determine the similarity of orbits and location. The metric m is

$$m = \sqrt{\left(\frac{q_1 - q_2}{q_{err}}\right)^2 + \left(\frac{\omega_1 - \omega_2}{\omega_{err}}\right)^2 + \left(\frac{\Omega_1 - \Omega_2}{\Omega_{err}}\right)^2 + \left(\frac{i_1 - i_2}{i_{err}}\right)^2 + \left(\frac{e_1 - e_2}{e_{err}}\right)^2 + \left(\frac{dist_{1-2}}{dist_{err}}\right)^2} \tag{4.2}$$

[4]These simulations were conducted before any revised orbital elements were available using STEREO data. Hence the estimated orbital elements used in this discussion differ from the uncertainties calculated in Section 3.2.

where q_x, ω_x, Ω_x, i_x, and e_x are the osculating orbital elements of the two orbits being compared (denoted by subscripts 1 and 2), q_{err}, ω_{err}, Ω_{err}, i_{err}, and e_{err} are the estimated uncertainties in the orbital elements cited above, $dist_{1-2}$ is the distance between the comets at the time being considered (in AU), and $dist_{err}$ was 0.1 AU (arbitrarily chosen). We explored a range of values for q_{err}, ω_{err}, Ω_{err}, i_{err}, e_{err}, and $dist_{err}$ to test the metric. We note that this is a crude metric which is not generalized for all orbits. In particular it is poor for orbits with small e and i for which ω and Ω are poorly constrained. However this is not a serious issue for our case since $e \sim 1$ and i is not too small. The key property of the metric is that m$\rightarrow$0 for identical orbits. Furthermore, we wanted the metric to respond to changing the assumed uncertainties in the orbital solutions in an easily quantifiable manner. To determine a potential linkage, we looked for solutions whose velocities differed by less than 5 m s^{-1}, which has been established by Sekanina (1977, 1978, 1982) as a reasonable upper limit for separation velocities imparted during fragmentation events.

The results for many individual simulations were promising but due to the large uncertainties in the orbital elements and the sensitivity to the position of Jupiter a definitive fragmentation history of the Kracht group remained elusive. However, we can make several generalizations.

1. The comets which arrived in temporal clusters with similar orbital elements evidently split from each other since the previous perihelion passage. The metric was nearly always minimized for these comets within the last orbit while earlier solutions were rarely of comparable quality.

2. Many solutions which agreed well in spatial location did not agree well in orbital elements. This was because of the nature of their highly eccentric orbits. The comets spend a large amount of their time near aphelion which is

confined to a small region of space because the orientations of the orbits are clustered around a very narrow range of ecliptic longitude and latitude of the perihelion point (L_π and B_π)[5]. Thus, many solutions were in similar locations but with orbital elements which differed by considerably more than could be generated by splitting with separation velocity less than 5 m s^{-1}, making their production via fragmentation at that location and time unlikely.

3. Due to the sensitivity of the orbits to close approaches with Jupiter, small differences in orbital elements can result in very divergent origins. This is illustrated in Figure 4.3. In this plot 200 orbits drawn from the error regions around the published orbital elements for C/1999 M3 are integrated backwards 150 years. While most orbits follow a similar orbital evolution (with a steadily widening envelope of elements), several solutions deviate dramatically, differing from the primary solution by more than 25° in ω and Ω, more than 15° in i, and having e and q which move in the opposite direction as the main solutions. The effects of close approaches to Jupiter can be seen as large jumps in the elements every ∼12 years, corresponding to the orbital period of Jupiter. Unless the uncertainty in the orbital elements is improved by observations of the same comet on multiple apparitions, it is unlikely that a unique history of the group will be found.

---

[5]A small range of L_π and B_π is exhibited for all the comets in each of the sungrazing families. Because the orientation of an orbit is not easily changed in the short term, the L_π and B_π values tend to correspond to the orientation of the original orbit of the progenitor. Despite the often divergent orbital elements, L_π and B_π are nearly always very similar and may be used to identify members of the family when the orbits are less certain. See Sections 4 and 5.3 of Sekanina (2002b) for further discussion and Equations 8 and 9 of the same work for equations for L_π and B_π.

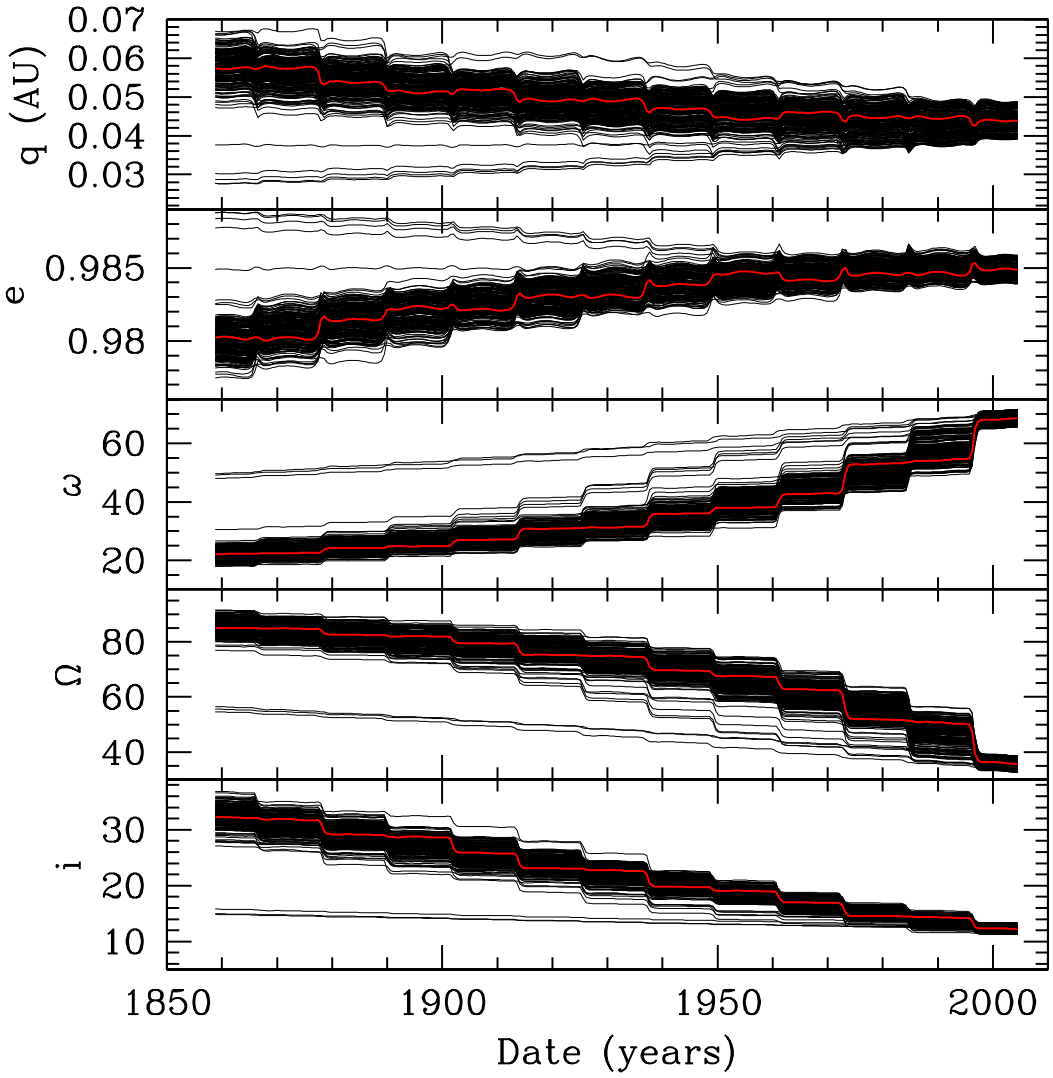

Figure 4.3: Backwards integration of Kracht comet C/1999 M3 and 200 comets with slightly different orbital elements. The thin black lines are the osculating orbital elements of each simulated comet and the heavy red line denotes the osculating orbital elements of the published orbital solution (for a link to C/2004 L10). The top panel plots the perihelion distance q in AU, the second panel plots eccentricity e, the middle panel plots argument of perihelion ω in degrees, the fourth panel plots longitude of ascending node Ω in degrees, and the bottom panel plots the inclination i in degrees.

4.3.2 Simulation 2: From the Past to the Present

Accepting that a unique solution for the Kracht group is unlikely at present, we next attempted to estimate the length of time over which the group has been evolving. Because of the orientation of the orbit relative to Jupiter, the angular elements (ω, Ω, and i) have been evolving in the same direction since the split from 96P/Machholz 1. The change is relatively constant but with jumps due to close approaches with Jupiter. The trend is for ω to increase, and for Ω and i to decrease with time, as shown in Figure 4.3. We hoped to estimate the time since the major clusters of Kracht comets split from each other based on these trends in the elements combined with the effects of fragmentation. Following the framework developed by Sekanina (1977, 1978, 1982), we explored the effects of fragmentation with varying velocities of separation in the radial (R = radial away from the Sun), transverse (T = transverse in the orbital plane), and normal (N = normal to the orbital plane) directions.

We started our simulations by integrating a comet in a typical Kracht orbit backwards to a specified time T_{frag}. We simulated a fragmentation event at T_{frag} by creating 100 orbits with random velocities added in the positive and negative RTN directions with the magnitude of the combined RTN velocity less than or equal to a set velocity v_{frag}. Next, we created fragmentation events for T_{frag} varying between 1750–2000 CE, considering fragmentation near perihelion and at various points around the orbit. The simulations were repeated for a range of v_{frag} for each fragmentation event (v_{frag} = 1–50 m s^{-1}). Then we adjusted the initial orbital elements of the "typical" Kracht orbit and repeated the simulations for a number of starting conditions in order to best replicate the distribution of orbits seen today.

We can make several generalizations of the results:

1. As expected, the spread in the orbital elements is larger the greater the sep-

aration velocity imparted during the fragmentation event, and the earlier the fragmentation event occurred.

2. The effect on the orbital period is larger the closer the fragmentation event occurs to perihelion. The effect on q, ω, Ω, and i is larger the closer the fragmentation event occurs to aphelion. These effects are similar, but of a smaller magnitude, to those of the Kreutz family discussed in Section 3.2.

3. The effect of a close approach to Jupiter is potentially larger than the previous two effects. As a result, splitting near perihelion, which maximizes the spread in the orbital period but has minimal effect on q, ω, Ω, and i, often leads to close approaches of a few fragments and subsequently results in orbits which have the largest spread in all elements.

We could not replicate the full range of orbits exhibited by the Kracht group with a single fragmentation event, but could replicate the spread in the angular elements (ω, Ω, i) with a range of scenarios. We have plotted three representative solutions in Figures 4.4–4.6[6]. For splitting with a high separation velocity ($v_{frag} \leq 50$ m s^{-1}), the distribution roughly matched the spread in elements seen for fragmentation near perihelion around 1947 (Figure 4.4). For splitting at a moderate separation velocity ($v_{frag} \leq 5$ m s^{-1}), the distribution was most similar for fragmentation near perihelion around 1897 (Figure 4.5). For splitting with a low separation velocity ($v_{frag} \leq 1$ m s^{-1}, the distribution was best matched for fragmentation near perihelion around 1788 (Figure 4.6). These solutions are not unique, and similar results could be obtained, for example, for fragmentation with lower separation velocities at even earlier times,

[6]Note that the nearly linear relationship of ω and Ω is a consequence of the Kracht orbit in which perturbations cause changes in ω and Ω which are opposite in sign and approximately equal in magnitude. Deviations from this line could be due to nongravitational forces, but are more likely due to uncertainty in the orbital elements.

or for fragmentation events with higher separation velocities but which occur farther from perihelion.

While the fragmentation scenarios often matched the spread in ω and Ω well (the left panels in Figures 4.4–4.6), the agreement with the range of i values was somewhat less successful, and the agreement with the observed range of q was only fair (the right panels of Figures 4.4–4.6). The agreement of the range of orbital periods (not plotted) varied with v_{frag}. High v_{frag} solutions matched the observed period distribution reasonably well ($\sigma_{period} = 0.25$ years), but solutions with $v_{frag} \leq 5$ m s^{-1} and $v_{frag} \leq 1$ m s^{-1} did not create a large enough spread in orbital periods ($\sigma_{period} = 0.02$ years for each).

The lack of agreement in all orbital parameters may be due to several factors. First, all of the subgroups of the Kracht family may not have been produced by a single fragmentation event. It has been shown that fragmentation likely occurs throughout the orbits for Kreutz comets (Sekanina 2000a, 2002a,b). It is likely that the same is true for Kracht comets, and is further evidenced by the fact that a number of fragments have apparently been produced since the previous perihelion passage of several comets. Therefore, it is quite likely that a model of the evolutionary history must use multiple fragmentation events. The exponentially increasing phase space required by such a simulation puts it beyond the scope of the current investigation. Second, the fragmentation may have occurred at a time which was not sampled in the current investigation. Due to the strong sensitivity to close approaches to Jupiter, a slightly different T_{frag} may have resulted in better agreement in all elements. Furthermore, while the range of 250 years was selected to be representative of a reasonable range of v_{frag}, it is possible that the separation velocity was even smaller and occurred still longer ago. Since the goal of the current investigation is to estimate the time necessary for the elements to evolve to the present

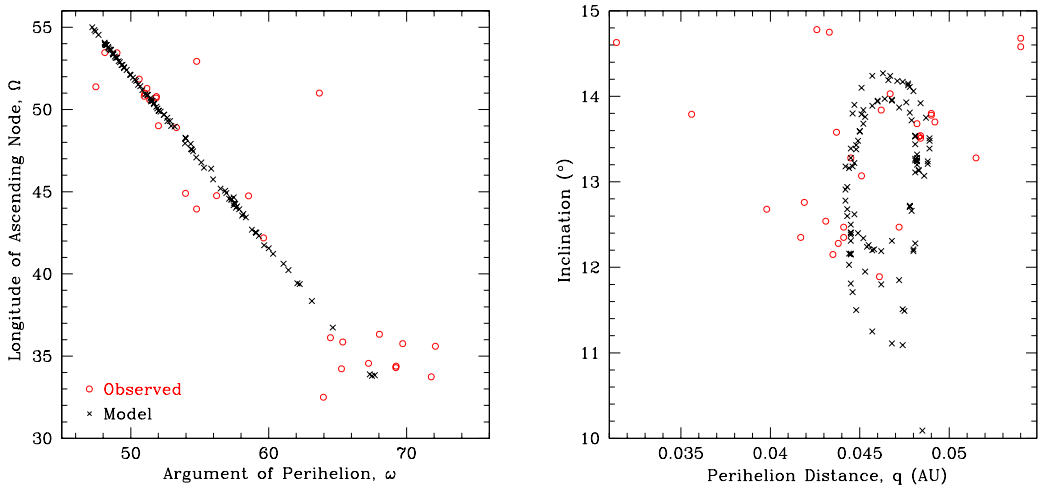

Figure 4.4: Distribution of the orbital elements for a generic Kracht comet which split near perihelion in 1947 at $v_{sep} \leq 50$ m s^{-1}. The red circles are the known members of the group observed from 1996-2007, the black crosses are simulated fragments.

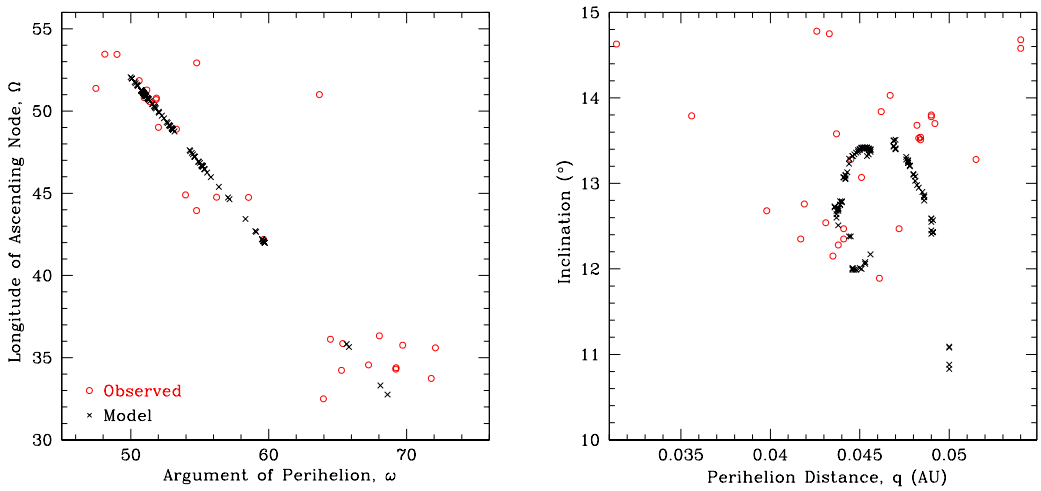

Figure 4.5: Similar to Figure 4.4, except the split occurred near perihelion in 1897 at $v_{sep} \leq 5$ m s^{-1}.

distribution rather than to determine the unique history, we feel the fragmentation scenarios explored are sufficient. Finally, the orbital elements of the known fragments may be inaccurate, particularly for the comets observed for very short arcs or only in C3. This uncertainty will remain until the fragments have been observed sufficiently well on three or more orbits.

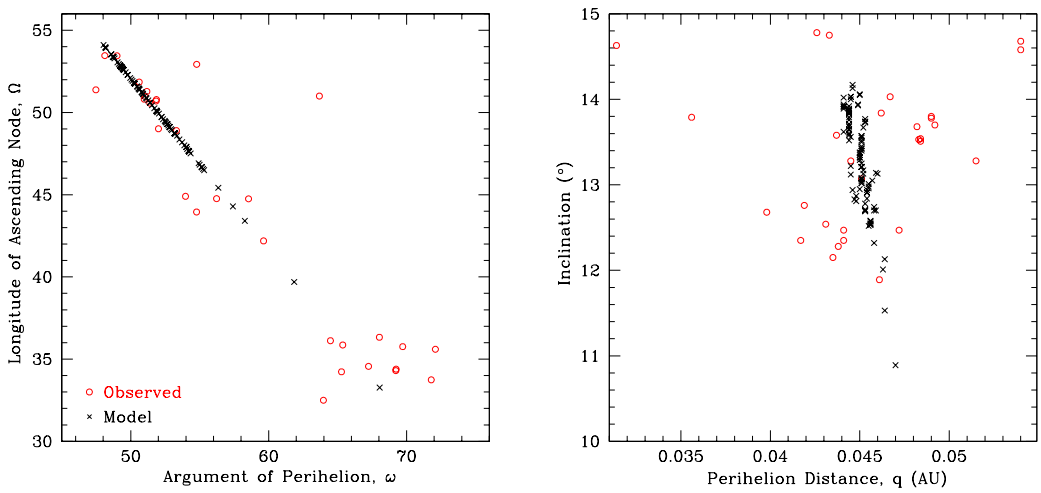

Figure 4.6: Similar to Figure 4.4, except the split occurred near perihelion in 1788 at $v_{sep} \leq 1$ m s^{-1}.

4.4 Photometry

We reduced the photometry of the Kracht and Marsden comets using the procedures discussed in Section 2.2. The detectability of comets in either group has a seasonal dependence due to the orientation of the group's orbit, which is illustrated in Figure 4.7 for the Marsden group and in Figure 4.8 for the Kracht group. Marsden comets are usually seen only in C2 and typically move from the bottom half of images to the top half, either left to right or right to left (for images oriented with north up and east to the left). Most Kracht comets are seen only in C2 and typically move horizontally across the CCD in a track which passes behind the occulting disk. Only the brightest comets in either group are seen in C3. Both groups of comets are typically only seen within ∼12 hours of perihelion and the time relative to perihelion at which they are seen is seasonal but also dependent on the phase angle and the intrinsic brightness of the comet. As with the Kreutz comets, the Marsden and Kracht comets that are seen simultaneously in the C2 orange filter and C3 clear filter appear ∼1 magnitude brighter in the C2 orange filter. The brightest few comets

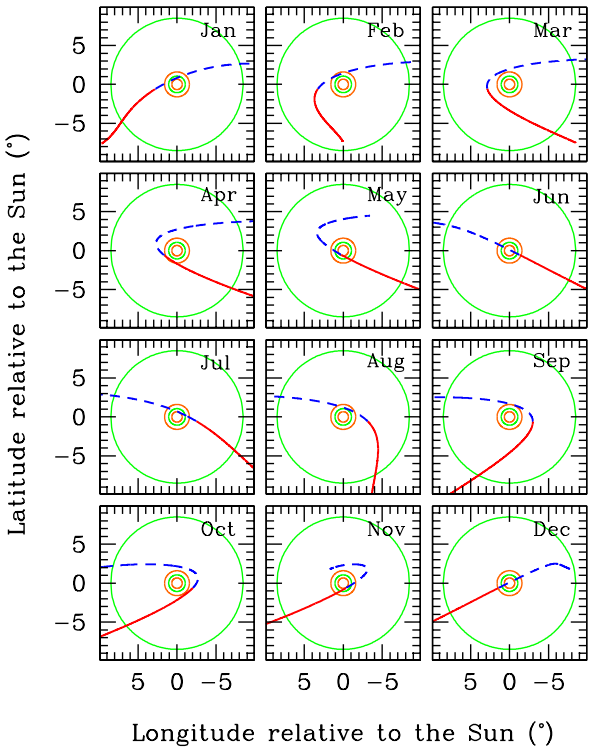

Figure 4.7: Monthly track across the SOHO coronagraphs for typical Marsden comets. The track is for a comet which reaches perihelion on the 15^{th} day of the month specified in the upper right corner of each plot. The red (solid) line is the orbit prior to perihelion and the blue (dashed) line is the orbit after perihelion. The green (C3) and orange (C2) circles denote the outer and inner radii of the SOHO coronagraphs, respectively.

appeared elongated in C2 images, while all appeared stellar in C3 images. None of the Marsden or Kracht comets have exhibited tails (many of the brightest Kreutz comets displayed tails but these are typically brighter than the brightest Marsden or Kracht comets).

The lightcurves of the Kracht comets are plotted in Figures B.10–B.13 and the Marsden comet lightcurves are in Figures B.14–B.17. We calculated the error bars in the same manner as the Kreutz error bars. Due to the seasonal effects on the viewing geometry and the lack of bright comets observed in either group, only a few Marsden or Kracht comets are observed continuously around perihelion. Instead, most are

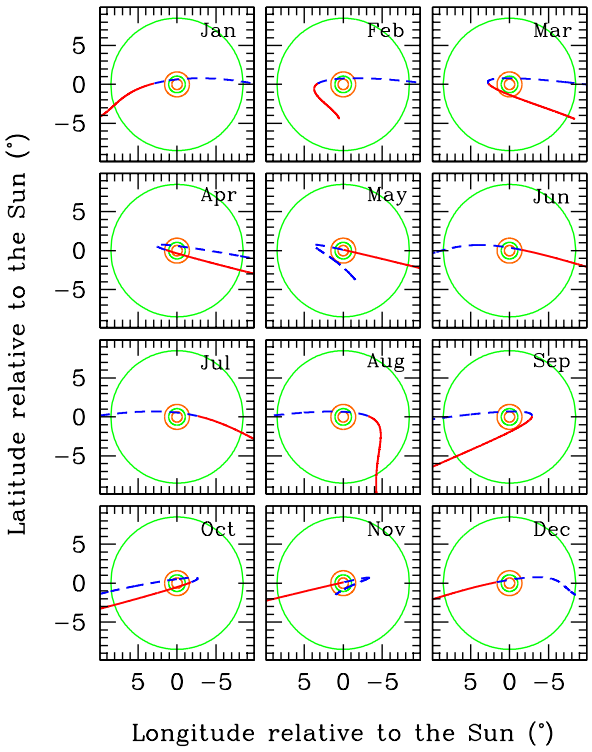

Figure 4.8: Same as Figure 4.7, but for typical Kracht comets.

observed for only a few hours either before or after perihelion. Due to the small number of observed comets and the frequent gaps in the lightcurves, it is impossible to construct a characteristic lightcurve of either group. However, it is clear that the lightcurves of Kracht and Marsden comets do not exhibit a consistent peak in brightness prior to perihelion as do the Kreutz comets (see Section 3.4). Most are too poorly observed to determine a peak. For those that have a discernible peak, the peaks tend to occur within ∼6 hours of perihelion and at distances smaller than 14 $R_{\odot}$, however they do not correlate with heliocentric distance, time relative to perihelion, or perihelion distance. Thus it appears that, as with the Kreutz comets, the time and distance at which a given comet reaches its peak brightness is a function of its unique history.

All of the comets which were observed twice appeared fainter on the second ap-

parition (with the possible exception of Marsden comet C/2000 C4 which is believed to have returned as C/2005 W1 and is discussed in Appendix C). The decrease in brightness is difficult to measure because the comets are often not seen at the same distances and in the same telescope, but is typically less than 1 magnitude. The only comet which was observed well enough to compare the lightcurve shapes was C/1999 J6 which returned as C/2004 V9. When the lightcurves are corrected only for the changing SOHO-centric distance (i.e. no phase correction), the shapes are virtually identical, with C/1999 J6 slightly brighter. However, when the phase corrected lightcurves are compared, their shapes vary dramatically and C/1999 J6 is significantly brighter. We discuss this discrepancy in more detail in Appendix C. We calculated the slope of brightening or fading for a handful of comets. These varied widely and since some comets peak before perihelion and some after, the slopes were not calculated over the same distances. With these caveats, these comets appear to brighten at between $\propto r^{-6}$ and $\propto r^{-10}$ and to fade more steeply, between $\propto r^{+7}$ and $\propto r^{+12}$.

The viewing geometry effects make it difficult to sample the groups at a uniform distance, time relative to perihelion, or even with the same telescope. We calculated a very rudimentary size by adding 1 magnitude to all C2 magnitudes to correct for the $\sim$1 magnitude difference between orange and clear filter magnitudes at similar distances in the Kreutz comets (Section 3.4.3) then converting the brightest point to an equivalent size in the same manner as in Section 3.4.4. This yields sizes between 1–10 meters in radius. However, unlike the Kreutz group, most Marsden and Kracht comets are observed to survive perihelion and the assumption that the nucleus totally disintegrates is invalid. A simple estimate of mass loss from a water ice nucleus due to erosion (e.g. Huebner (1967); Iseli *et al.* (2002)) yields $\Delta R \approx 30$ meters per orbit for a density of 0.35 g cm^{-3} while Sekanina and Chodas (2005)

estimated the erosion rate of C/1999 J6 = C/2004 V10 to be $\Delta R \approx 6$ meters in radius per orbit. Since many of the comets were seen on two orbits, they must have been at least ΔR larger the first time they were observed. If we approximate the change in brightness from one apparition to the next at 1 magnitude, assume this change is due entirely to a difference in surface area which is proportional to the radius squared, and set the erosion rate at $\Delta R \approx 10$ meter in radius per orbit, we arrive at nuclei that were $\sim$30 meters in radius when first observed. If we instead use $\Delta R = 6$ or 30 meters, the size when first observed could range from 20–100 meters in radius. With the lack of consistency between observations and numerous assumptions required to estimate a nuclear size, it would be unreasonable to estimate a size distribution of either family.

4.5 Family Trees

We summarize the overall fragmentation tree of the Kracht and Marsden comets in Figures 4.9 and 4.10, respectively, and give a table of the potential third apparitions in Table 4.2. Observations three or more times will improve the estimate of the nuclear size and erosion rate, improve the orbital elements (which will allow more specific dynamical integrations), and potentially allow estimates of nongravitational forces.

Using the fragmentation trees of the two groups, we can now assess the rate of splitting. We specify whether or not each comet was a product of splitting since its previous perihelion passage. If a comet was unobserved on its subsequent perihelion passage it is considered to have disappeared and its split status cannot be determined. If two or more comets were produced by the same fragmentation event, this is only counted as one split since on the previous apparition they were one

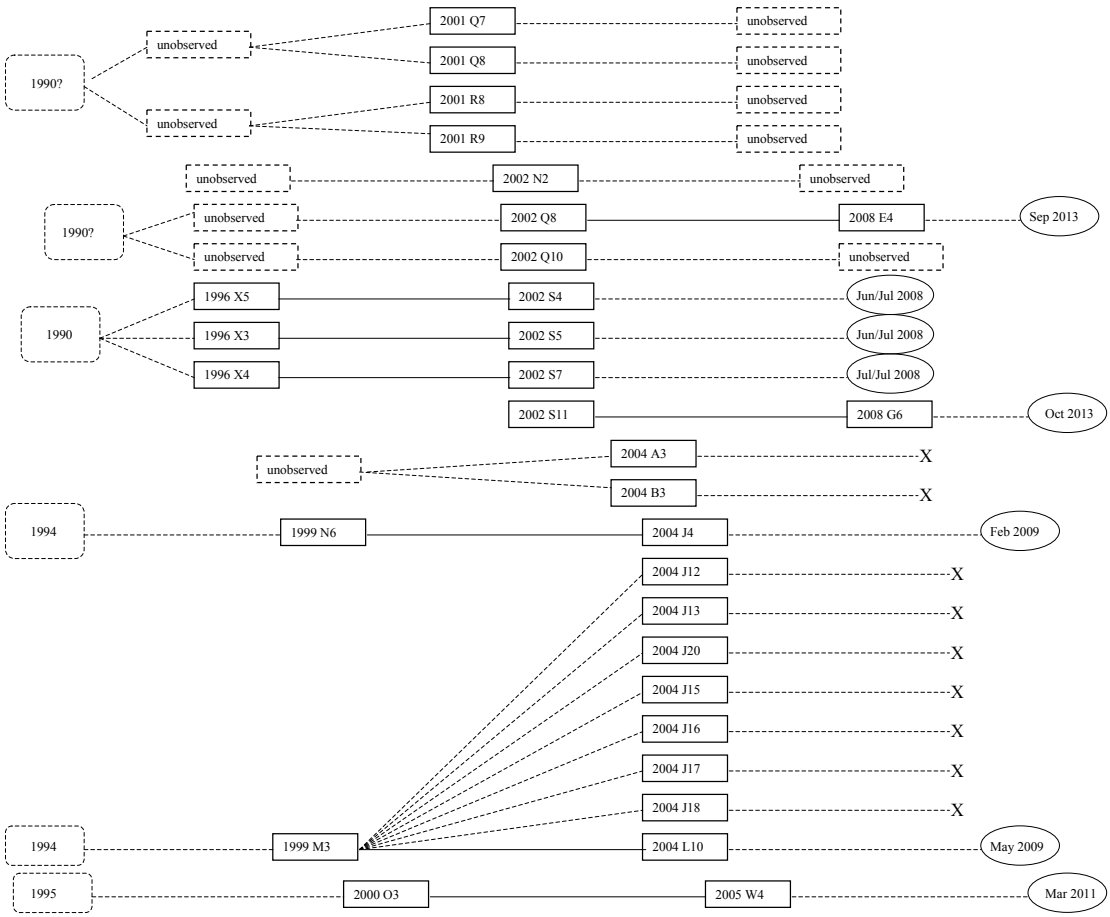

Figure 4.9: Fragmentation tree of the Kracht comets. The solid rectangles are observed comets, dashed rectangles are comets which likely reached perihelion since 1996 but went unobserved, dashed rectangles with rounded corners are comets which likely reached perihelion before 1996 (when SOHO started observing), ovals are predicted third apparitions (with estimated dates) for the brightest objects, and X's denote comets which are unlikely to be seen again.

comet. For the Kracht group we find that 6 comets likely split on their previous orbit (resulting in a total of 19 observed fragments), 11 comets did not split, 5 disappeared, and 8 were observed twice. For the Marsden group we find that 7 comets likely split on their previous orbit (resulting in a total of 18 observed fragments), 14 did not split, 11 disappeared, and 8 were observed twice. Thus, we estimate that $\sim \frac{1}{3}$ of the Marsden and Kracht comets split each orbit, $\sim$60% of the observed comets were a product of fragmentation on their previous orbit, and roughly half disappear

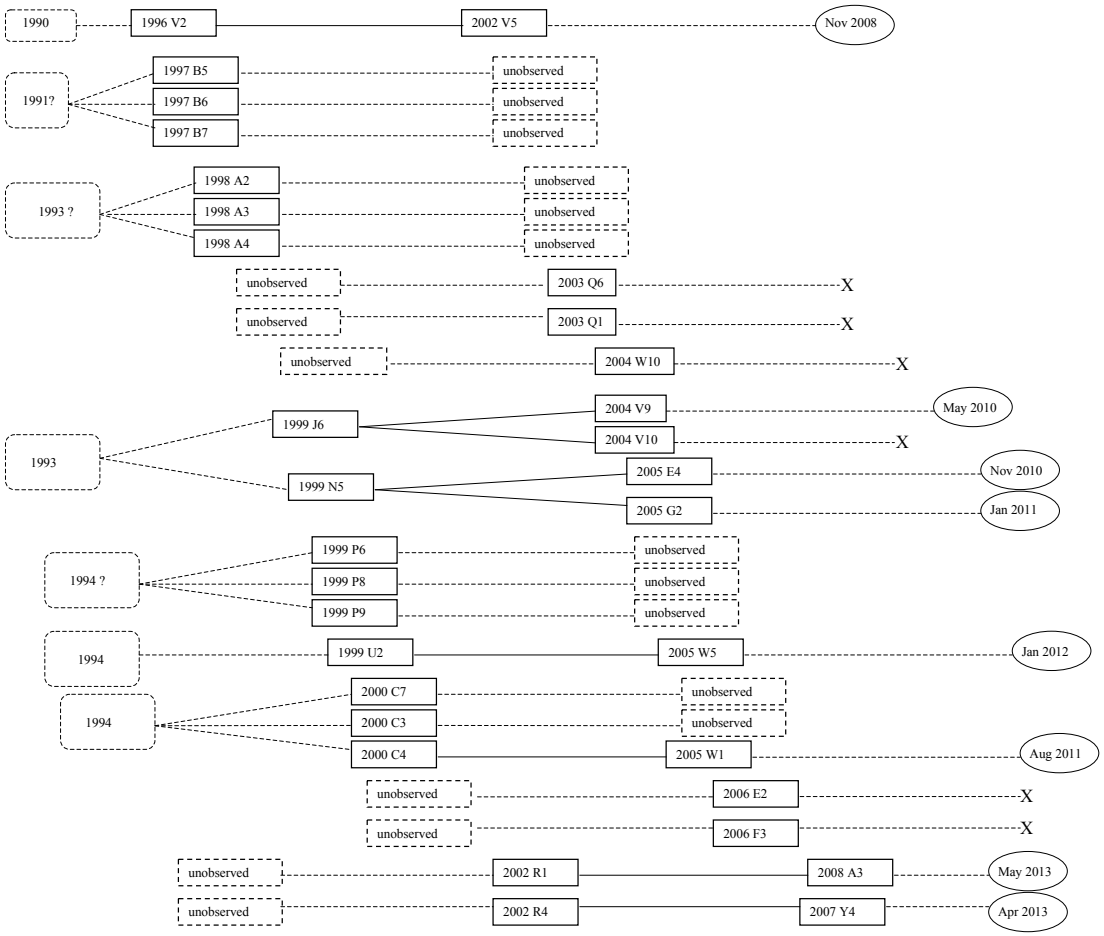

Figure 4.10: Fragmentation tree of the Marsden comets. The symbols are the same as in Figure 4.9.

each orbit. This is a lower limit on the splitting rate since if a comet splits but only the brightest fragment is seen then it will appear as though no split occurred. Furthermore, data gaps may prevent the recovery of some fragments and geometric effects may prevent or allow the observation of other fragments.

First Apparition	Second Apparition	Third Apparition	Group
1996 X3, X4, X5	2002 S4, S5, S7[a]	2008 Jun 28–Jul 4	Kracht
1996 V2	2002 V5	2008 Nov 12	Marsden
1999 N6	2004 J4	2009 Feb 27	Kracht
1999 M3	2004 L10	2009 May 29	Kracht
1999 J6	2004 V9	2010 May 9	Marsden
1999 N5	2005 E4	2010 Nov 8	Marsden
1999 N5	2005 G2	2011 Jan 17	Marsden
2000 O3	2005 W4	2011 Mar 19	Kracht
2000 C4	2005 W1	2011 Aug 30	Marsden
1999 U2	2005 W5	2012 Jan 6	Marsden
2002 R4	2007 Y4	2013 Apr 10	Marsden
2002 R1	2008 A3	2013 May 30	Marsden
2002 Q8	2008 E4	2013 Sep 9	Kracht
2002 S11	2008 G6	2013 Oct 26	Kracht

[a] 2002 S4 and S7 should be visible however 2002 S5 may be too faint.

Table 4.2: Predicted returns of Marsden and Kracht comets.

4.6 Discussion

4.6.1 Fragmentation Rate and Size Estimate

Our studies of the Kracht and Marsden families reveal that they are populations in flux. On every orbit roughly 33% of the comets fragment, and about half are not observed on subsequent orbits. Each group currently has 7–8 fragments which are likely large enough to be seen on subsequent perihelion passages (Table 4.2). Assuming the brightness scales with nuclear size in a similar manner as the Kreutz comets, even the "large" fragments are probably less than 30 meters in radius and the faint comets are likely smaller than 5 meters in radius. We roughly estimate the erosion rate at $\Delta R \approx 10$ meters in radius per orbit, meaning that the faintest comets are not likely to survive until the next perihelion passage and even the brightest

fragments will only survive for another few orbits.

The high erosion rate, temporal clustering, and dynamical simulations indicate that the fragments being seen today are very young, and each group was probably contained in 5–10 larger comets in the 1980s. These likely split from each other in a series of fragmentation events over the preceding 50–250 years, with close approaches to Jupiter most responsible for the spread of orbits seen today. Integrating the water ice erosion rate for generic Kracht and Marsden orbits since 950 CE, a comet which is just visible today was 3–4 km in radius when it split from the Machholz complex progenitor (assuming no subsequent splitting). We assume the fragments seen today represent the last surviving bits from a single 3–4 km proto-Kracht comet and a single 3–4 km proto-Marsden comet which represent first generation fragments from the Machholz complex progenitor, and progressively split later into the comets seen by SOHO. If the other first generation fragments of the Machholz complex (which each became 96P/Machholz 1, the Daytime Arietids, and the Southern δ Aquarids) were of comparable size, the progenitor of the complex was likely 5–7 km in radius, about the size of a large Jupiter family comet or a typical long period comet. Of course, such objects may have split multiple times making those size estimates extremely uncertain.

4.6.2 Are These Comets Active?

The absence of tails and the likelihood that the Kracht and Marsden comets have been in 5–6 year orbits with perihelion distances smaller than 1 AU for some 2000 years raise the question of whether they are still active or are dormant nuclei either depleted of volatiles or covered in enough inactive regolith to prevent outgassing. The lack of a visible tail for comets as faint as the Marsden and Kracht comets is unremarkable. Most Kreutz comets with tails appeared brighter than magnitude 5

(the approximate brightest magnitude of Marsden and Kracht comets), and except for the very brightest comets, tails were generally seen at distances smaller than $\sim$10 $R_\odot$.

Typical Kracht and Marsden comets appear magnitude $\sim$8 or fainter near perihelion. Assuming a 4% albedo, a perihelion distance of 10 $R_\odot$, and ignoring phase angle, a bare nucleus would need to be about 8 km in radius to appear this bright. This is unrealistic as it would require a population of at least 50–60 objects of this size to repeatedly pass undetected through the inner solar system. Furthermore, as pointed out by Meyer (2003), Marsden comets which reach perihelion in mid-May pass within 0.025 AU of Earth in mid-June. An 8 km comet would appear about magnitude 7 (ignoring phase) at this time. C/1999 J6 reached perihelion 1999 May 11.59 and was not seen from the ground. While it was not discovered in SOHO images until 2000, it is unlikely that a magnitude 7–8 object could pass so close to Earth without being observed.

A second argument against these being dormant nuclei is the lightcurve shape. While there is no characteristic shape of Marsden and Kracht lightcurves, the observed lightcurves deviate significantly from the r^{-2} shape which would be expected of an asteroid reflecting sunlight. Not only does the brightness peak at times other than perihelion, but when calculable, the slopes of brightening are much steeper than r^{-2}, consistent with an increasing coma surface area due to outgassing.

4.6.3 Qualitative Discussion of the Activity

Having established that the Marsden and Kracht comets are active (at least in the SOHO field of view), how then can we explain their activity? As with the Kreutz group, the lightcurve shape of Kracht and Marsden comets is an amalgamation of numerous processes which depend on the heliocentric distance. The processes

driving the activity are likely similar to those acting on the Kreutz at comparable distances (Section 3.6.4). We restrict this discussion to the circumstances which differ between the Kreutz and the Marsden and Kracht groups.

Beyond the SOHO field of view, the comets which survived intact since their previous perihelion passage are probably less active than those which experienced fragmentation and have freshly exposed surfaces. While no Kracht or Marsden comet has been seen beyond 19 $R_\odot$, we do not interpret this as a significant turn-on (inbound) or turn-off (outbound) point for activity. Instead, it is a product of the viewing geometry and the fact that the Marsden and Kracht comets are generally very faint. Because the brightest comets reach only apparent magnitude 5–6, they are evidently very small (or have only a small active area) and do not reach the threshold for detection until $\sim$19 $R_\odot$.

If the Marsden and Kracht comets are similar in composition to the Kreutz comets, we would expect their lightcurves to peak between 10–14 $R_\odot$. This occurs prior to perihelion for most, but since some have q as large as 12 $R_\odot$ and roughly half the Kreutz have peaks inside of 12 $R_\odot$, some fraction of Marsden and Kracht comets may peak at or after perihelion. While the lightcurve coverage is sparse for most Marsden and Kracht comets, there is no consistent peak in brightness prior to perihelion, nor is there a consistent fading after perihelion. In fact, many lightcurves appear relatively flat. Therefore we cannot assess the similarity of composition.

After perihelion we would expect the brightness behavior to be similar to the pre-perihelion brightness. However, comets which split after perihelion should be brighter due to the newly exposed volatiles and (until they are far enough apart to be resolved) a greater surface area in the aperture. Due to the high rate of splitting in the Marsden and Kracht comets, the rates of fading probably vary widely from comet to comet, making it difficult to predict their brightnesses at elongations large

enough to be observable from the ground.

4.6.4 Compositional Differences?

The lightcurve coverage is insufficient to determine if the Marsden and Kracht comets peak at 10–14 $R_{\odot}$. However, if they do not, it may indicate that they have a different composition than the Kreutz comets which may be diagnostic of differences in their formation regions. Bailey *et al.* (1992) suggest that the progenitor of the Kreutz group may have been captured from the Oort cloud within the past ≈1 My. It is unclear where 96P/Machholz 1 (from which the Marsden and Kracht families are believed to have split prior to 950 CE) originated, as orbital integrations indicate it is in a secular Kozai resonance (Kozai 1962) with Jupiter in which it oscillates between a high inclination orbit with perihelion distance near 1 AU to a low inclination sungrazing (or nearly sungrazing) orbit over a period of ∼4000 years (Bailey *et al.* 1992; Green *et al.* 1990; Rickman and Froeschle 1988). However, the Tisserand parameters of 96P and of the ten pairs of Kracht and Marsden comets with published elliptical orbits are between 1.80–1.99, suggesting the Machholz complex progenitor was from the Oort cloud (T_J<2). Schleicher (2007) found that for 96P "the CN-to-OH ratio is low by about a factor of 200; C_2 and C_3 are also low but by factors of 10–20 from 'typical' composition (based on A'Hearn *et al.* (1995))". Schleicher speculates that 96P might represent a new compositional class of comets. This finding is tantalizing and encourages further study of the components of the Machholz complex.

Chapter 5

Summary and Conclusions

5.1 Overview

First recognized over 100 years ago and studied extensively since then, the Kreutz group is the prototypical sungrazing family. It has produced some of the most spectacular comets in recorded history, including the comet of 1106 CE, C/1882 R1, and C/1965 S1 Ikeya-Seki. Kreutz comets have highly inclined orbits (i∼143°) with perihelion distances q∼1–2 $R_\odot$, and periods of 500–1000 years. The group has more than 1200 known members, the vast majority of which have been discovered by SOHO since 1996. These fragments are small (less than 50 meters in radius) and short lived, as they were produced since their previous perihelion passage and are destroyed before they reach perihelion.

As they approach the Sun, the Kreutz comets follow a typical lightcurve shape. They brighten steadily, reach a peak at 10–14 $R_\odot$, and fade interior to this. The brightest comets are seen in both C3 (the outer coronagraph) and C2 (the inner coronagraph). Because of seasonal geometric effects, many comets are seen only in C2. Most comets are not seen at all heliocentric distances, but they all follow the general trend of the group at the distances over which they are observed. The

comets which are seen beyond $\sim$20 $R_\odot$ (generally the brightest ones) are usually first seen brightening at a rate near $\propto r^{-7.3}$ but transition to a brightening rate near $\propto r^{-3.8}$ between 20–30 $R_\odot$. We suspect this change of slope corresponds to a short lived tail formation event which releases large amounts of dust into the coma, and the steeper slope does not extend much beyond the SOHO field of view ($\sim$30 $R_\odot$).

The distance of the peak in brightness is not bimodal as previously suggested (Biesecker *et al.* 2002) but ranges from 10.5–14 $R_\odot$ with a peak near 12 $R_\odot$. The distance correlates to the shape of the lightcurve, with the comets which peak at the largest distances having more gradual slopes of brightening and fading while comets which peak at smaller distances have steeper slopes of brightening and fading. This is likely a manifestation of the comets having a continuum of slightly different compositions which are also influenced by their unique fragmentation histories, shapes, and rotation periods. The comets appear brighter in the C2 and C3 orange filters than the C3 clear filter by $\sim$1 magnitude, although the difference varies with heliocentric distance, reaching a maximum near 19 $R_\odot$. We concur with previous authors (e.g. Biesecker *et al.* (2002); Sekanina (2003)) that this difference in brightness is due to sodium emission.

Assuming that the comets seen by SOHO are representative of the distribution of comets throughout the Kreutz orbit, the family contains some 20,000 comets larger than 5 meters in radius. The total mass of these small fragments is $\sim 4\times10^{14}$g, much smaller than the estimated mass for the largest group members observed from the ground. The cumulative size distribution is $N(>R)\propto R^{-2.2}$ and the cumulative mass distribution is $N(>m)\propto m^{-0.73}$. Interestingly, the size distribution exponent α=2.2 is similar to that found for the nuclei of Jupiter family comets, although this likely has no significance since the distributions were produced by different processes. If the comets were allowed to continue in their orbits instead of disintegrating on the

subsequent perihelion passage, they would likely continue to fragment, steepening the slope of the size distribution. If it is assumed that the cometesimals which formed the original Kreutz progenitor have maintained their integrity (their internal strength is stronger than their connection to neighboring cometesimals), then continued fragmentation should cause the size distribution to reflect the true size distribution of the cometesimals where the Kreutz progenitor formed. The Weidenschilling (2004) two-dimensional model for the formation of comets predicts they are composed of components ranging in size up to ∼100 meters. Thus the size distribution seen in the Kreutz today may be close to the primordial distribution, and the discontinuity in the cumulative size distribution between the ground observed and SOHO observed comets is reflective of two distinct populations: large bodies composed of 1–100 meter components and the components themselves.

Study of the Kracht and Marsden families provides an intimate look at the destruction of a comet. Dynamical simulations imply that the Kracht and Marsden comets were once part of a larger comet, the largest remnant of which is likely 96P/Machholz 1. Over the last millennium these comets have steadily migrated from high inclination orbits with perihelion distances near 1 AU to (relatively) low inclination orbits with perihelion distances around 0.05 AU. As this has proceeded, the ever smaller perihelion distances have caused increasingly more erosion. Compounding the problem, they have been subject to repeated fragmentation. The temporal clustering of arrivals suggests that fragmentation is common, and the spread in the orbital elements implies that fragmentation events have been occurring for at least the last 50–250 years and probably since the split with 96P.

The combination of increasing erosion and rampant fragmentation is quickly depleting the number of observable comets in the two families. SOHO has been operational for more than 12 years, or roughly two orbital periods of the Kracht and

Marsden comets. While there were numerous data gaps early in the mission, the coverage has been quite good since 2000 and it is doubtful that any large members of the families have gone unobserved. Thus, the total observable population of the groups is less than 60. Of these, only 8 Marsden and 7 Kracht comets are likely to be large enough to be seen on future perihelion passages. Geometric effects and data gaps will undoubtedly cause some of these comets to go unobserved while fragmentation and phase angle effects will likely produce some unexpected new members.

Despite the possibility of detecting a few new members, the long term outlook for the Kracht and Marsden families is grim. The already small nuclei (probably 5–30 meters in radius) lose 6–30 meters in radius per orbit at the current perihelion distance, so most are unlikely to survive more than a few additional orbits. We are fortunate to have the opportunity to study this wealth of cometary fragments on a regular basis for perhaps another decade, even more so since we can compare what we learn from them with their readily observable relative 96P/Machholz 1.

The picture is not so bleak if one views the disappearance of the Marsden and Kracht comets not as the termination of two groups of comets but in the larger framework of the Machholz complex. The potential remains that there are undiscovered components of the complex. We hinted at this when discussing the questionable Marsden comets C/2003 Q1 and C/2003 Q6 (Appendix C), suggesting that they may be members of an extended population between the current Marsden and Kracht groups dubbed the "quasi-Marsden precursors" by Sekanina and Chodas (2005). Several Marsden and Kracht comets were not initially identified as such because alternate orbital solutions were initially published. Once the group was recognized, a number of orbits were recomputed and other members were found (Meyer 2003). It is possible that other members of the Machholz complex have already been

observed by SOHO and similarly misidentified. Furthermore, as discussed by Ohtsuka *et al.* (2003) and Sekanina and Chodas (2005), 96P and any as yet unobserved "quasi-Machholz precursors" will migrate into Marsden orbits in the future. Thus, even if the Marsden and Kracht comets are depleted in the next few perihelion passages, the chance remains that the near-Sun environment will be repopulated by their relatives in the coming decades, and opportunities to study the end states of comets will continue.

5.2 Key Results

Our study of the sungrazing comets observed by SOHO has included photometric reductions and analysis, physical modeling, and dynamical modeling. We have focused our studies on the Kreutz, Marsden, and Kracht groups, presenting the first published lightcurves of more than 700 of these comets and revised lightcurves for another 200. In the interest of space these lightcurves will be published separately in the International Comet Quarterly[1] and the Planetary Data System[2]. Reduced images of each of these comets have been submitted to the Planetary Data System for archiving and will soon be publicly available. We summarize our most important results below.

- The Kreutz lightcurves do not have a bimodal distance of peak brightness as previously reported by Biesecker *et al.* (2002). Instead, they reach a peak in brightness over a range from 10.5–14 $R_\odot$ with a maximum around 12 $R_\odot$. This suggests that there is a continuum of compositions among the members rather than two distinct compositions.

[1] http://cfa-www.harvard.edu/icq/icq.html

[2] http://pdssbn.astro.umd.edu/

- Most Kreutz lightcurves brighten near $\propto r^{-7.3}$ when they first become visible then exhibit a change in brightening rate between 20–30 $R_\odot$, brightening near $\propto r^{-3.8}$ from 16–24 $R_\odot$. It is unclear how far outward the $\propto r^{-7.3}$ extends as the only Kreutz comet seen beyond the SOHO field of view prior to perihelion was C/1965 S1 Ikeya-Seki which brightened at $\propto r^{-4.1}$ from 1.02–0.03 AU, but was not observed between 50–20 $R_\odot$. Its lightcurve from 20–50 $R_\odot$ after perihelion was sparse, but did not deviate significantly from the $\propto r^{-3.9}$ rate it exhibited from 0.04–1.63 AU post-perihelion. The rate of brightening of the SOHO observed Kreutz from 16–24 $R_\odot$ is similar to the rates of fading of the ground observed members of the family as well as the canonical rate of brightening for most comets. The increased activity which results in the steeper lightcurve when first visible may be responsible for tail formation, and Sekanina (2000b) found that tails were produced between 20–30 $R_\odot$ in a sample of 11 comets.

- The lightcurves of the Marsden and Kracht comets do not display a characteristic shape. Their observability suffers from severe seasonal effects due to the geometry of the orbit, but it appears that they reach a peak in brightness within ∼6 hours of perihelion, have no preference for peaks before or after perihelion, and display no trend with perihelion distance. As with the Kreutz group, individual lightcurve shapes are likely due to the unique history of each fragment.

- The size range of the observed Kreutz comets is 2–50 meters in radius. The cumulative size distribution is $N(>R) \propto R^{-2.2}$. The largest fragment in this distribution should be ∼500 meters in radius, consistent with C/1887 B1 and C/1945 X1 (the two smallest ground observed members) being the two largest members. Six other ground observed comets were much larger than this, in-

dicating that either the size distribution does not hold at the largest sizes or that the distribution is not uniform throughout the orbit. If the distribution of comets seen by SOHO is consistent throughout the orbit, there are ∼20,000 comets larger than 5 meters in the Kreutz group. These have a total mass of $\sim 4 \times 10^{14}$ g which is much smaller than the likely mass of the largest ground observed members. From these arguments we conclude that either the Kreutz family is not collisionally evolved or that the distribution is not uniform throughout the orbit.

- The flux of Kreutz comets reaching perihelion has increased during the mission. After correcting for the changing discovery circumstances, the average comets year^{-1} increased from an average of 83.5±8.4 from 1997–2002 to 125.1±7.6 from 2003–2007. The increase is not restricted to the smallest comets, as there was an 80% increase in comets brighter than magnitude 6, suggesting the increase is due to a changing distribution around the orbit rather than an improvement in the discovery capabilities.

- The sizes of the Marsden and Kracht comets are uncertain, but likely to be smaller than 30 meters. The faintest ones will not be reobserved, but many of the 16 members which have apparently been seen on two apparitions will likely be seen a third time. However, even the largest fragments will not survive more than a few more orbits.

- Fragmentation is pervasive and ongoing in the Kreutz, Marsden, and Kracht groups. Approximately 8% of Kreutz comets arrive in clusters smaller than 0.2 days, suggestive of fragmentation events since aphelion. The presence of comets belonging to each of the subgroups in the family indicates that substantial fragmentation occurred near the previous perihelion passage. Thus it

is likely that several generations of splitting have occurred since the previous perihelion passage of these comets, when they were still a part of their parent comet. Approximately 33% of Marsden and Kracht comets fragment each perihelion passage. The members of these groups seen by SOHO were likely contained in 5–10 larger fragments just a few orbits ago. Dynamical simulations of the Kracht group show that the orbital distribution can be explained by low velocity fragmentation events and close approaches to Jupiter over the last 50–250 years.

5.3 The Future of Sungrazer Observations

5.3.1 STEREO

While SOHO continues to operate, the next advance in space-based coronagraphs, Solar TErrestrial RElations Observatory (STEREO), is already in operation. STEREO is nominally a two year mission to observe the Sun in 3-D, with two identical spacecraft. One spacecraft orbits ahead (dubbed STEREO-A) and the other trails the Earth (dubbed STEREO-B). They are gradually moving away from each other, and after two years will be 90° apart, each one 45° from the Earth (as viewed from the Sun). Each spacecraft has two coronagraphs (COR1 and COR2) and two heliospheric imagers (HI1 and HI2). COR1 has an annular field of view from 1.3–4.0 $R_\odot$ with a resolution of 7.5 arcsec pixel^{-1}, and a bandpass of 650–660 nm. COR2 has an annular field of view from 2–15 $R_\odot$ with a resolution of 15 arcsec pixel^{-1} and a bandpass of 650–750 nm. HI1 is centered 13.28° from the Sun with a circular 20° field of view, a resolution of 35 arcsec pixel^{-1}, and a bandpass of 650–750 nm. HI2 is centered 53.36° from the Sun with a circular 70° field of view, a resolution of 240 arcsec pixel^{-1}, and a bandpass of 400–1000 nm. The heliospheric imagers

on STEREO-A look back at the Earth-Sun line, while the heliospheric imagers on STEREO-B look ahead at the Earth-Sun line (Kaiser 2005).

While the bandpasses, imaging sequences, and processing techniques are not as favorable for discovering comets as those of SOHO, STEREO recently discovered its first Kreutz comets which were apparently unobserved by SOHO (Battams *et al.* 2008). It has also observed a number of Kreutz comets which have also been seen by SOHO (Marsden and Battams 2008a,b; Marsden and Baldwin 2008), although no Marsden, Kracht, or Meyer group comets as of May 2008. The additional observations yielded improved orbital calculations and increased lightcurve coverage. STEREO cannot rival SOHO in sheer quantity of sungrazer detections, but the quality of the observations of the comets it does observe is superior due to its smaller angular resolution over a larger range of distances relative to SOHO.

STEREO allows simultaneous imaging of comets from two different viewing geometries (three when combined with SOHO). Comparison of the apparent magnitudes for each spacecraft will allow a direct calculation of the scattering phase dependence (see the discussion in Section 2.3.2). The dependence of the scattering on the phase angle will allow estimates of the sizes of typical particles in the coma and of the dust to gas ratio of the coma. This will also improve the correction of the apparent magnitudes in the SOHO field of view, since the comets Marcus (2007b) used to calculate the phase dependence (Equation 2.5) were observed at much larger heliocentric distances and may have had different compositions, dust size distributions, and dust to gas ratios than do sungrazing comets.

5.3.2 Ground Based Telescopes

In the next few years, several large scale ground-based surveys are scheduled to begin collecting data: Pan-STARRS (Hawaii), LSST (Chile), and the Discovery Channel Telescope (Arizona). With the preponderance of large survey telescopes largely dedicated to searching for comets and near Earth objects, what are the chances that sungrazing comets will be observed from the ground?

A survey for Kreutz comets would look for them several months prior to perihelion. Due to the range of orbits, it is necessary to survey a wide area (at least 10 square degrees) ideally with non-sidereal tracking at the expected rate of motion of the comets in that field of view. Because the comets are not known prior to being seen by SOHO, regions of the sky statistically likely to contain them must be chosen. The survey would ideally be carried out in the southern hemisphere with a telescope capable of imaging at relatively small solar elongations. Most of the planned surveys will observe too far from the Sun to discover Kreutz comets, although Pan-STARRS has plans to look for near-Earth objects at "sweet spots" some 60° from the Sun along the ecliptic which may be promising, although a comparable survey in the southern hemisphere would be preferable.

The magnitude of the Kreutz comets at these distances is unknown, but based on a preliminary search we undertook using the KPNO 4-m in January 2005, the rate of brightening is likely steeper than $\propto r^{-3.5}$. Even if the slope of the brightening is much steeper than this, the flux of Kreutz comets is large enough that we are hopeful that the occasional large comet will be detected. If such a comet were bright enough, high resolution photometry might allow determination of the rotation rate and size. Discovery of a comet prior to its entering the SOHO field of view would allow the SOHO team to plan observing sequences such as cycling through the

range of filters available on C2 and C3 (perhaps with a higher cadence and shorter observing times since the brightest comets saturate the detector) and alignment of the UVCS spectrograph.

With their short orbital periods and orbits which can come very close to the Earth, the Marsden and Kracht comets are a better target than the Kreutz comets, despite their apparently smaller sizes and much fewer numbers. Marsden comets pass within 0.025 AU in June (post perihelion) and 0.35 AU in July/August (pre-perihelion). Kracht comets pass within 0.1 AU in mid-June (post-perihelion) and 0.25 AU (pre-perihelion) in July/August (Meyer 2003). The best candidate for future observation is Marsden comet C/2004 V9 which is expected to reach perihelion 2010 May 9. This is the brightest comet in the Marsden or Kracht groups, has the most favorable geometry for observation from the ground, and if observed in 2010, would be seen for the third time. If it fades $\propto r^{-4}$ from its brightness near perihelion it would be about magnitude 10 at closest Earth approach. If instead it is inactive and behaves like an asteroid of radius 30 meters it would be about magnitude 19 at closest Earth approach (ignoring phase effects). Furthermore, the close approach might allow it to be observed in the radar, which would vastly improve the orbital certainty and yield information about the size, shape, and rotation. C/2004 L10 is the best Kracht candidate for observation from the ground, with perihelion around 2009 May 29. However it is likely smaller than C/2004 V9 and will pass at a larger distance. Finally, the Kracht comet C/2008 E4 may have a reasonably close approach to Earth prior to its next return around 2013 September 9, however since it has only been observed twice, the orbital uncertainty is considerably larger than it would be for C/2004 V9 or C/2004 L10 after they have been observed three times, and its closest approach to Earth is much larger.

It is unlikely that the Meyer group will be observable from the ground. While

it is has more members than either the Marsden or Kracht groups, there are far fewer members than in the Kreutz family. The brightest comets in the group have only reached magnitude ∼5, making them difficult to observe beyond the SOHO field of view unless they pass close to the Earth. The high inclination of the orbit prevents close approaches to the Earth, and the lack of apparent repeat observations or suspected linkages to ground observed objects makes it impossible to search along a known orbit.

One additional sungrazer which merits consideration for observing from the ground but has not been discussed to this point is P/1999 R1=P/2003 R5=P/2007 R5. This has now been reobserved twice by SOHO and is the first confirmed periodic comet discovered by SOHO (Battams *et al.* 2007). Its third return was predicted by Hönig (2006) who attempted to recover it from the ground prior to the 2007 perihelion passage, but could not detect it to a limiting magnitude of ∼19 (Hönig 2007, private communication). Now that it has been seen three times, the orbital uncertainty is considerably better which will allow deeper integrations over a smaller area. This comet is of particular interest as it is near a 3:1 resonance with Jupiter and appears to have been in a stable ∼4.0 year orbit for many orbits. While the comet appeared diffuse in C2 images (Knight and Battams 2007), it is uncertain how long a comet could remain active in such an orbit, and it has been suggested that it is really an asteroid or defunct comet nucleus (with the apparent diffusivity in C2 attributed to a varying PSF as it crosses the detector). Ground based observations might lend further insight into its origin and current state, particular if a high quality lightcurve can be used to estimate its size (assuming it is inactive at larger distances) or brightness as a function of heliocentric distance.

Appendix A

Orbital Elements of Sungrazing Comets

This appendix lists the orbital elements of various sungrazing comets. Table A.1 lists the likely members of the Kreutz family seen from the ground. Table A.2 lists the Kreutz comets seen by SMM and Solwind from 1979–1989. Table A.3 lists all Marsden comets seen by SOHO. Table A.4 lists all Kracht comets seen by SOHO. In the interest of space we have not listed the elements of the Meyer and Kreutz comets seen by SOHO, however any reader wishing to use these may contact the author for a complete list.

Due to space limitations, the sources cited for all SOHO observed orbital elements are omitted from the bibliography. We instead direct the reader to the Minor Planet Electronic Circular (MPEC) or International Astronomical Union Circular (IAUC) cited in the table. We note that in a few instances (mostly comets discovered before 1998), the electronic and paper circulars disagree. In these cases we quote the elements given on the paper circulars. Where the elements given on a later circular superseded the elements on an earlier circular, we only give the later

Name	Perihelion Date	q (AU)	e	$\omega(^\circ)$	$\Omega(^\circ)$	i $(^\circ)$	Source
372 BCE	Winter 372 BCE	—	—	—	—	—	K99
X/1106 C1	1106 Jan 26.5	—	—	—	—	—	SC07
C/1843 D1	1843 Feb 27.911	0.00553	0.999914	82.64	2.83	144.35	M89
C/1880 C1	1880 Jan 28.118	0.00549	1.0	86.24	7.08	144.66	M89
X/1882 K1	1882 May 17.463	0.00534	1.0	86.16	7.69	144.50	K03
C/1882 R1	1882 Sep 17.724	0.00775	0.999907	69.59	346.96	142.00	M89
C/1887 B1	1887 Jan 11.934	0.00483	1.0	83.51	3.88	144.38	M89
C/1945 X1	1945 Dec 27.965	0.00752	1.0	72.06	350.50	141.87	M89
C/1963 R1	1963 Aug 23.956	0.00506	0.999946	86.16	7.24	144.58	M89
C/1965 S1	1965 Oct 21.184	0.00779	0.999915	69.05	346.30	141.86	M89
C/1970 K1	1970 May 14.486	0.00888	1.0	61.29	336.32	139.07	M89

Table A.1: Orbital elements of probable members of the Kreutz family which were observed from the ground. The elements are for an epoch close to perihelion. Orbits with e=1.0 had only parabolic solutions. The sources are as follows: K99 = Kronk (1999), SC07 = Sekanina and Chodas (2007), M89 = Marsden (1989), K03 = Kronk (2003).

elements and only cite the later circular.

Name	Perihelion Date	q (AU)	$\omega(^\circ)$	$\Omega(^\circ)$	i $(^\circ)$	Satellite	Source
C/1979 Q1	1979 Aug 30.949	0.00480	67.67	344.30	141.45	Solwind	M89
C/1981 B1	1981 Jan 27.100	0.00792	65.43	341.41	140.67	Solwind	M89
C/1981 O1	1981 Jul 20.336	0.00612	68.43	345.26	141.70	Solwind	M89
C/1981 V1	1981 Nov 4.532	0.00450	77.68	356.87	143.84	Solwind	M89
C/1981 W1	1981 Nov 20.61	0.0048	97.36	24.63	135.48	Solwind	IAUC8566
C/1983 N2	1983 Jul 7.89	0.0049	81.43	359.55	142.23	Solwind	IAUC8573
C/1983 S2	1983 Sep 25.188	0.00753	78.58	357.98	143.98	Solwind	M89
C/1984 O2	1984 Jul 28.556	0.01541	56.67	329.74	136.38	both	M89
C/1984 Q1	1984 Aug 23.22	0.0049	81.04	355.72	144.14	Solwind	IAUC8573
C/1987 T2	1987 Oct 6.069	0.00538	80.59	0.46	144.25	SMM	M89
C/1987 U4	1987 Oct 18.027	0.00627	82.63	2.96	144.46	SMM	M89
C/1988 M1	1988 Jun 27.784	0.00516	85.88	6.96	144.70	SMM	M89
C/1988 Q1	1988 Aug 21.819	0.00591	82.25	2.50	144.43	SMM	M89
C/1988 T1	1988 Oct 12.072	0.00513	88.08	9.65	144.78	SMM	M89
C/1988 U1	1988 Oct 24.864	0.00579	86.14	7.28	144.71	SMM	M89
C/1988 W1	1988 Nov 18.369	0.00590	91.08	13.32	144.79	SMM	M89
C/1989 L1	1989 Jun 2.578	0.00557	84.72	5.54	144.63	SMM	M89
C/1989 N3	1989 Jul 8.772	0.00462	91.80	14.20	144.78	SMM	M89
C/1989 S1	1989 Sep 28.855	0.00476	87.50	8.94	144.76	SMM	IAUC4884

Table A.2: Orbital elements of Kreutz comets observed by Solwind and SMM from 1979–1989. The elements are for an epoch close to perihelion. Due to the short orbital arc, all solutions are only for parabolic orbits ($e = 1.0$). C/1984 O2 was observed by both SMM and Solwind. The sources are as follows: M89 = Marsden (1989), IAUC8566 = Kracht and Marsden (2005a), IAUC8573 = Kracht and Marsden (2005c), IAUC4884 = St. Cyr *et al.* (1989).

Name	Perihelion Date	q (AU)	$\omega(^\circ)$	$\Omega(^\circ)$	$i(^\circ)$	Source
C/1996 V2	1996 Nov 11.78	0.0488	11.84	89.36	33.41	MPEC 2005-F31
C/1997 B5	1997 Jan 29.51	0.0512	23.98	78.00	25.10	MPEC 2006-C49
C/1997 B6	1997 Jan 29.61	0.0501	23.13	76.41	24.95	MPEC 2006-C49
C/1997 B7	1997 Jan 29.65	0.0490	22.39	74.98	24.78	MPEC 2006-C49
C/1998 A2	1998 Jan 03.74	0.0410	26.31	80.78	27.93	MPEC 2002-E25
C/1998 A3	1998 Jan 09.30	0.0419	22.97	80.73	27.35	MPEC 2002-E25
C/1998 A4	1998 Jan 10.79	0.0431	21.35	81.03	26.87	MPEC 2002-F70
C/1999 J6	1999 May 11.59	0.0492	22.47	81.69	26.53	IAUC 7832
C/1999 N5	1999 Jul 11.24	0.0496	27.20	82.49	27.08	MPEC 2002-F03
C/1999 P6	1999 Aug 05.11	0.0494	21.49	82.01	26.57	MPEC 2002-F43
C/1999 P8	1999 Aug 14.99	0.0494	21.28	81.85	26.56	MPEC 2002-F43
C/1999 P9	1999 Aug 15.04	0.0493	21.51	81.74	26.55	MPEC 2002-F43
C/1999 U2	1999 Oct 25.23	0.0492	22.22	82.05	27.05	MPEC 1999-U29
C/2000 C7	2000 Feb 04.48	0.0481	22.34	81.06	24.89	MPEC 2002-K48
C/2000 C3	2000 Feb 04.59	0.0487	23.47	81.85	24.97	IAUC 7832
C/2000 C4	2000 Feb 05.17	0.0487	23.05	81.95	24.97	IAUC 7832
C/2002 R1	2002 Sep 02.54	0.0492	33.67	70.43	22.19	MPEC 2002-R57
C/2002 R4	2002 Sep 03.30	0.0520	20.16	85.69	28.31	MPEC 2002-S35
C/2002 V5	2002 Nov 12.42	0.0506	19.13	86.61	34.24	MPEC 2003-C02
C/2003 Q1	2003 Aug 20.97	0.0320	52.38	43.43	29.33	MPEC 2004-J19
C/2003 Q6	2003 Aug 26.51	0.0366	33.17	56.30	25.43	MPEC 2004-J19
C/2004 V10	2004 Nov 08.45	0.0488	22.79	81.86	26.40	MPEC 2004-X73
C/2004 V9	2004 Nov 08.56	0.0492	22.51	81.51	26.52	MPEC 2004-X73
C/2004 W10	2004 Nov 29.26	0.0467	25.29	82.11	25.97	MPEC 2005-A13
C/2005 E4	2005 Mar 10.54	0.0487	22.24	80.60	26.43	MPEC 2005-E87
C/2005 G2	2005 Apr 14.26	0.0492	23.53	80.69	26.84	MPEC 2005-H24
C/2005 W1	2005 Nov 17.28	0.0482	23.44	80.29	24.88	MPEC 2005-W07
C/2005 W5	2005 Nov 29.91	0.0494	22.26	81.77	26.91	MPEC 2005-X14
C/2006 E2	2006 Mar 15.42	0.0482	21.86	80.94	24.50	MPEC 2006-F50
C/2006 F3	2006 Mar 25.54	0.0510	19.10	85.31	23.02	MPEC 2006-F50
C/2007 Y4	2007 Dec 22.16	0.0505	23.03	82.08	28.59	MPEC 2008-B49
C/2008 A3	2008 Jan 15.75	0.0493	33.70	70.18	22.28	MPEC 2008-B61

Table A.3: Orbital elements of the Marsden comets observed by SOHO. The elements are for an epoch close to perihelion. Due to the short orbital arc, all solutions are only for parabolic orbits ($e = 1.0$). Due to space limitations, the sources cited here are omitted from the bibliography. We instead direct the reader to the Minor Planet Electronic Circular (MPEC) or International Astronomical Union Circular (IAUC) cited.

Name	Perihelion Date	q (AU)	$\omega(^\circ)$	$\Omega(^\circ)$	$i(^\circ)$	Source
C/1996 X3	1996 Dec 06.17	0.0426	63.68	51.00	14.78	MPEC 2006-C49
C/1996 X4	1996 Dec 06.28	0.0492	51.86	50.79	13.70	MPEC 2006-C49
C/1996 X5	1996 Dec 06.33	0.0490	51.17	51.28	13.78	MPEC 2006-C49
C/1999 M3	1999 Jun 30.70	0.0441	68.03	36.33	12.35	MPEC 2002-E18
C/1999 N6	1999 Jul 12.30	0.0435	63.97	32.50	12.15	MPEC 2002-F03
C/2000 O3	2000 Jul 30.94	0.0540	48.12	53.46	14.58	MPEC 2000-Q09
C/2001 Q7	2001 Aug 21.80	0.0445	54.77	43.95	13.28	MPEC 2002-F43
C/2001 Q8	2001 Aug 24.81	0.0451	56.22	44.76	13.07	MPEC 2002-O35
C/2001 R8	2001 Sep 06.67	0.0437	59.63	42.19	13.58	MPEC 2002-O35
C/2001 R9	2001 Sep 07.32	0.0472	53.31	48.90	12.47	MPEC 2002-O35
C/2002 N2	2002 Jul 11.92	0.0490	54.78	52.93	13.80	MPEC 2002-Q02
C/2002 Q8	2002 Aug 25.92	0.0462	47.47	51.38	13.84	MPEC 2002-Q46
C/2002 Q8	2002 Aug 25.93	0.0479	51.16	50.38	13.70	MPEC 2008-F32
C/2002 Q10	2002 Aug 27.50	0.0484	51.02	50.99	13.54	MPEC 2002-R02
C/2002 S4	2002 Sep 18.22	0.0484	50.98	50.81	13.51	MPEC 2002-T16
C/2002 S5	2002 Sep 19.33	0.0467	52.01	49.01	14.03	MPEC 2002-T16
C/2002 S7	2002 Sep 21.06	0.0483	51.38	50.57	13.53	MPEC 2002-T25
C/2002 S11	2002 Sep 30.34	0.0482	51.84	50.70	13.68	MPEC 2002-T75
C/2004 A3	2004 Jan 16.16	0.0433	58.54	44.75	14.75	MPEC 2004-M04
C/2004 B3	2004 Jan 18.27	0.0515	53.97	44.90	13.28	MPEC 2004-M04
C/2004 J4	2004 May 05.33	0.0417	69.22	34.30	12.35	MPEC 2004-M71
C/2004 J12	2004 May 12.91	0.0398	71.79	33.74	12.68	MPEC 2004-N04
C/2004 J13	2004 May 13.85	0.0441	64.48	36.12	12.47	MPEC 2004-N04
C/2004 J15	2004 May 14.75	0.0438	67.24	34.56	12.28	MPEC 2004-N05
C/2004 J16	2004 May 14.97	0.0314	69.24	34.39	14.63	MPEC 2004-N05
C/2004 J17	2004 May 15.55	0.0356	72.09	35.60	13.79	MPEC 2004-N05
C/2004 J18	2004 May 15.69	0.0461	65.28	34.23	11.89	MPEC 2004-N05
C/2004 L10	2004 Jun 14.10	0.0431	69.72	35.76	12.54	MPEC 2004-O05
C/2005 W4	2005 Nov 23.49	0.0540	49.00	53.45	14.68	MPEC 2005-X14
C/2008 E4	2008 Mar 3.01	0.0499	50.61	51.85	13.13	MPEC 2008-F32
C/2008 G6	2008 Apr 13.54	0.0483	57.03	49.13	14.35	MPEC 2008-L29

Table A.4: Same as Table A.3 but for the Kracht comets observed by SOHO.

Appendix B

Plots of Selected Lightcurves

In this appendix we plot the lightcurves of the Kreutz comets observed to peak in C3 and all Kracht and Marsden comets discovered by January 2006. This excludes a few Marsden and Kracht comets which have been discovered since then: Kracht comets C/2004 J20 (which was not discovered until mid-2007) and C/2008 E4 and Marsden comets C2006 E2, C/2006 F3, C/2007 Y4, C/2008 A3, and C/2008 G6. The comets are plotted by group in chronological order of perihelion time. Table B.1 lists the Kreutz comets with a reliably determined peak. These are plotted in Figures B.1–B.9. The Kracht comets are in Figures B.10–B.13 and the Marsden comets are in Figures B.14–B.17.

SOHO internal numbers are given in each plot and the corresponding IAU designation is listed in the caption. All magnitudes have been normalized to Δ=1 AU and phase angle = 90° as discussed in Section 2.2. C2 orange filter images are orange triangles, C3 clear filter images are green circles, and C3 orange filter images are orange asterisks. Open points denote images in which the vignetting was greater than 4.0.

Since all Kreutz comets were observed prior to perihelion we plot the brightness as a function of distance. However, since the Kracht and Marsden comets were

observed both before and after perihelion and with a range of perihelion distances, we found the lightcurves to be most informative when plotted as a function of time relative to perihelion. The vast majority of the Kracht and Marsden comets are near the detection threshold resulting in much noisier lightcurves than for the Kreutz comets. Thus most of these comets are simply detected and no meaningful photometric interpretation can be made from the lightcurve, however we include them for completeness.

Table B.1: Kreutz comets which have a reliably determined peak in C3. The distance of the peak is likely only good to ± 0.5 $R_\odot$. The apparent visual magnitude of the peak is given for C3 and for C2 when possible. When the C2 peak is not visible, the maximum observed brightness is listed. The group identification is based on the shape of the lightcurve as discussed in Section 3.4.1. Comets are listed in order of perihelion time. The comets which are italicized saturated the detector. The internal SOHO numbers are included for comparison with Biesecker *et al.* (2002). The lightcurves of these comets are plotted in Figures B.1–B.9.

Designation	SOHO #	Distance of Peak ($R_\odot$)	C2 Peak Magnitude	C3 Peak Magnitude	Group
C/1996 O4	23	12.3	—	5.4	C
C/1996 Q3	2	11.5	—	6.4	C
C/1996 S3	3	13.0	—	5.5	A
C/1997 L3	12	10.6	—	5.0	C
C/1997 M1	15	11.1	—	5.7	C
C/1997 P1	19	12.6	—	3.3	A
C/1997 Q2	25	12.8	—	4.3	A
C/1997 T2	31	10.9	<5.6	6.4	C
C/1998 G4	47	11.4	<3.8	4.6	C
C/1998 H2	48	13.0	<1.1	2.1	A
C/1998 K10	*54*	*10.8*	*0.6*	*0.8*	—
C/1998 K11	*55*	*10.9*	*0.1*	*0.5*	—
C/1998 L1	56	12.8	<5.5	5.4	B
C/1999 C1	58	12.5	—	5.4	A
C/1999 O3	74	11.7	—	5.7	C
C/1999 S1	86	12.6	—	4.8	A
C/2000 B1	97	12.3	—	4.3	A
C/2000 B6	98	11.3	—	6.3	C
C/2000 C6	104	11.1	—	5.2	C
C/2000 D1	106	11.2	—	5.1	C
C/2000 E1	107	12.2	—	5.3	A
C/2000 H2	*111*	*9.7*	*0.5*	*0.7*	—
C/2000 T1	204	12.9	<3.4	4.3	A
C/2001 C3	293	11.6	—	5.9	A
C/2001 C2	294	12.1	—	4.2	A
C/2001 C6	296	10.8	<5.6	5.3	C
C/2001 R2	*347*	*12.8*	*<3.8*	*2.9*	—
C/2001 U4	361	13.7	<6.3	7.3	A
C/2001 U7	365	14.0	<4.3	5.5	A

Continued on next page

Table B.1 – continued from previous page

Designation	SOHO #	Distance of Peak ($R_\odot$)	C2 Peak Magnitude	C3 Peak Magnitude	Group
C/2001 U9	*367*	*13.1*	*<1.4*	*2.8*	—
C/2002 J3	443	10.7	<2.9	4.1	C
C/2002 Q7	503	12.3	—	5.6	B
C/2002 S2	517	12.4	<4.0	3.7	B
C/2002 W12	556	12.5	<4.8	6.4	A
C/2003 A3	579	11.8	—	5.4	A
C/2003 C2	584	12.3	—	4.0	A
C/2003 C5	587	12.1	—	6.4	B
C/2003 F3	592	12.8	<4.2	4.4	C
C/2003 F5	594	12.6	<3.0	3.8	A
C/2003 K7	*614*	*10.8*	*-0.0*	*-0.1*	—
C/2003 L5	624	12.9	3.0	4.0	B
C/2003 O5	644	11.1	<5.0	4.2	C
C/2003 Q2	652	12.3	—	5.2	A
C/2003 Q5	655	11.9	—	4.9	C
C/2003 Q7	657	11.5	—	4.5	C
C/2003 V5	687	12.0	<4.8	5.9	A
C/2003 W6	694	12.0	<4.4	6.0	A
C/2004 A2	724	12.0	—	4.7	B
C/2004 D4	744	12.9	—	4.5	A
C/2004 F6	750	12.3	<5.0	5.3	A
C/2004 O1	819	11.8	—	4.8	B
C/2004 P7	828	12.2	—	5.8	B
C/2004 Q3	829	12.0	—	6.3	B
C/2004 Q4	830	11.8	—	6.1	B
C/2004 R4	833	12.7	—	5.8	B
C/2004 T7	844	11.5	<5.5	6.9	B
C/2005 C3	907	11.3	—	5.0	B
C/2005 D5	913	12.2	<6.4	5.5	A
C/2005 E6	917	11.3	<5.9	5.3	C
C/2005 F1	925	10.8	<6.2	6.2	B
C/2005 L7	972	11.1	3.3	4.3	B
C/2005 N9	993	12.6	<5.5	5.2	B
C/2005 O3	995	12.3	<6.2	4.5	A
C/2005 P1	999	12.2	—	6.5	A
C/2005 S1	1024	13.7	<3.8	4.1	A
C/2005 T11	1031	13.2	<5.3	5.8	A
C/2005 V9	1047	12.2	<4.0	4.9	A
C/2005 Y9	1078	12.2	<4.9	6.3	A
C/2006 A5	1087	11.7	<3.7	3.9	A
C/2006 B3	1091	11.2	—	6.2	A
C/2006 B6	1094	11.2	—	5.8	C

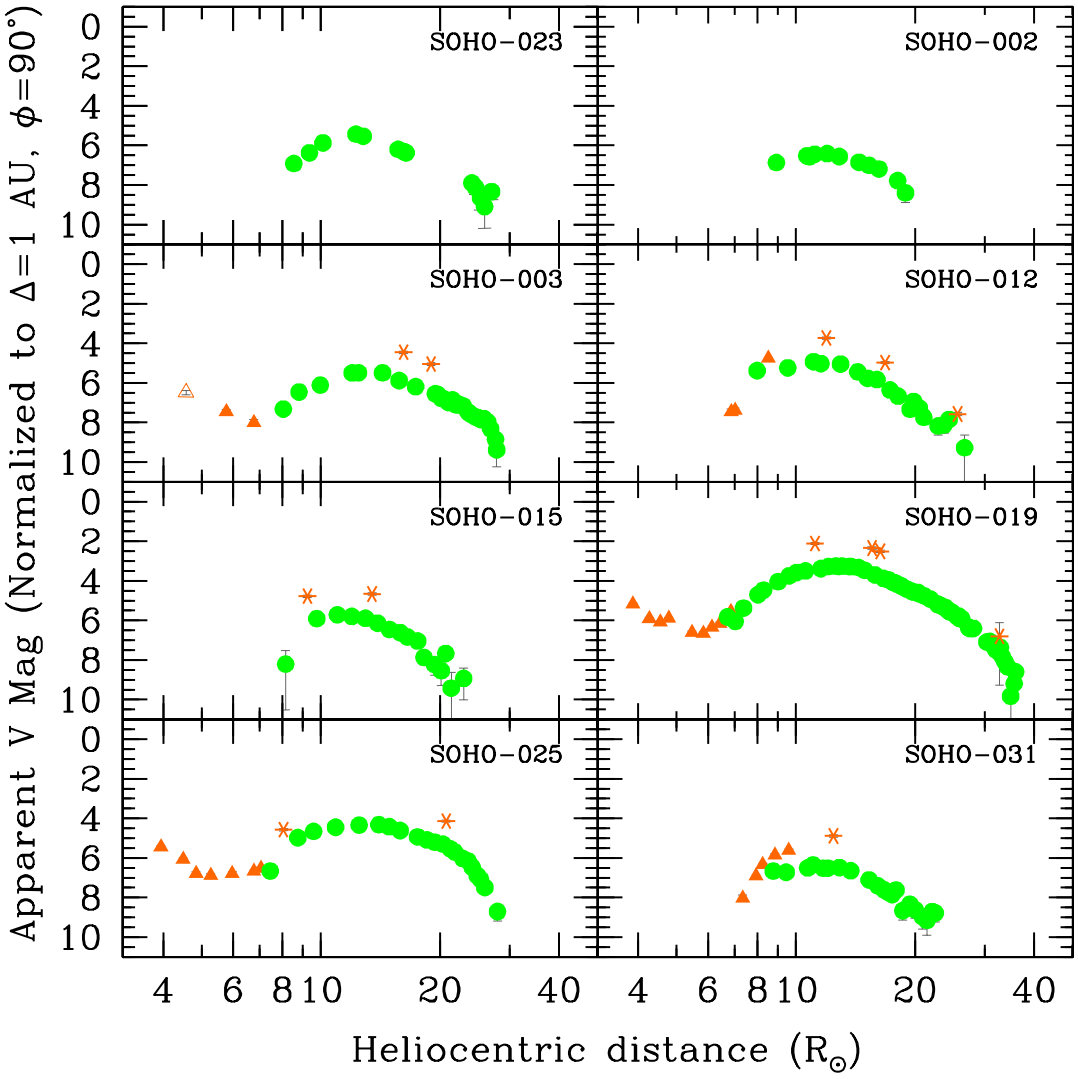

Figure B.1: Lightcurves of Kreutz comets observed to peak in C3. Starting on the top row and moving left to right, these are: C/1996 O4 (SOHO-023), C/1996 Q3 (002), C/1996 S3 (003), C/1997 L3 (012), C/1997 M1 (015), C/1997 P1 (019), C/1997 Q2 (025), and C/1997 T2 (031). Orange triangles are C2 orange filter images, orange asterisks are C3 orange filter images, and green triangles are C3 clear filter image. Solid points have vignetting less than 4, while open points have vignetting greater than 4.

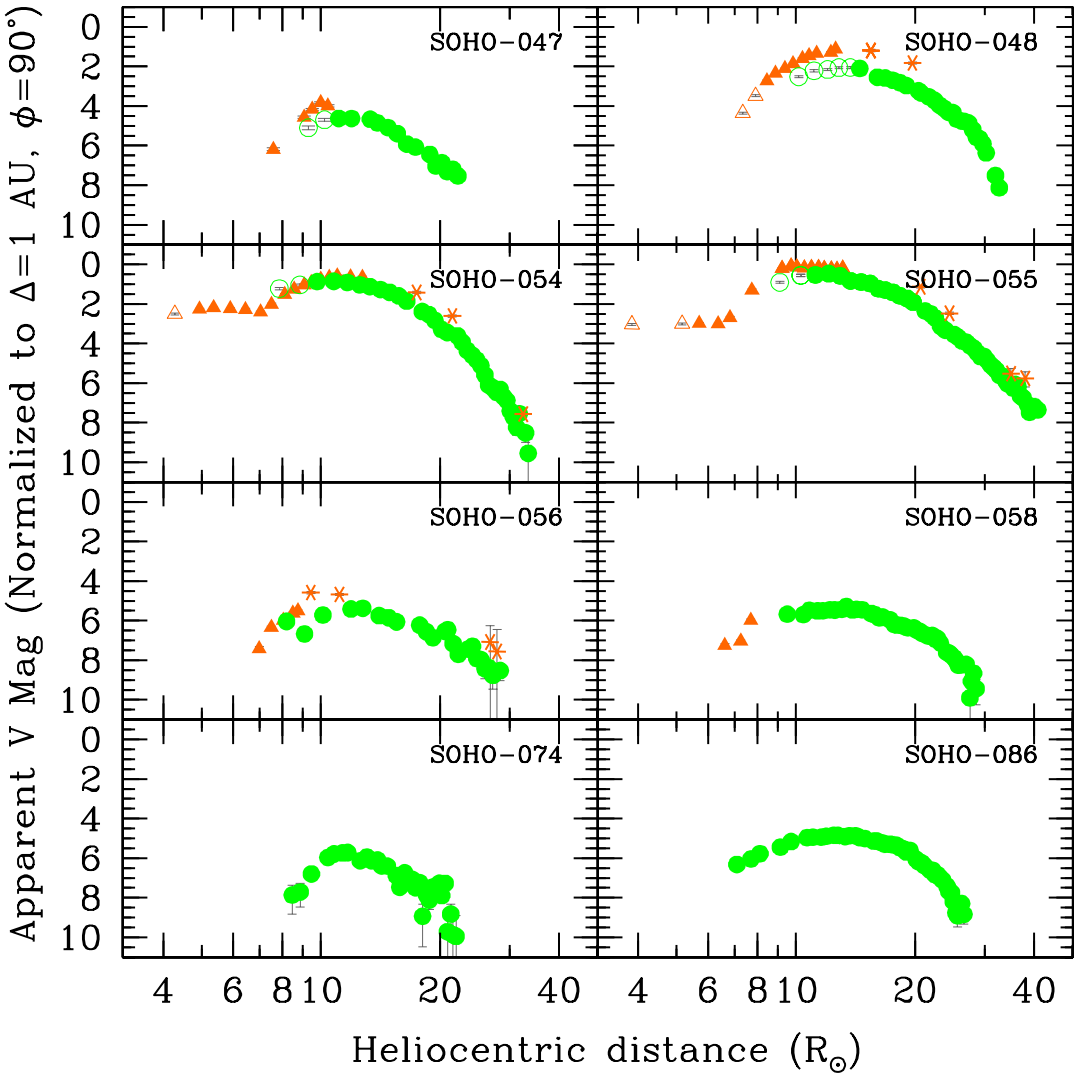

Figure B.2: Lightcurves of Kreutz comets observed to peak in C3. Starting on the top row and moving left to right, these are: C/1998 G4 (SOHO-047), C/1998 H2 (048), C/1998 K10 (054), C/1998 K11 (055), C/1998 L1 (056), C/1999 C1 (058), C/1999 O3 (074), and C/1999 S1 (086). The symbols are as given in Figure B.1.

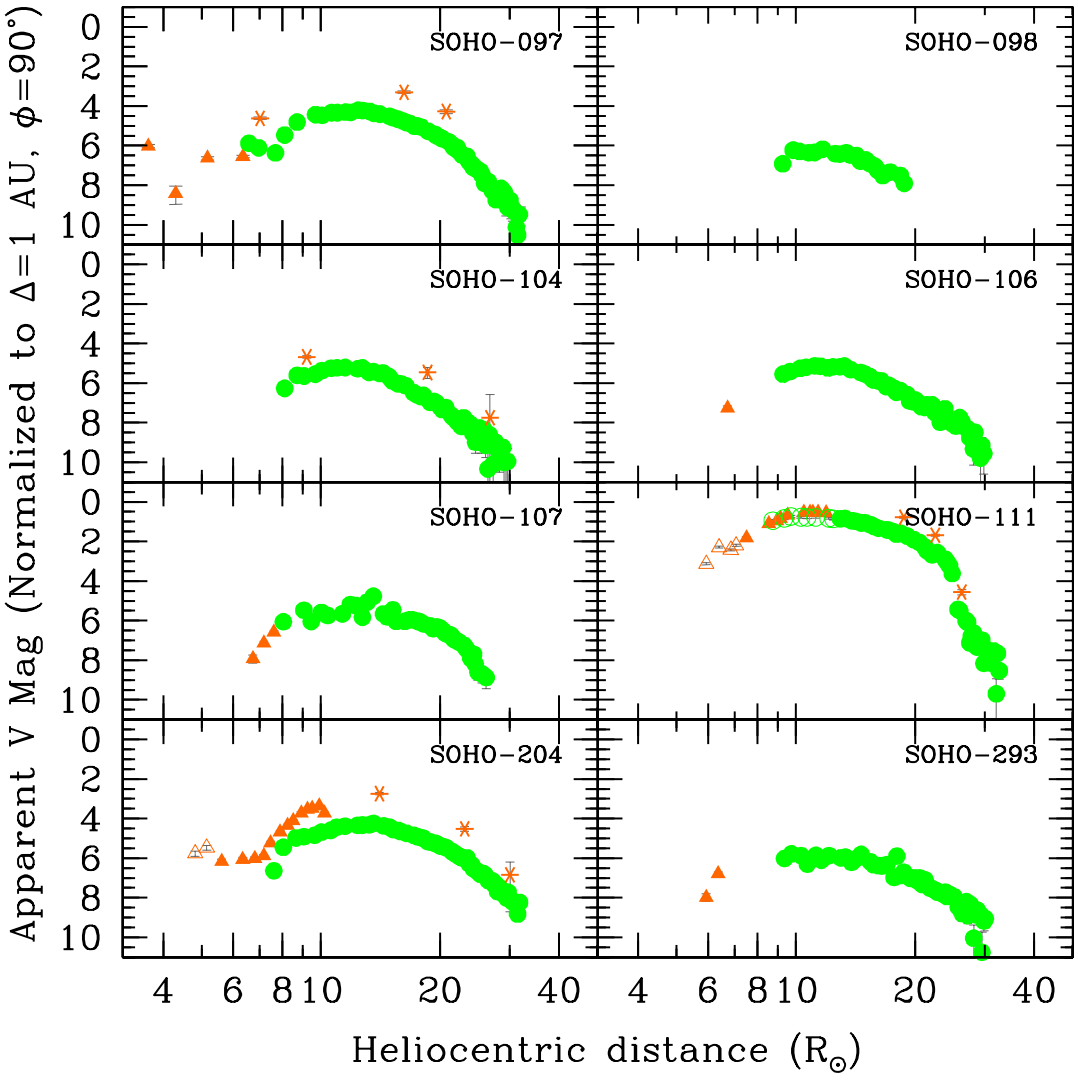

Figure B.3: Lightcurves of Kreutz comets observed to peak in C3. Starting on the top row and moving left to right, these are: C/2000 B1 (SOHO-097), C/2000 B6 (098), C/2000 C6 (104), C/2000 D1 (106), C/2000 E1 (107), C/2000 H2 (111), C/2000 T1 (204), and C/2001 C3 (293). The symbols are as given in Figure B.1.

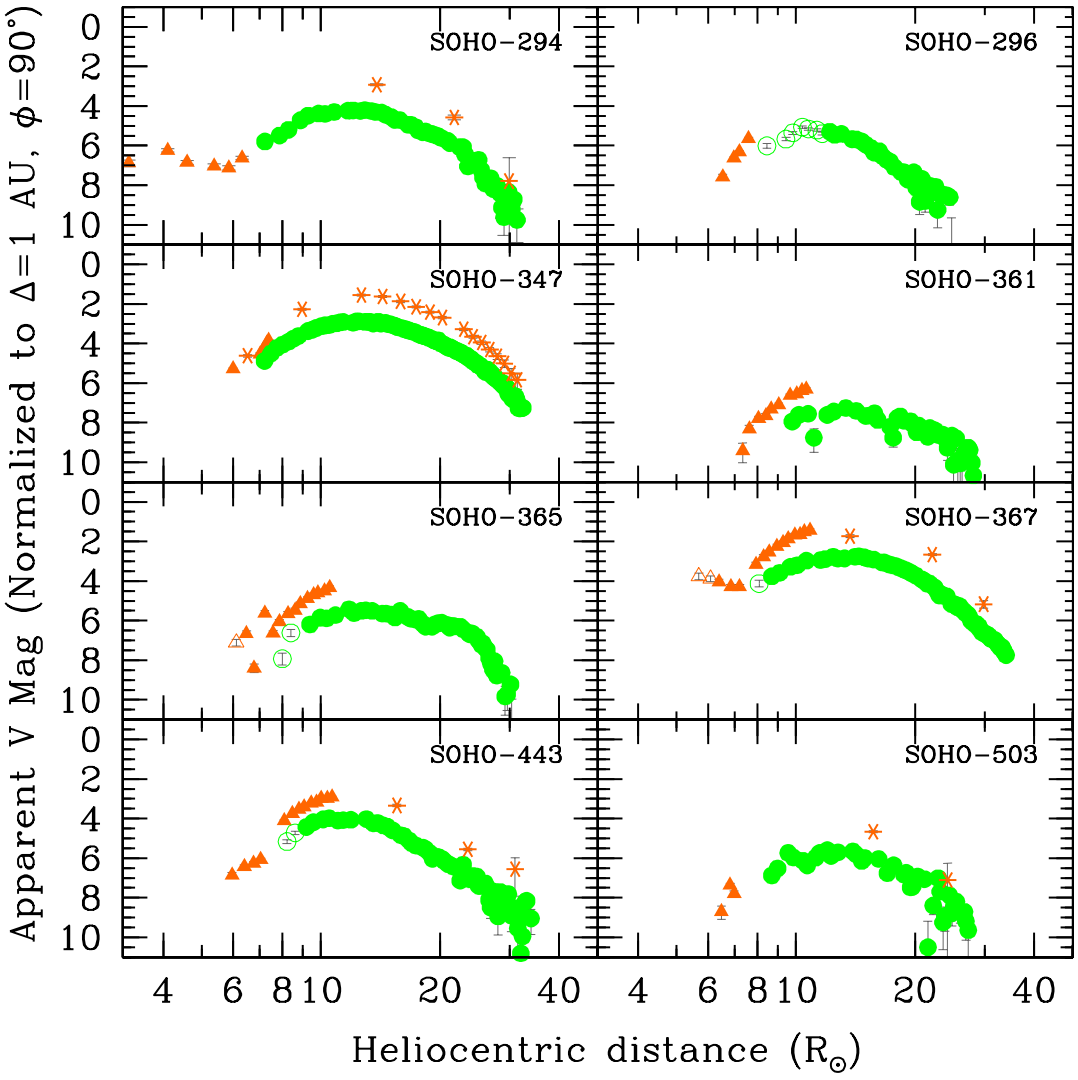

Figure B.4: Lightcurves of Kreutz comets observed to peak in C3. Starting on the top row and moving left to right, these are: C/2001 C2 (SOHO-294), C/2001 C6 (296), C/2001 R2 (347), C/2001 U4 (361), C/2001 U7 (365), C/2001 U9 (367), C/2002 J3 (443), and C/2002 Q7 (503). The symbols are as given in Figure B.1.

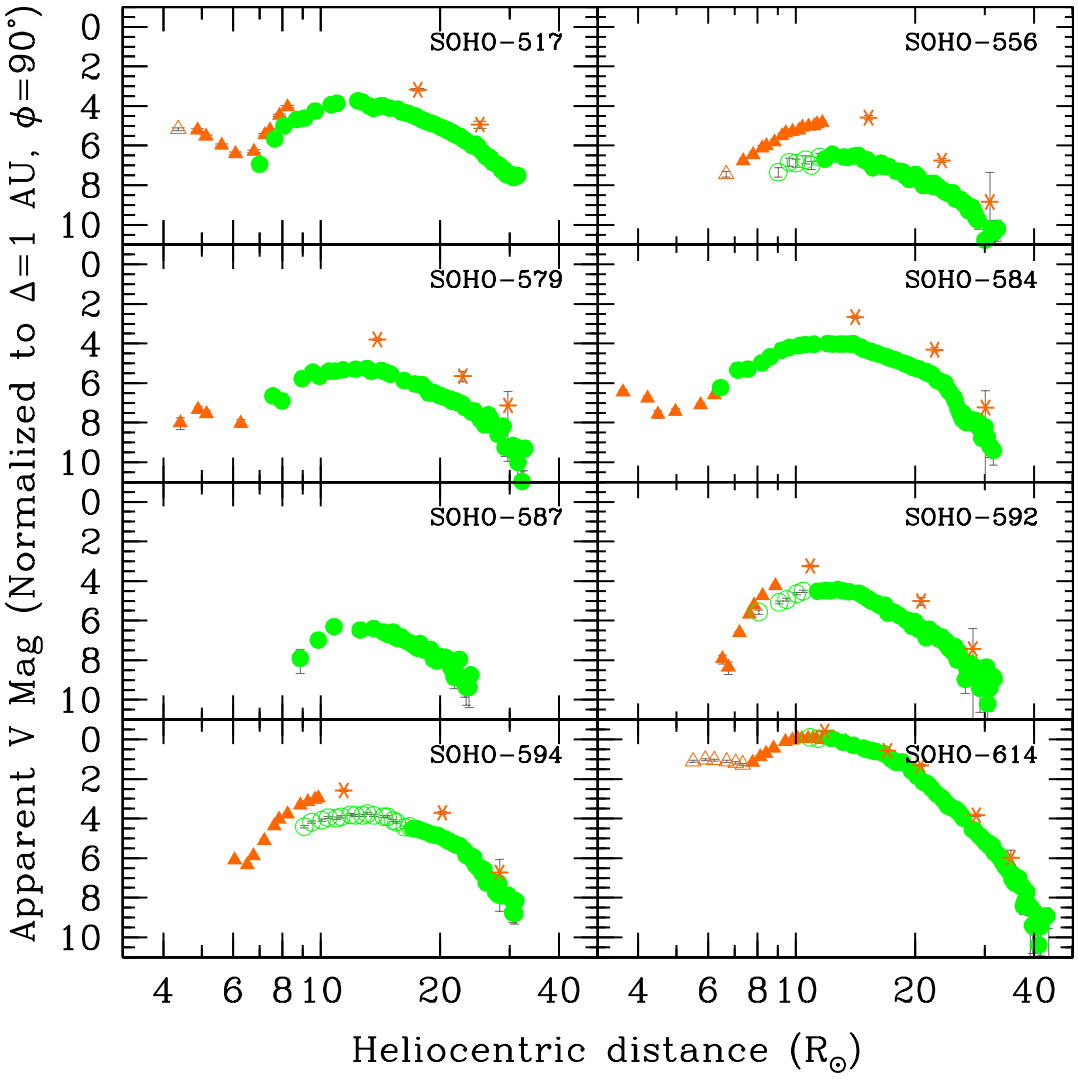

Figure B.5: Lightcurves of Kreutz comets observed to peak in C3. Starting on the top row and moving left to right, these are: C/2002 S2 (SOHO-517), C/2002 W12 (556), C/2003 A3 (579), C/2003 C2 (584), C/2003 C5 (587), C/2003 F3 (592), C/2003 F5 (594), and C/2003 K7 (614). The symbols are as given in Figure B.1.

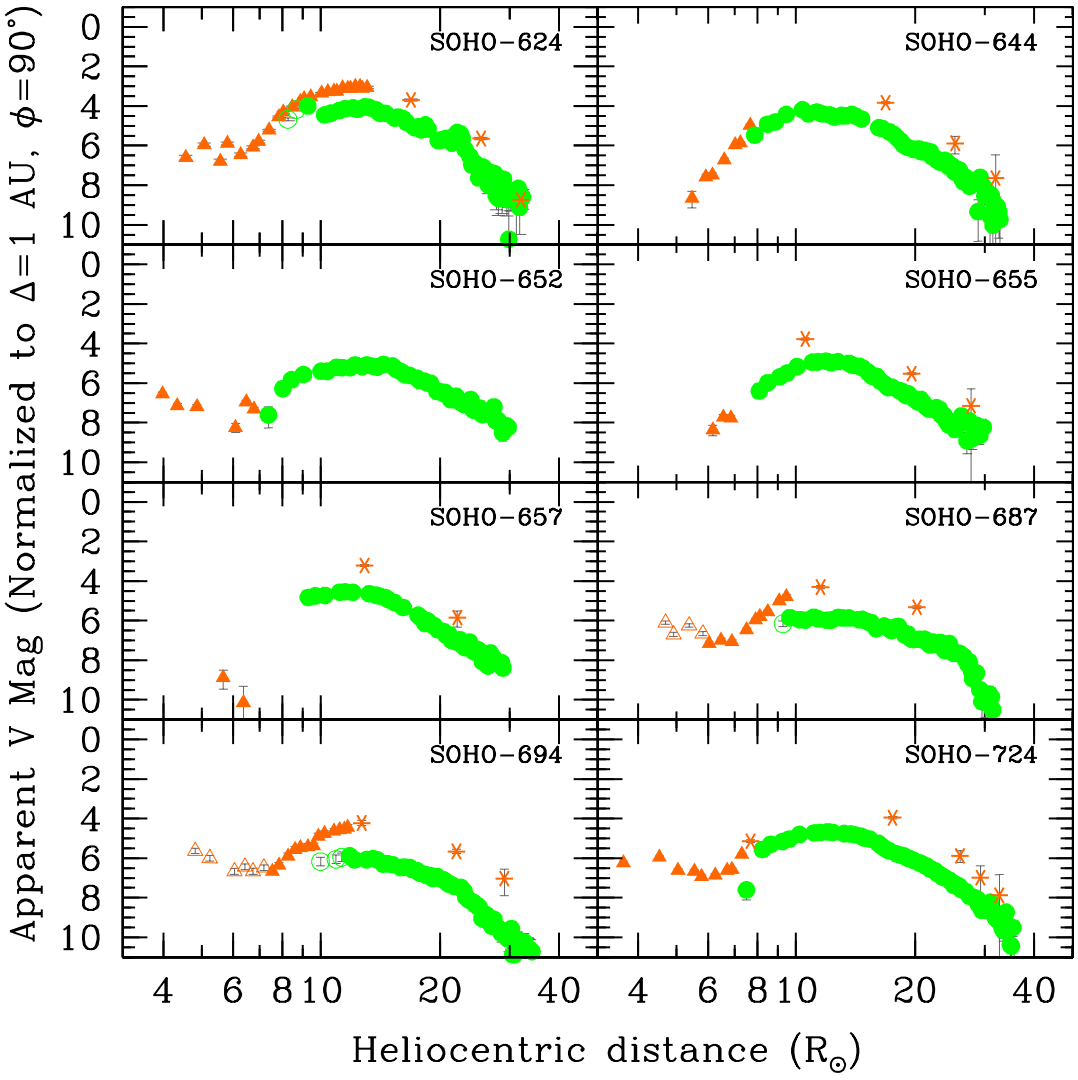

Figure B.6: Lightcurves of Kreutz comets observed to peak in C3. Starting on the top row and moving left to right, these are: C/2003 L5 (SOHO-624), C/2003 O5 (644), C/2003 Q2 (652), C/2003 Q5 (655), C/2003 Q7 (657), C/2003 V5 (687), C/2003 W6 (694), and C/2004 A2 (724). The symbols are as given in Figure B.1.

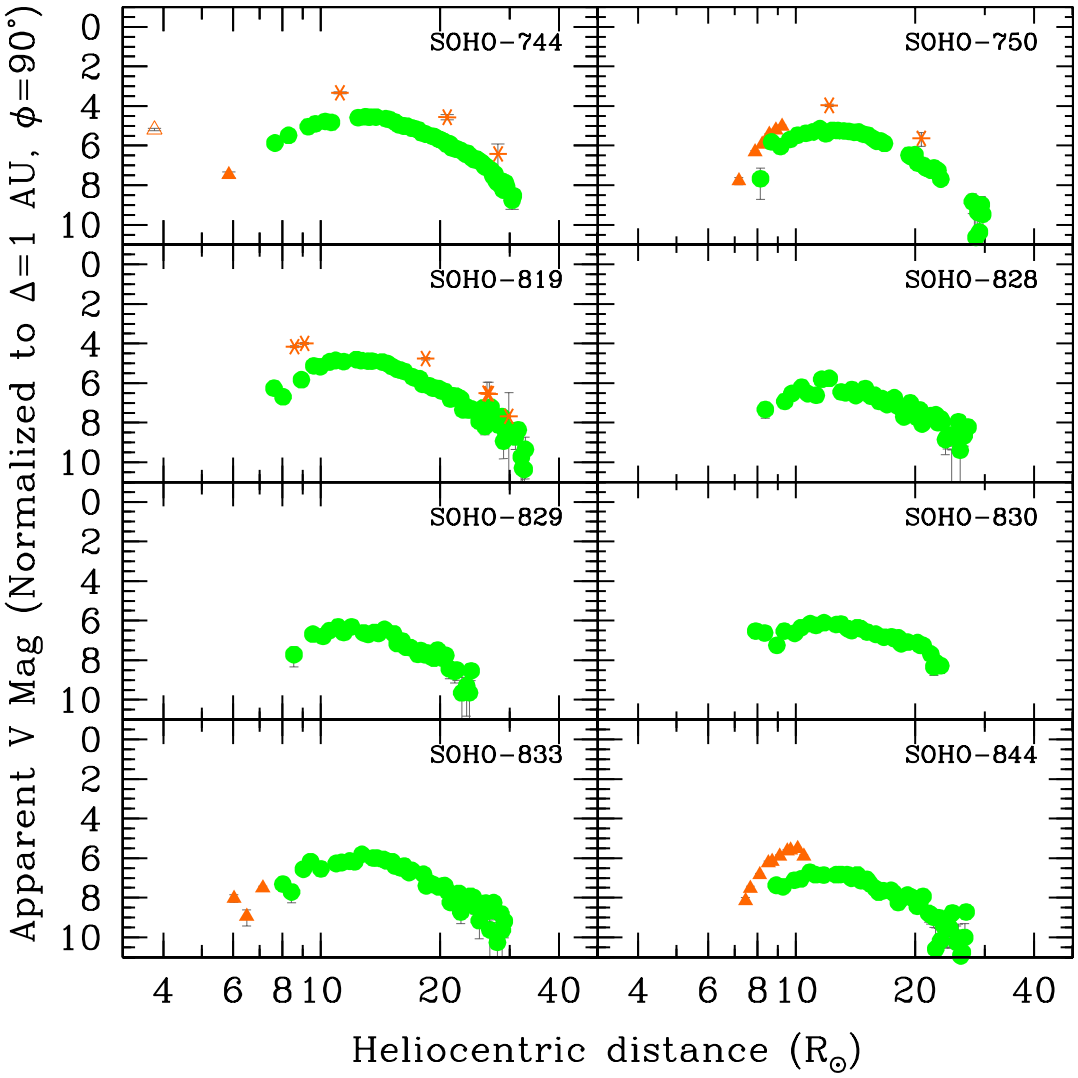

Figure B.7: Lightcurves of Kreutz comets observed to peak in C3. Starting on the top row and moving left to right, these are: C/2004 D4 (SOHO-744), C/2004 F6 (750), C/2004 O1 (819), C/2004 P7 (828), C/2004 Q3 (829), C/2004 Q4 (830), C/2004 R4 (833), and C/2004 T7 (844). The symbols are as given in Figure B.1.

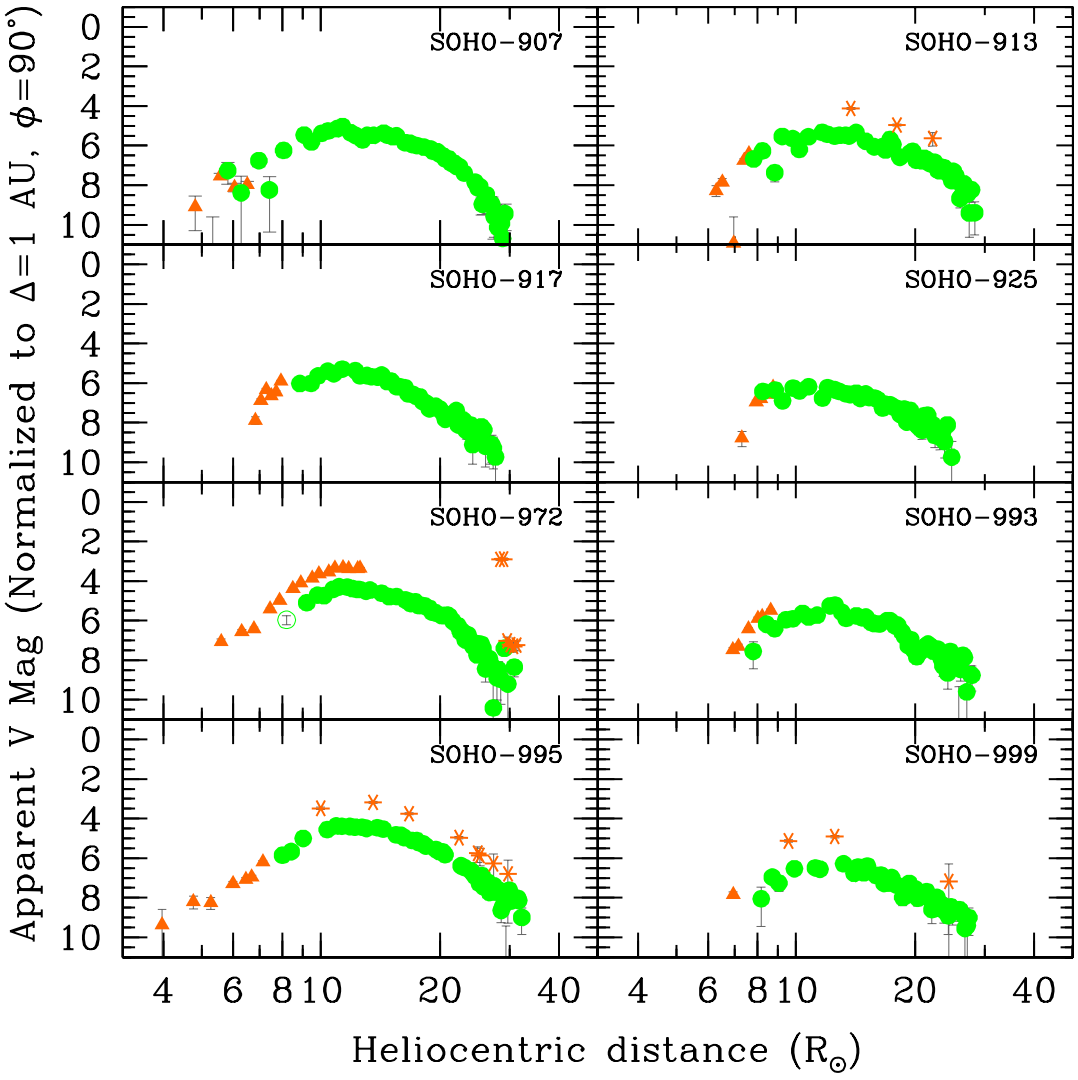

Figure B.8: Lightcurves of Kreutz comets observed to peak in C3. Starting on the top row and moving left to right, these are: C/2005 C3 (SOHO-907), C/2005 D5 (913), C/2005 E6 (917), C/2005 F1 (925), C/2005 L7 (972), C/2005 N9 (993), C/2005 O3 (995), and C/2005 P1 (999). The symbols are as given in Figure B.1.

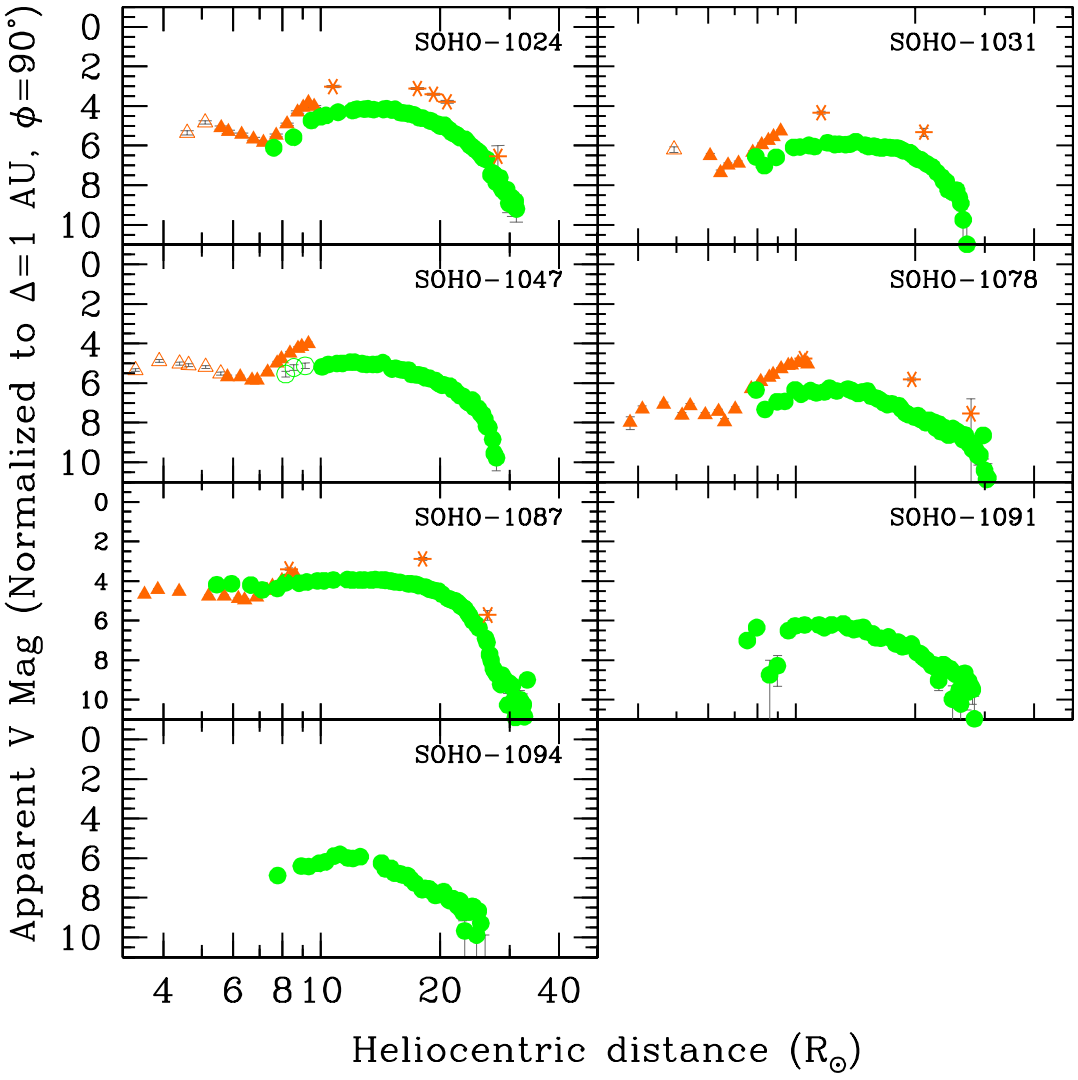

Figure B.9: Lightcurves of Kreutz comets observed to peak in C3. Starting on the top row and moving left to right, these are: C/2005 S1 (SOHO-1024), C/2005 T11 (1031), C/2005 V9 (1047), C/2005 Y9 (1078), C/2006 A5 (1087), C/2006 B3 (1091), and C/2006 B6 (1094). The symbols are as given in Figure B.1.

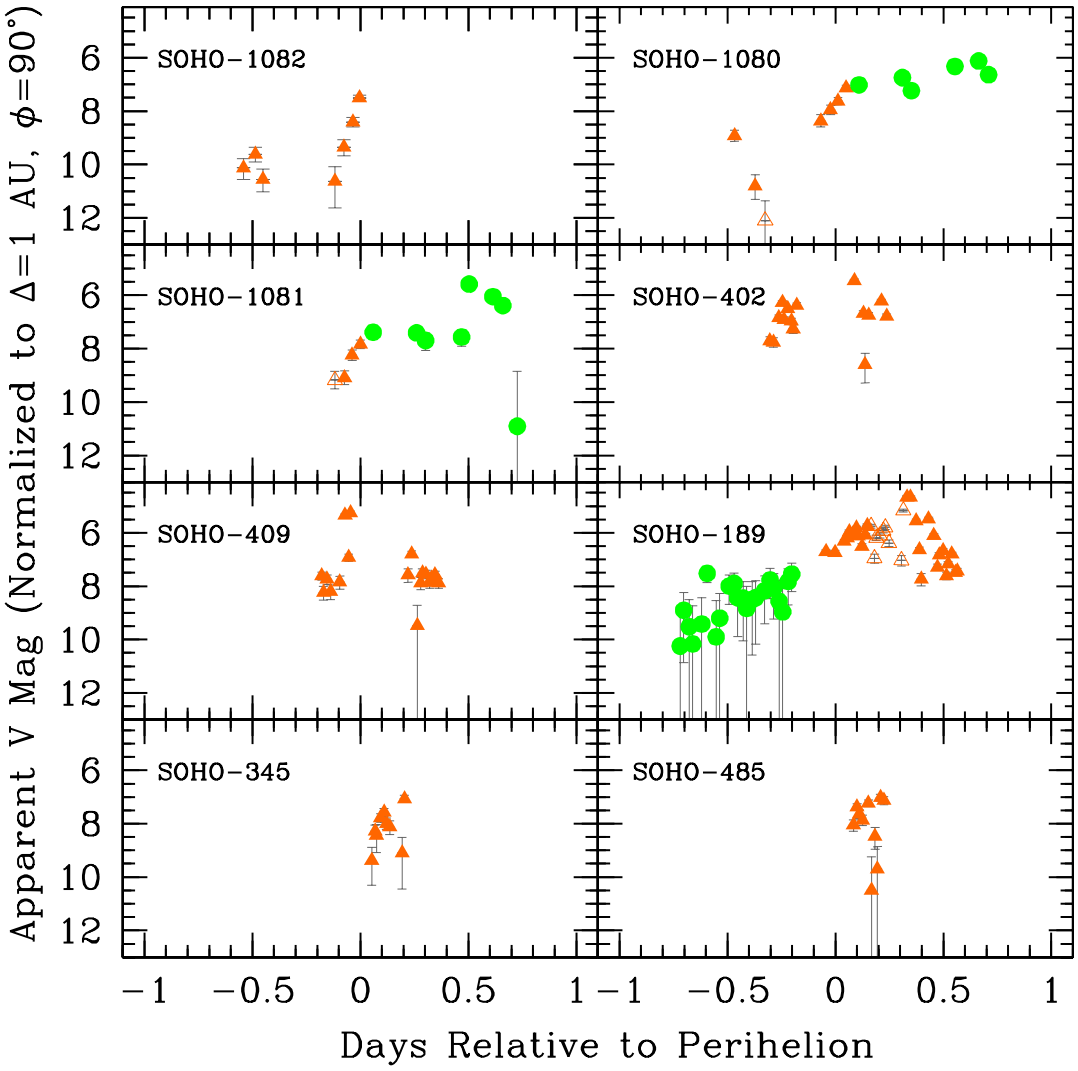

Figure B.10: Lightcurves of Kracht comets. Starting on the top row and moving left to right, these are: C/1996 X3 (SOHO-1082), C/1996 X4 (1080), C/1996 X5 (1081), C/1999 M3 (402), C/1999 N6 (409), C/2000 O3 (189), C/2001 Q7 (345), and C/2001 Q8 (485). The symbols are as given in Figure B.1.

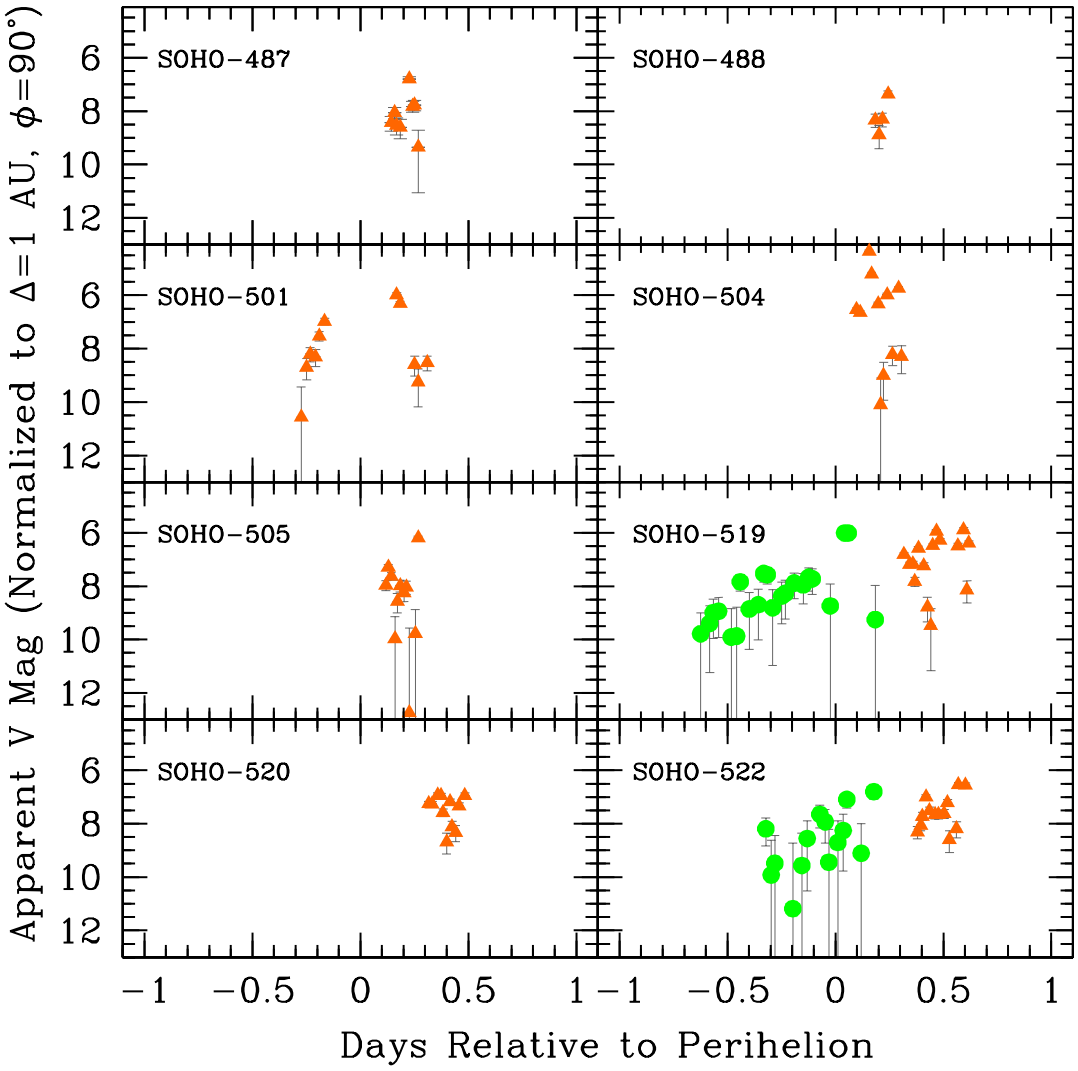

Figure B.11: Lightcurves of Kracht comets. Starting on the top row and moving left to right, these are: C/2001 R8 (SOHO-487), C/2001 R9 (488), C/2002 N2 (501), C/2002 Q8 (504), C/2002 Q10 (505), C/2002 S4 (519), C/2002 S5 (520), and C/2002 S7 (522). The symbols are as given in Figure B.1.

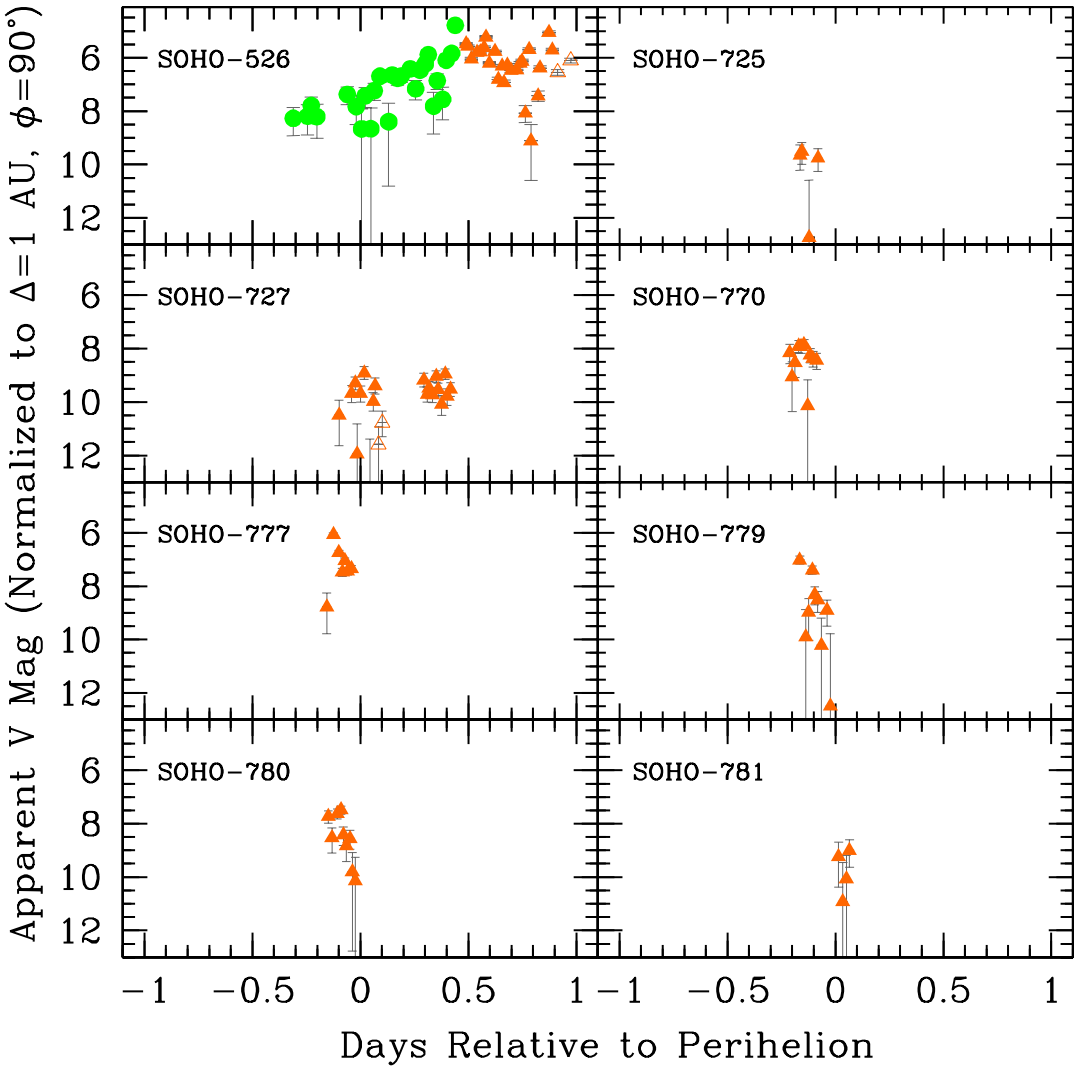

Figure B.12: Lightcurves of Kracht comets. Starting on the top row and moving left to right, these are: C/2002 S11 (SOHO-526), C/2004 A3 (725), C/2004 B3 (727), C/2004 J4 (770), C/2004 J12 (777), C/2004 J13 (779), C/2002 J15 (780), and C/2002 J16 (781). The symbols are as given in Figure B.1.

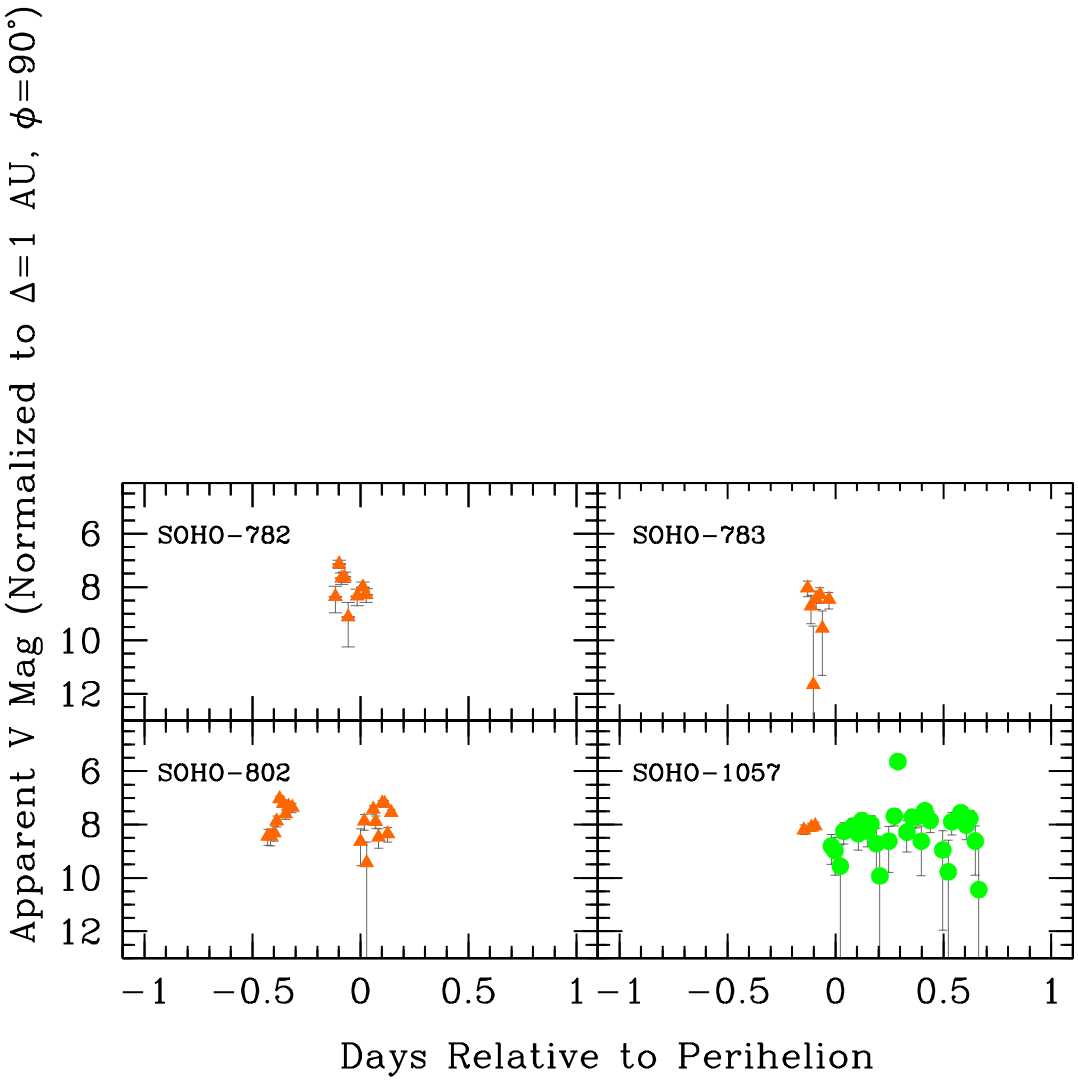

Figure B.13: Lightcurves of Kracht comets. Starting on the top row and moving left to right, these are: C/2004 J17 (SOHO-782), C/2002 J18 (783), C/2004 L10 (802), and C/2005 W4 (1057). The symbols are as given in Figure B.1.

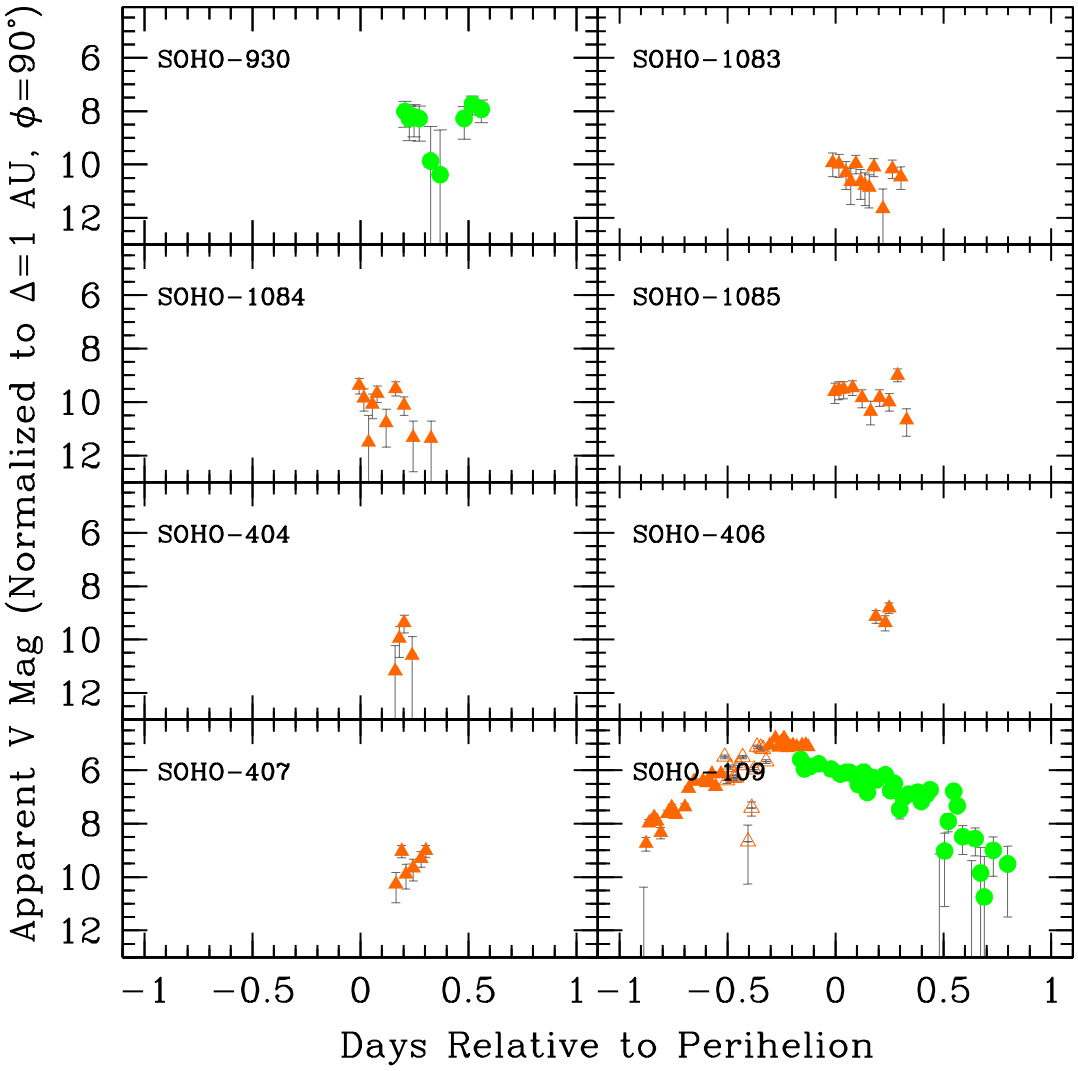

Figure B.14: Lightcurves of Marsden comets. Starting on the top row and moving left to right, these are: C/1996 V2 (SOHO-930), C/1997 B5 (1083), C/1997 B6 (1084), C/1997 B7 (1085), C/1998 A2 (404), C/1998 A4 (406), C/1998 A4 (407), and C/1999 J6 (109). The symbols are as given in Figure B.1.

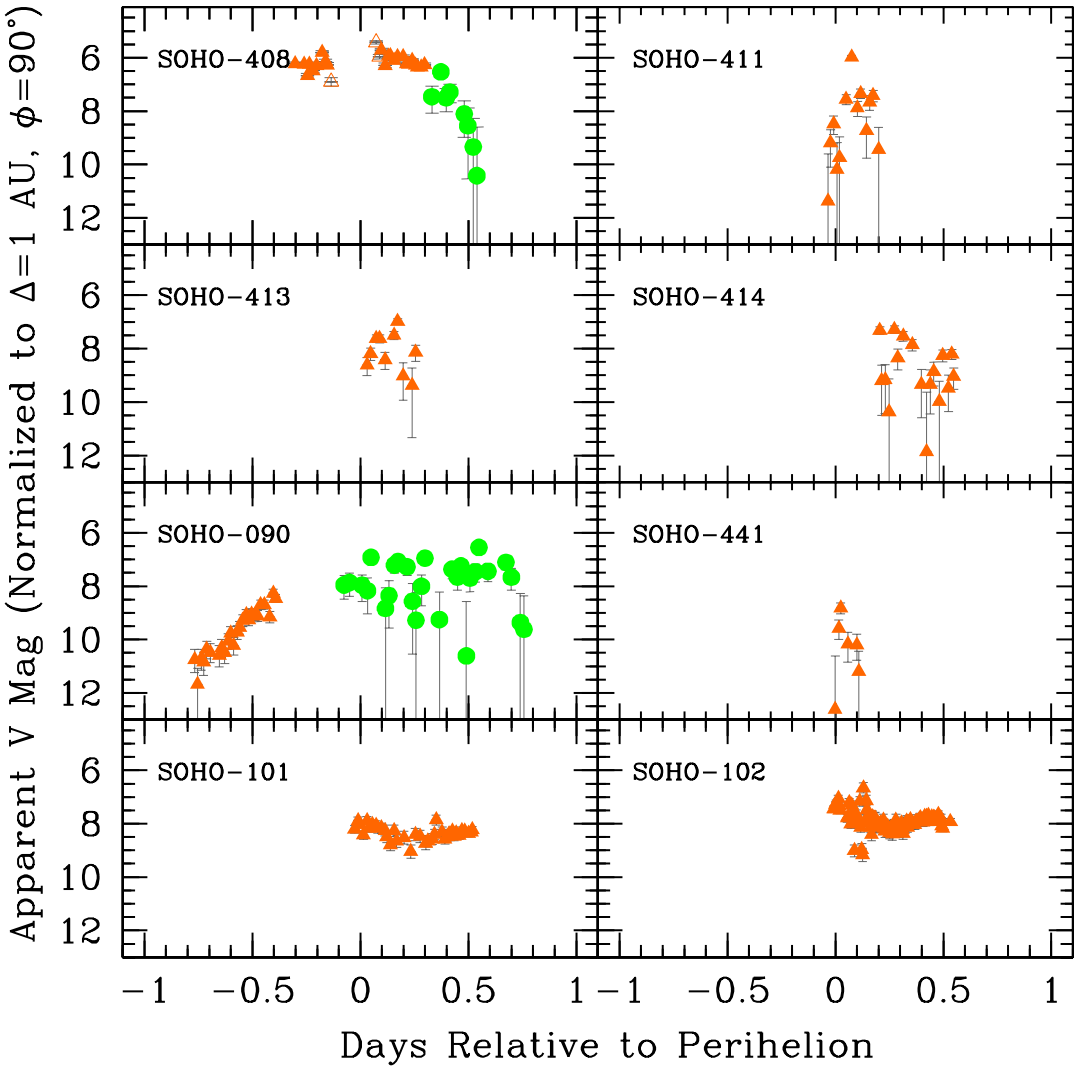

Figure B.15: Lightcurves of Marsden comets. Starting on the top row and moving left to right, these are: C/1999 N5 (SOHO-408), C/1999 P6 (411), C/1999 P8 (413), C/1999 P9 (414), C/1999 U2 (090), C/2000 C7 (441), C/2000 C3 (101), and C/2000 C4 (102). The symbols are as given in Figure B.1.

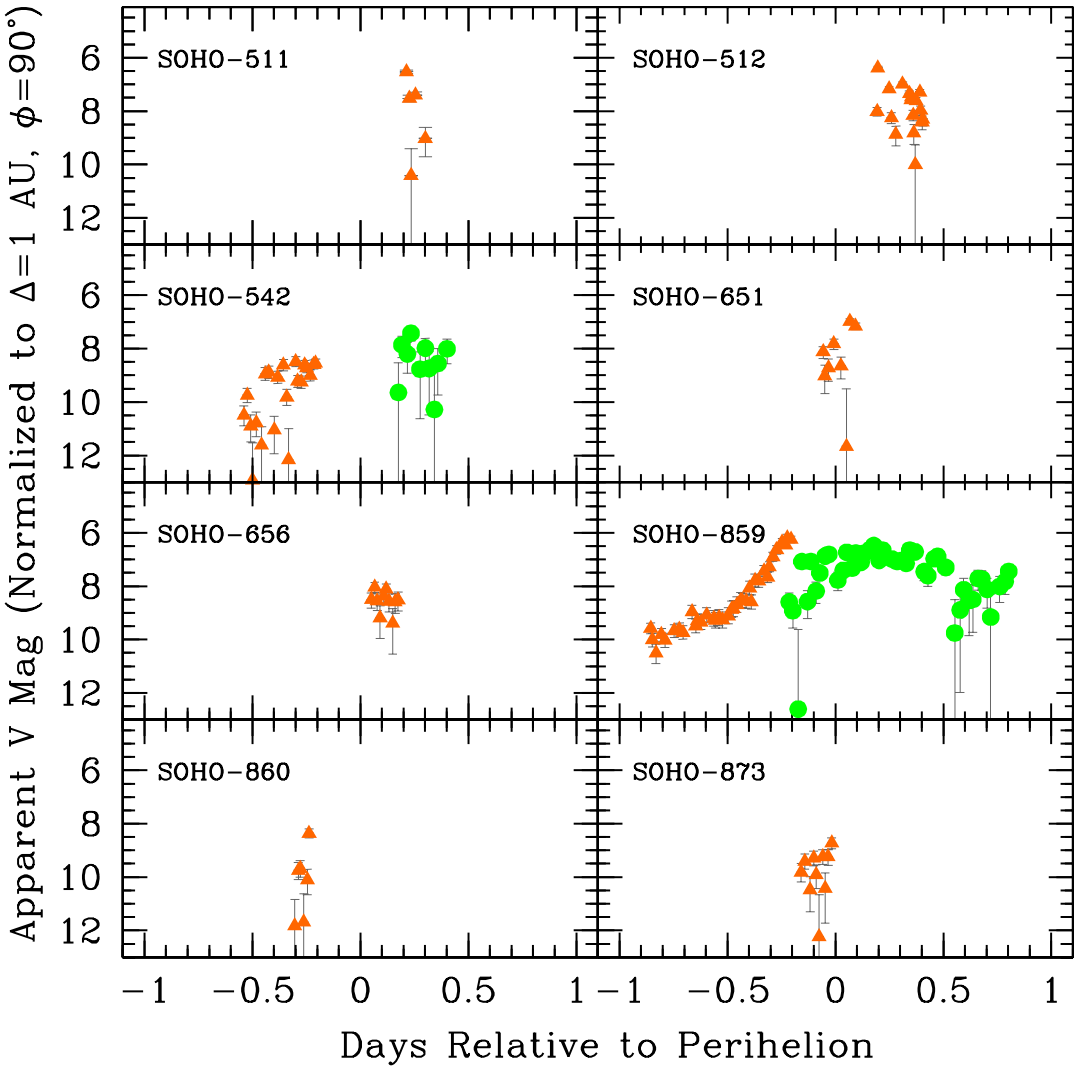

Figure B.16: Lightcurves of Marsden comets. Starting on the top row and moving left to right, these are: C/2002 R1 (SOHO-511), C/2002 R4 (512), C/2002 V5 (542), C/2003 Q1 (651), C/2003 Q6 (656), C/2004 V9 (859), C/2004 V10 (860), and C/2004 W10 (873). The symbols are as given in Figure B.1.

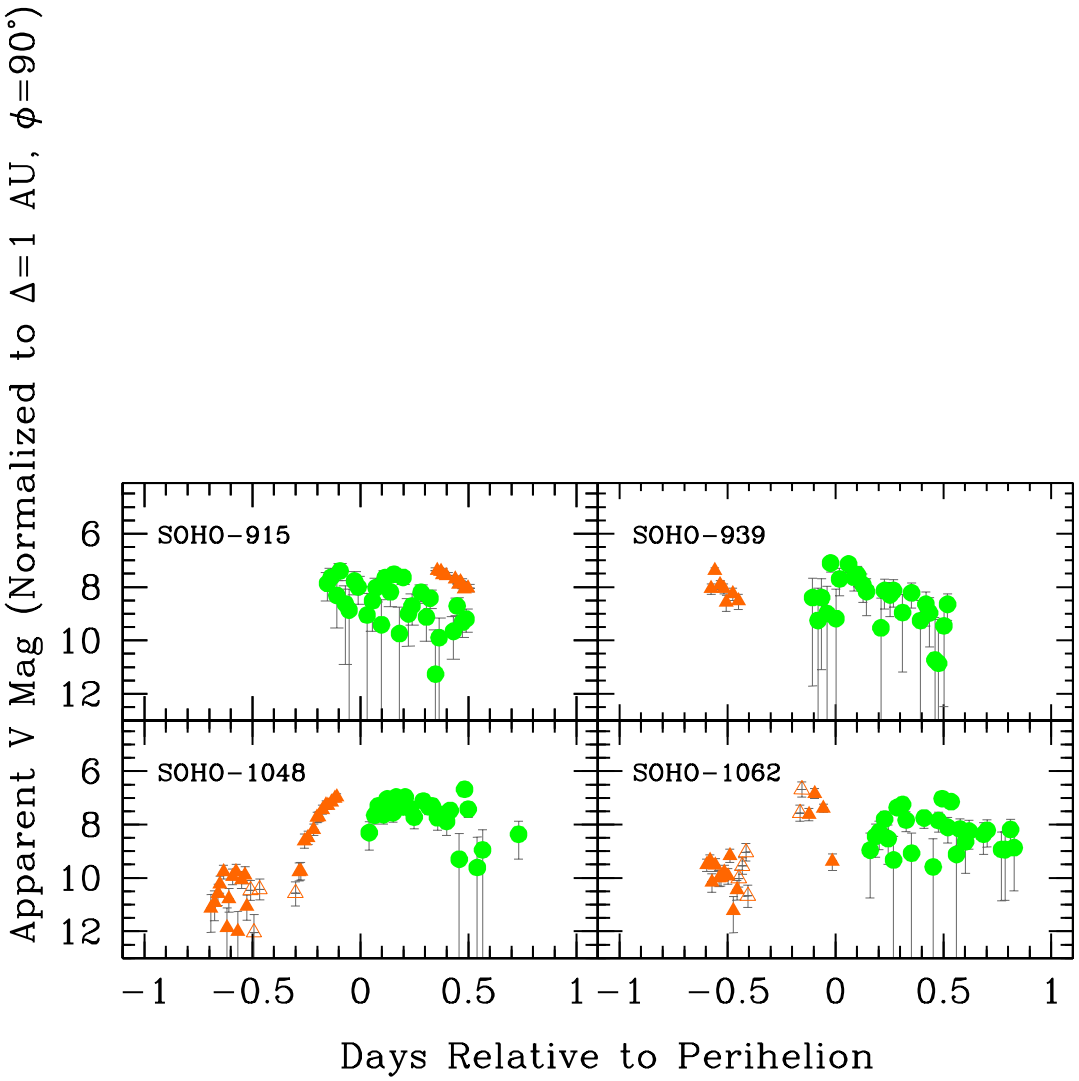

Figure B.17: Lightcurves of Marsden comets. Starting on the top row and moving left to right, these are: C/2005 E4 (915), C/2005 G2 (939), C/2005 W1 (1048), and C/2005 W5 (1062). The symbols are as given in Figure B.1.

Appendix C

A Summary of Each Kracht and Marsden Comet

Combining our photometry and dynamical investigation with the orbital fitting work of Brian Marsden (as published on IAUCs and MPECs) and Rainer Kracht (private communications 2007–2008 and orbits published on his website[1]), we summarize the past, present, and future of observations of the known Kracht and Marsden comets below. Comets are listed in chronological order of arrival and are grouped where appropriate.

C.1 Kracht Group

- **C/1996 X3, X4, X5** – These comets arrived within 0.16 days of each other, making it very likely they were produced by a fragmentation event since their last perihelion passage. Kracht suggested possible linkages with C/2002 S4, S5, and S7 with a period of 5.79 years (Kracht *et al.* 2006). He also suggested C/2002 S11 as a possible return but it now appears to be linked with C/2008

[1] http://www.rkracht.de/soho/kracht1.htm

G6 which would preclude a linkage with C/1996 X3, X4, or X5 (Uchina *et al.* 2008). C/1996 X3 was evidently the faintest of the three since it was the only one not observed in C3. C/2002 S5 was also only observed in C2 while C/2002 S4 and S7 were observed in both C2 and C3. C/1996 X5 was slightly brighter than C/1996 X4 and C/2002 S4 was slightly brighter than C/2002 S7. The photometry suggests C/1996 X3 returned as C/2002 S5, C/1996 X4 returned as S7, and C/1996 X5 returned as C/2002 S4, although the lightcurves are noisy enough that the linkages of C/2002 S4 and S7 could be reversed.

- **C/1999 M3** – Marsden and Chodas have linked this with C/2004 L10 with a period of 4.95 years (Otterstedt *et al.* 2004). Kracht reports that C/2004 J12, J13, J15, J16, J17, J18, and J20 can be linked with C/1999 M3 (with periods of 4.86–4.87 years) but that C/2004 J4 cannot. Dynamically it is almost certain that C/2004 J12, J13, J15, J16, J17, J18, and J20 split from each other since their previous perihelion passage. C/2004 J4 arrived close enough in time to this cluster to be consistent with fragmentation near the previous perihelion passage (Sekanina and Chodas (2005) find that a difference of ∼10 days in perihelion can be explained by breakup near perihelion), however C/2004 L10 arrive some 29 days after the last comet in the cluster (C/2004 J18), a separation much too large to be explained by a reasonable separation velocity. Thus it is unclear dynamically which of these comets are the return(s) of C/1999 M3. The photometry is consistent with any of these linkages. All were observed only in C2, and C/1999 M3 was marginally brighter than any of the potential 2004 returns. C/1999 M3 appeared star-like, and did not show any hint of elongation which might be indicative of a train of fragments.

- **C/1999 N6** – Marsden and Chodas have linked this with C/2004 J4 or J18 (Otterstedt *et al.* 2004) however Kracht reports that he could only link it with C/2004 J4 (Kracht, private communication 2008). A linkage with C/2004 J4 gives a period of 4.81 years. C/1999 N6 was perhaps 1 magnitude fainter than C/1999 M3 and is thus a less likely parent for the cluster of C/2004 J12, J13, J15, J16, J17, J18, and J20. C/1999 N6 is marginally brighter than C/2004 J4. C/1999 M3 and C/1999 N6 were separated by only 12 days and their orbital elements are similar. We could not link them on the previous orbit (in 1994), however they are likely to have fragmented within the preceding few orbits.

- **C/2000 O3** – Marsden and Hoenig have linked this with C/2005 W4 with a period of 5.32 years (Hoenig and Marsden 2005; Zhou *et al.* 2005). C/2000 O3 is the best observed Kracht comet and C/2005 W4 is also well observed, making this the strongest apparent linkage in the family. The photometry is consistent with this linkage as well, as C/2000 O3 was brighter than C/2005 W4 even after correcting for the fact that C/2005 W4 was observed almost entirely in the C3 clear filter while C/2000 O3 was observed in the C2 orange filter (where comets appear $\sim$1 magnitude brighter due to sodium emission).

- **C/2001 Q7, Q8, R8, R9** – None of these comets have been linked to any subsequent comets and given their faintness when observed in 2001, it is likely all are now below the threshold for detection by SOHO. If they had orbital periods shorter than $\sim$5.7 years they should have passed through the SOHO field of view sometime in early to mid-1996. Given the faintness of the comets in 2001 and the infrequency of observations taken in 1996, it is reasonable to assume these comets were not observed. All four comets may have been

produced since the previous perihelion in 1996, although likely from two separate parent fragments (one which produced C/2001 Q7 and Q8 and the other which produced C/2001 R8 and R9). The parents of C/2001 Q7, Q8, R8, and R9 were likely the same comet within a few orbits prior to 1996.

- **C/2002 N2** – Kracht searched for the return of this comet in February 2008 assuming a linkage with one of the cluster of C/1996 X3, X4, or X5 (Kracht, private communication 2008). It has not been recovered and has likely disappeared. Depending on the orbital period, it is likely to have been in the SOHO field of view from mid-1996 until mid-1997. However, the faintness in 2002 makes it plausible to have been missed on its previous apparition.

- **C/2002 Q8, Q10** – Kracht linked C/2002 Q8 to C/2008 E4 with a period of 5.52 years (Zhou *et al.* 2008). C/2002 Q10 has not been recovered and given that it was at least 1 magnitude fainter than C/2002 Q8 it may have disappeared. Kracht has searched images from 1997 February 14–15 based on the linkage of C/2002 Q8 with C/2008 E4 but did not find anything. This linkage will have to wait until 2013 before it can be confirmed.

- **C/2002 S4, S5, S7** – As discussed above, these are believed to be the returns of C/1996 X3, X4, and X5. Kracht predicts these comets will return 2008 June 28–July 4[2]. We expect that C/2002 S4 and S7 should be bright enough to be observed again, although C/2002 S5 may not be.

- **C/2002 S11** – Kracht suggested a link to C/1996 X3, X4, or X5 (Kracht *et al.* 2006) but Kracht and Marsden have since linked it to C/2008 G6 with a period of 5.53 years (Uchina *et al.* 2008). This later linkage precludes C/2002 S11 being linked to C/1996 X3, X4, or X5. Kracht searched images from

[2]http://www.rkracht.de/soho/links.htm

1997 March 16–17 but did not find anything (Kracht, private communication 2008). C/2002 S11 was one of the best observed Kracht comets, visible for more than a day and observed by both C2 and C3. It is troubling that it was not recovered in 1997 images. Until this can be observed again around 2013 October 26 we consider this linkage tentative.

- **C/2004 A3, B3** – These comets arrived roughly 2 days apart. They were faint and benefited from favorable viewing geometry and so are unlikely to be observed again. Even if they were bright enough to be seen on their previous perihelion passage, there is a good chance they were missed because SOHO was not operational for roughly four months between June 1998 and January 1999, corresponding to orbital periods of 5–5.5 years. Their orbital elements deviate by more than most comets in temporal clusters, but C/2004 A3 was only observed in 5 images and as such its orbit is highly uncertain. It is likely they split from each other since their previous perihelion passage.

- **C/2004 J4, J12, J20, J13, J15, J16, J17, J18, L10** – These have all been discussed previously in regards to C/1999 M3 and N6. There is some confusion as to the direct parent of each of these, but it is highly likely that J12, J13, J15, J16, J17, J18, and J20 split since their previous perihelion passage, and that all of these are second or third generation fragments of the same progenitor. None were bright enough to be likely to be observed again, although C/2004 L10 has the best chance, with a return around 2009 May 29 (for a linkage with C/1999 M3). If it is observable, C/2004 J4 is expected to return around 2009 February 27 (for a linkage with C/1999 N6).

- **C/2005 W4** – This has already been discussed as the likely return of C/2000 O3. It was bright enough that we expect it to be visible on its next perihelion

passage around 2011 March 19.

- **C/2008 E4** – This has already been discussed as the likely return of C/2002 Q8. We have not yet calculated the photometry for this comet so we cannot predict the likelihood of its being visible on its next perihelion passage around 2013 September 9.

- **C/2008 G6** – This has already been discussed as the likely return of C/2002 S11. We have not yet calculated the photometry for this comet so we cannot predict the likelihood of its being visible on its next perihelion passage around 2013 October 26.

C.2 Marsden Group

- **C/1996 V2** – We propose that this returned as C/2002 V5 with a period of 6.0 years, although we are not aware of any attempts to link the observations. This was only observed in C3 because no C2 images were taken for several days around its perihelion. As a result the uncertainty in the orbit is likely unusually large. The photometry is consistent with a linkage with C/2002 V5.

- **C/1997 B5, B6, B7** – Battams suggested that two of these comets returned as C/2002 R1 or R4 (Kracht *et al.* 2006), however C/2002 R1 and R4 have now been linked with C/2008 A3 and C/2007 Y4 (Kracht *et al.* 2008; Yuan *et al.* 2008), respectively, which preclude a link with C/1997 B5, B6, or B7. The photometry also disagrees with this linkage, as C/1997 B5, B6, and B7 were all slightly fainter than C/2002 R1 and R4. The geometry was particularly favorable for the observation of C/1997 B5, B6, and B7, and it is not surprising that they have not been reobserved. Their very close arrival times (ΔT=0.14

days) suggest they fragmented since their previous perihelion passage.

- **C/1998 A2, A3, A4** – No linkages have been suggested. The geometry was particularly favorable for the observation of these comets and it is unsurprising that they have not been reobserved. They likely split from each other near their previous perihelion passage.

- **C/1999 J6** – This is the best observed and brightest Marsden or Kracht comet, and the linkage with C/2004 V9 (Otterstedt *et al.* 2004) is quite certain, yielding a period of 5.49 years. This was discussed extensively in Sekanina and Chodas (2005) who found that C/2004 V9 and V10 split from each other a few months before the 1999 perihelion but were still too close together to be resolved. The authors fit their erosion model to the lightcurve of C/1999 J6, estimating its diameter was 48 meters before the perihelion passage in 1999 and 23 meters following the 2004 return. They predict it will be bright enough to be reobserved at its next two perihelion passages in 2010 and 2015. Our lightcurves support the linkage as well[3]. Marsden suggests that C/1999 J6 and

[3]We note that these two comets exhibit a bizarre phase dependence. When the lightcurves normalized only to unit SOHO-centric distance are compared, C/1999 J6 and C/2004 V9 appear virtually identical, with similar slopes of brightening and fading, a similar distance of peak brightness, and only a very slight decrease in brightness in C/2004 V9. However, the phase curves of these two comets are reversed, with C/1999 J6 observed at low phase prior to perihelion and high phase after perihelion while C/2004 V9 is at very high phase prior to perihelion and low phase after perihelion. As a result, the phase corrected lightcurves show C/1999 J6 as substantially brighter. The apparently identical non-phase corrected lightcurves may simply be a coincidence, however applying a correction which induces an unexpected lightcurve shape is troubling. Applying the Kolokolova *et al.* (2004) lightcurve, which has a less dramatic correction at high phase angles also causes C/1999 J6 to be much brighter, although the effect on the shape of the curve is less severe. It is possible that the dust in the coma of C/1999 J6 and C/2004 V9 is of a different size than the

C/1999 N5 likely split from each other near perihelion in 1993 (MPEC 2005-E87), noting that "the remaining slight discordances being understandable on account of the poor quality of even the C2 observations". However, we note that while the orbital elements may be reasonably uncertain (as we have concluded elsewhere), the time of perihelion is certainly well known to within a few hours, and the separation between the perihelion times of C/1999 J6 and C/1999 N5 is ≈31 days. Sekanina and Chodas (2005) found that a separation velocity of 3 m s^{-1} will result in differences in the perihelion time of ∼10 days, and our own simulations show differences of ∼20 days for a separation velocity of 5 m s^{-1}. Thus, the temporal separation of C/1999 J6 and C/1999 N5 would require a relatively high separation velocity in 1993. While we have

---

dust for the comets used to derive the phase function (although one of the comets used to construct the phase curve was 96P/Machholz 1 which is likely linked to the Marsden and Kracht comets). Marcus (2007b) finds that the scattering curve for radius R=0.05 μm particles is relatively flat while the scattering curves for R=0.25 μm and R=1.25 μm show increasing intensities at large scattering angles (and the increase is larger for R=1.25 μm than for R=0.25 μm). Thus, if the dust of C/1999 J6 and C/2004 V9 was dominated by small particles its response to the changing phase angle would be minimal. This raises the possibility that the dust of all the Marsden (and most likely Kracht) comets is smaller than normal and that the phase correction is too severe for these comets. Alternatively, if δ_{90} is very small (ie. extremely gassy) the phase correction would also be very small. It is possible that the dust to gas light ratio is not the same in the Kreutz, Marsden, and Kracht comets. Thus a larger fraction of the observed light in the Marsden (and possibly Kracht) comets may come from the gas in the coma, likely sodium. We note that the phase correction has produced sensible results when applied to all other SOHO observed comets (with the possible exception of C/2000 C3 and C4 as discussed in the footnote below), and that the conclusions from the photometric analysis of the Marsden and Kracht comets is unchanged even if the phase correction is not applied. Therefore, we note the curious nature of the phase correction to C/1999 J6 and C/2004 V9 and the possibility that the phase correction for these comets is too severe, but stand by the conclusions.

not explored dynamical simulations of this link, a split one or more revolutions earlier (e.g. 1988 or before) would require a more reasonable fragmentation velocity.

- **C/1999 N5** – Marsden has linked this to C/2005 E4 with a period of 5.67 years (Oates *et al.* 2005; Oates and Marsden 2005). The photometry is consistent with this linkage, as C/1999 N5 is slightly brighter than C/2005 E4, even after considering that it appears ∼1 magnitude brighter because it was observed in the C2 orange filter while C/2005 E4 was only observed in the C3 clear filter. Marsden has suggested that C/1999 N5 and C/1999 J6 were coincident at their previous perihelion passage (Oates *et al.* 2005) although we favor a split date in 1988 or before, as discussed above. Marsden has also suggested that C/1999 N5 is linked to C/2005 G2 with a period of 5.76 years, and that C/2005 G2 and C/2005 E4 split from each other near perihelion in 1999 (Kracht *et al.* 2005). The large temporal separation of C/2005 E4 and G2 (35 days) argues against this scenario, however there are no other plausible candidates which were observed around this time. C/2005 G2 was much too bright to have been C/1999 P6, P8, or P9, but is consistent with a linkage with C/1999 N5.

- **C/1999 P6, P8, P9** – These were all faint when detected in 1999 and were unsurprisingly not reobserved. Their close perihelion times (particularly C/1999 P8 and P9 which arrived 0.05 days apart) suggest that these fragmented from each other recently, likely since their last perihelion passage.

- **C/1999 U2** – Sekanina, Chodas, and Kracht have suggested that this was likely reobserved as C/2005 W5 with a period of 6.10 years (Kracht *et al.* 2005). Our photometry supports this linkage, with C/1999 U2 approximately

0.5–1.0 magnitude brighter.

- **C/2000 C3, C4, C7** – Marsden suggested that C/2000 C4 likely returned as C/2005 W1 with a period of 5.78 years (Battams and Marsden 2005; Su *et al.* 2005). Sekanina and Chodas (2005) determined that C/2000 C3 and C7 likely split from each other 400–800 days after perihelion in 1994. Our photometry is consistent with C/2000 C4 being the largest fragment (and hence most likely to return), although C/2000 C3 was only ∼0.5 magnitudes fainter and seemed likely to have been reobserved. C/2000 C7 was barely detected and was unlikely to be reobserved. However, the photometry suggests that C/2005 W1 may have been brighter than C/2000 C4. Direct comparison of the lightcurves is difficult because C/2000 C4 was only observed in the C2 orange filter and at very high phase angle while C/2005 W1 was observed in the C3 clear filter at a moderate phase angle at the same distance. This is the only potential linkage in either data set whose second apparition is brighter than the first. We cannot suggest a more suitable linkage for either C/2000 C4 or C/2005 W1, so we must wait until the comet returns around 2011 August 30 to determine whether this linkage is valid.[4]

[4]The lightcurves of C/2000 C3 and C4 illustrate the need to correct for phase angle in sungrazing comets. Both were observed for ∼12 hours and the raw (uncorrected) lightcurves brightened smoothly, peaked ∼6 hours after perihelion, then faded gradually. However, the lightcurve shape corresponded exactly to the phase angle, which peaked at ∼160° precisely when the lightcurves peaked. Our phase correction has flattened the peak, although there is now an inverted peak at the distance where the original peak was. It is possible that the Marcus (2007b) model is overcorrecting at large phase angle. At phase angles larger than 150° it is derived from only two comets, the data points coming from SOHO observations. Marcus (2007b) suggests that the scattering slope of these two comets could be contaminated by the comet's dust tail (causing it to brighten more steeply) since the aperture used for photometry on the SOHO images was much larger than the

- **C/2002 R1** – Kracht has suggested this is linked to C/2008 A3 with a period of 5.37 years (Kracht *et al.* 2008). Battams had previously speculated that it might be the return of C/1997 B5, B6, or B7 (Kracht *et al.* 2006), however the more conclusive C/2008 A3 linkage rules this out. For the linkage with C/2008 A3, the comet should have been visible around 1997 April 19, however nothing has been discovered in these images. It is difficult to estimate how bright this comet should have been in 1997 as the photometry for C/2002 R1 is unreliable. The background fluctuated wildly from image to image, and while the comet was well observed, the magnitude could not be calculated with any certainty. In Figure B.16 we plot the 5 images for which the background looked reasonable, however the comet was seen in an additional 30 images which were not plotted. The perihelion times of C/2002 R1 and R4 suggest a linkage, but they differ substantially in all other orbital elements and given their apparent linkages, it is likely their similar perihelion times are merely coincidental.

- **C/2002 R4** – Battams has suggested this is linked with C/2007 Y4 with a period of 5.30 years (Yuan *et al.* 2008). For this linkage, the comet should have been visible around 1997 May 15, however nothing has been discovered

---

apertures for the other comets in the study. Alternatively, the dust in the coma of C/2000 C3 and C4 may be smaller than the dust in the coma of the comets used to derive the phase curve, as suggested for C/1999 J6, above (although one of the comets used to construct the phase curve was 96P/Machholz 1 which is likely linked to the Marsden and Kracht comets). Another possibility is that the dust to gas light ratio may be lower than the assumed $\delta_{90} = 0.16$ (the value for the Kreutz comets in the orange filter). When the Kolokolova *et al.* (2004) model is applied (which has a less dramatic correction at large phase), the peak at large phase angle reappears (although less severely)! As discussed in the footnote to C/1999 J6 above, the phase correction behaves sensibly and we are confident in the analysis, however as C/2000 C3 and C4 illustrate, it may be slightly too strong a correction at very large phase.

in these images. As with C/2002 R1, it is difficult to estimate how bright this comet should have been in 1997 as the photometry for C/2002 R5 is unreliable. In Figure B.16 we plot the 18 images for which the background looked reasonable, however the comet was seen in an additional 27 images which were not plotted. Marsden notes that for the assumed orbit, the comet would have passed within 0.063 AU of the Earth on 1997 June 14 (Yuan *et al.* 2008).

- **C/2002 V5** – This is likely the return of C/1996 V2 as discussed above. We expect it to be bright enough to be reobserved at its next perihelion passage around 2008 November 12.

- **C/2003 Q1, Q6** – These two comets were faint and it is not surprising that they were not seen previously. They are unlikely to be observed on future orbits as well. Their close arrival times suggest they split recently, but the difference between their other elements is large. The fact that their elements differ so substantially from the rest of the Marsden group suggests they are more closely related to each other than to any other Marsden comets. Meyer[5] has labeled these as uncertain members of the Marsden group but notes that by excluding the worst observation of C/2003 Q6, he can bring its elements closer to the mean Marsden group. If the elements are correct, the comets may belong to the as yet unobserved "Quasi-Marsden precursors" as shown on Figure 2 of Sekanina and Chodas (2005). There is no reason to think that there should be distinct gaps between the components of the Machholz complex, and there may even be other unrecognized members of the Machholz complex contained in the population of "non-group" comets observed by SOHO.

[5]http://www.comethunter.de/groups/marsden.html

- **C/2004 V9, V10** – These are believed to be linked to C/1999 J6 and to have split from each other a few months prior to perihelion in 1999, as discussed above. C/2004 V9 is the dominant object, and should be visible around 2010 May 9 and likely on at least one subsequent orbit. C/2004 V10 was barely detected and is not expected to be observed again.

- **C/2004 W10** – This was barely detected under favorable viewing geometry and is unlikely to have been seen before or to be seen again.

- **C/2005 E4** – This is believed to be the return of C/1999 N5 and to have fragmented from C/2005 G2 near perihelion in 1999, as discussed above. It is likely to be bright enough to be observable on its next perihelion passage around 2010 November 8.

- **C/2005 G2** – This is believed to be the return of C/1999 N5 and to have fragmented from C/2005 E4 near perihelion in 1999, as discussed above. It is likely to be bright enough to be observable on its next perihelion passage around 2011 January 17.

- **C/2005 W1** – This is believed to be the return of C/2000 C4, as discussed above. It should be bright enough to be observable on its next perihelion passage around 2011 August 30.

- **C/2005 W5** – This is believed to be the return of C/1999 U2, as discussed above. It should be bright enough to be observable on its next perihelion passage around 2012 January 6.

- **C/2006 E2, F3** – No linkages have been suggested for these comets. Their arrival ∼10 days apart suggests they may have split from each other near their previous perihelion passage. We have not yet calculated the photometry for

these comets, but note that C/2006 E2 is likely the more massive fragment, having an astrometric baseline of 23 hours (compared to C/2006 F3 which was only visible for 8 hours). The 23 hour baseline for C/2006 E2 suggests it is reasonably bright, and it is surprising that it was not observed previously. Of the two, C/2006 E2 is more likely to be observed on its next perihelion passage.

- **C/2007 Y4** – This is believed to be the return of C/2002 R4, as discussed above. We have not yet calculated the photometry for this comet so we cannot predict the likelihood of its being visible on its next perihelion passage around 2013 April 10.

- **C/2008 A3** – This is believed to be the return of C/2002 R1, as discussed above. We have not yet calculated the photometry for this comet so we cannot predict the likelihood of its being visible on its next perihelion passage around 2013 May 30.

Bibliography

A'Hearn, M. F., M. J. S. Belton, W. A. Delamere, J. Kissel, K. P. Klaasen, L. A. McFadden, K. J. Meech, H. J. Melosh, P. H. Schultz, J. M. Sunshine, P. C. Thomas, J. Veverka, D. K. Yeomans, M. W. Baca, I. Busko, C. J. Crockett, S. M. Collins, M. Desnoyer, C. A. Eberhardy, C. M. Ernst, T. L. Farnham, L. Feaga, O. Groussin, D. Hampton, S. I. Ipatov, J.-Y. Li, D. Lindler, C. M. Lisse, N. Mastrodemos, W. M. Owen, J. E. Richardson, D. D. Wellnitz, and R. L. White 2005. Deep Impact: Excavating Comet Tempel 1. *Science* **310**, 258–264.

A'Hearn, M. F., and M. R. Combi 2007. Deep Impact at Comet Tempel 1. *Icarus* **187**, 1–3.

A'Hearn, M. F., R. L. Millis, D. G. Schleicher, D. J. Osip, and P. V. Birch 1995. The ensemble properties of comets: Results from narrowband photometry of 85 comets, 1976-1992. *Icarus* **118**, 223–270.

Asphaug, E., and W. Benz 1996. Size, Density, and Structure of Comet Shoemaker-Levy 9 Inferred from the Physics of Tidal Breakup. *Icarus* **121**, 225–248.

Bailey, M. E., J. E. Chambers, and G. Hahn 1992. Origin of sungrazers - A frequent cometary end-state. *A&A* **257**, 315–322.

Battams, K., K. Baldwin, and B. G. Marsden 2008. Comets C/2008 D1, C/2008 D2, C/2008 D3, C/2008 D4 (stereo). *IAU Circ.* **8926**.

Battams, K., and B. G. Marsden 2005. Comet C/2005 W1 (SOHO). *IAU Circ.* **8631**.

Battams, K., B. Zhou, R. Kracht, B. G. Marsden, and S. Hoenig 2007. P/2007 r5 = 1999 R1 = 2003 R5 (soho). *IAU Circ.* **8871**.

Bemporad, A., G. Poletto, J. Raymond, and S. Giordano 2007. A review of SOHO/UVCS observations of sungrazing comets. *Planet. Space Sci.* **55**, 1021–1030.

Bemporad, A., G. Poletto, J. C. Raymond, D. A. Biesecker, B. Marsden, P. Lamy, Y.-K. Ko, and M. Uzzo 2005. UVCS Observation of Sungrazer C/2001 C2: Possible Comet Fragmentation and Plasma-Dust Interactions. *ApJ* **620**, 523–536.

Bertaux, J. L., J. Costa, T. Mäkinen, E. Quémerais, R. Lallement, E. Kyrölä, and W. Schmidt 1999. Lyman-alpha observations of comet 46 P/Wirtanen with swan on SOHO: H2O production rate near 1997 perihelion. *Planet. Space Sci.* **47**, 725–733.

Biesecker, D. A., P. Lamy, O. C. St. Cyr, A. Llebaria, and R. A. Howard 2002. Sungrazing Comets Discovered with the SOHO/LASCO Coronagraphs 1996-1998. *Icarus* **157**, 323–348.

Biver, N., D. Bockelée-Morvan, P. Colom, J. Crovisier, F. Henry, E. Lellouch, A. Winnberg, L. E. B. Johansson, M. Gunnarsson, H. Rickman, F. Rantakyrö, J. K. Davies, W. R. F. Dent, G. Paubert, R. Moreno, J. Wink, D. Despois, D. J. Benford, M. Gardner, D. C. Lis, D. Mehringer, T. G. Phillips, and H. Rauer 2002. The 1995 2002 Long-Term Monitoring of Comet C/1995 O1 (HALE BOPP) at Radio Wavelength. *Earth Moon and Planets* **90**, 5–14.

Boehnhardt, H. 2004. *Split comets*, pp. 301–316. Comets II.

Brueckner, G. E., R. A. Howard, M. J. Koomen, C. M. Korendyke, D. J. Michels, J. D. Moses, D. G. Socker, K. P. Dere, P. L. Lamy, A. Llebaria, M. V. Bout, R. Schwenn, G. M. Simnett, D. K. Bedford, and C. J. Eyles 1995. The Large Angle Spectroscopic Coronagraph (LASCO). *Sol. Phys.* **162**, 357–402.

Bzowski, M., and M. Królikowska 2005. Are the sungrazing comets the inner source of pickup ions and energetic neutral atoms? *A&A* **435**, 723–732.

Carusi, A., E. Perozzi, G. B. Valsecchi, and L. Kresak 1985. First results of the integration of motion of short-period comets over 800 years. In A. Carusi and G. B. Valsecchi (Eds.), *IAU Colloq. 83: Dynamics of Comets: Their Origin and Evolution*, Volume 115 of *Astrophysics and Space Science Library*, pp. 319–340.

Chen, J., and D. Jewitt 1994. On the rate at which comets split. *Icarus* **108**, 265–271.

Chochol, D., V. Rusin, L. Kulcar, and V. Vanysek 1983. Emission features in the solar corona after the perihelion passage of Comet 1979 XI. *Ap&SS* **91**, 71–77.

Combi, M. R., J. T. T. Mäkinen, J.-L. Bertaux, and E. Quemérais 2005. Temporal deconvolution of the hydrogen coma. *Icarus* **177**, 228–245.

Combi, M. R., A. A. Reinard, J.-L. Bertaux, E. Quemerais, and T. Mäkinen 2000. SOHO/SWAN Observations of the Structure and Evolution of the Hydrogen Lyman-α Coma of Comet Hale-Bopp (1995 O1). *Icarus* **144**, 191–202.

Danby, J. M. A. 1992. *Fundamentals of Celestial Mechanics*. Richmond: Willman-Bell, —c1992, 2nd ed.

Domingo, V., B. Fleck, and A. I. Poland 1995. The SOHO Mission: an Overview. *Sol. Phys.* **162**, 1–37.

Dones, L., P. R. Weissman, H. F. Levison, and M. J. Duncan 2004. *Oort cloud formation and dynamics*, pp. 153–174. Comets II.

England, K. J. 2002. Early Sungrazer Comets. *Journal of the British Astronomical Association* **112**, 13–28.

Fernández, J. A., G. Tancredi, H. Rickman, and J. Licandro 1999. The population, magnitudes, and sizes of Jupiter family comets. *A&A* **352**, 327–340.

Fernández, Y. R., C. M. Lisse, M. S. Kelley, N. Dello Russo, A. T. Tokunaga,

C. E. Woodward, and D. H. Wooden 2007. Near-infrared light curve of Comet 9P/Tempel 1 during Deep Impact. *Icarus* **191**, 424–431.

Gehrz, R. D., and E. P. Ney 1992. 0.7- to 23-micron photometric observations of P/Halley 2986 III and six recent bright comets. *Icarus* **100**, 162–186.

Green, D. W. E., H. Rickman, A. C. Porter, and K. J. Meech 1990. The strange periodic comet Machholz. *Science* **247**, 1063–1067.

Groussin, O., M. F. A'Hearn, J.-Y. Li, P. C. Thomas, J. M. Sunshine, C. M. Lisse, K. J. Meech, T. L. Farnham, L. M. Feaga, and W. A. Delamere 2007. Surface temperature of the nucleus of Comet 9P/Tempel 1. *Icarus* **187**, 16–25.

Grynko, Y., K. Jockers, and R. Schwenn 2004. The phase curve of cometary dust: Observations of comet 96P/Machholz 1 at large phase angle with the SOHO LASCO C3 coronagraph. *A&A* **427**, 755–761.

Halley, E. 1705. *Philosophical Transactions*.

Hasegawa, I. 1966. . *The Heavens (in Japanese)* **47**, 31.

Hasegawa, I. 1979. Orbits of Ancient and Medieval Comets. *PASJ* **31**, 257–270.

Hasegawa, I., and S. Nakano 2001. Possible Kreutz Sungrazing Comets Found in Historical Records. *PASJ* **53**, 931–949.

Hoenig, S., and B. G. Marsden 2005. Comets C/2005 T6, T7, T8, W4, W5 (SOHO). *IAU Circ.* **8638**.

Hönig, S. F. 2006. Identification of a new short-period comet near the sun. *A&A* **445**, 759–763.

Huebner, W. F. 1967. Diminution of Cometary Heads Due to Perihelion Passage. *Zeitschrift fur Astrophysik* **65**, 185–193.

Iseli, M., M. Küppers, W. Benz, and P. Bochsler 2002. Sungrazing Comets: Properties of Nuclei and in Situ Detectability of Cometary Ions at 1 AU. *Icarus* **155**, 350–364.

Jewitt, D. 1991. Cometary photometry. In R. L. Newburn, Jr., M. Neugebauer, and J. Rahe (Eds.), *IAU Colloq. 116: Comets in the post-Halley era*, Volume 167 of *Astrophysics and Space Science Library*, pp. 19–65.

Kaiser, M. L. 2005. The STEREO mission: an overview. *Advances in Space Research* **36**, 1483–1488.

Kimura, H., I. Mann, D. A. Biesecker, and E. K. Jessberger 2002. Dust Grains in the Comae and Tails of Sungrazing Comets: Modeling of Their Mineralogical and Morphological Properties. *Icarus* **159**, 529–541.

Kirkwood, D. 1880. On the great southern comet of 1880. *The Observatory* **3**, 590–592.

Knight, M., and K. Battams 2007. P/2007 R5 = 1999 R1 = 2003 R5 (SOHO). *IAU Circ.* **8872**.

Knight, M. M., K. J. Walsh, M. F. A'Hearn, R. A. Swaters, B. A. Zauderer, N. H. Samarasinha, R. Vázquez, and H. Reitsema 2007. Ground-based visible and near-IR observations of Comet 9P/Tempel 1 during the Deep Impact encounter. *Icarus* **187**, 199–207.

Kolokolova, L., M. S. Hanner, A.-C. Levasseur-Regourd, and B. Å. S. Gustafson 2004. Physical properties of cometary dust from light scattering and thermal emission. *Comets II*, 577–604.

Kozai, Y. 1962. Secular perturbations of asteroids with high inclination and eccentricity. *AJ* **67**, 591–598.

Kracht, R., K. Battams, G. V. Williams, and B. G. Marsden 2006. Comets C/1996 X3, 1996 X4, 1996 X5, 1997 B5, 1997 B6, 1997 B7 (soho). *Minor Planet Electronic Circulars*, C49.

Kracht, R., D. Hammer, B. G. Marsden, Z. Sekanina, and P. Chodas 2005. Comets C/1999 U2, 2005 W5 (soho). *Minor Planet Electronic Circulars*, Y27.

Kracht, R., S. Hoenig, D. Hammer, and B. G. Marsden 2002. COMETS C/1999 M3, 2002 E1 (SOHO). *Minor Planet Electronic Circulars*, E18.

Kracht, R., X. Leprette, K. Battams, and B. G. Marsden 2005. Comets C/1996 N3, 1997 J5, 1998 U7 (soho). *Minor Planet Electronic Circulars*, H24.

Kracht, R., and B. G. Marsden 2005a. Comet C/1981 W1 (Solwind). *IAU Circ.* **8566**.

Kracht, R., and B. G. Marsden 2005b. Comet C/1984 R1 (Solwind). *IAU Circ.* **8583**.

Kracht, R., and B. G. Marsden 2005c. Comets C/1983 N2 and C/1984 Q1 (Solwind). *IAU Circ.* **8573**.

Kracht, R., R. Matson, B. Zhou, K. Battams, B. G. Marsden, and T. Hoffman 2008. Comets C/2007 Y8, 2007 Y9, 2007 Y10, 2008 A3 (soho). *Minor Planet Electronic Circulars*, B61.

Kresák, L. 1966. A meteor mission into the orbit of sun-grazing comets. *Bulletin of the Astronomical Institutes of Czechoslovakia* **17**, 188–195.

Kreutz, H. 1888. *Untersuchungen uber das comentesystem 1843 I, 1880 I und 1882 II.* Kiel, Druck von C. Schaidt, C. F. Mohr nachfl., 1888.

Kreutz, H. 1891. Untersuchungen uber das System der Cometen 1843 I, 1880 I und 1882 II II. Theil,. *Publication der Koeniglichen Sternwarte in Kiel* **6**.

Kreutz, H. 1901. Anzeige betr. Ergänzungshefte zu den Astr. Nachrichten. *Astronomische Nachrichten* **155**, 63.

Kronk, G. W. 1999. *Cometography : a catolog of comets*. Cometography : a catolog of comets / Gary W. Kronk. Cambridge, U.K. ; New York : Cambridge University Press, 1999.

Kronk, G. W. 2003. *Cometography*. Cometography, by Gary W. Kronk, pp. 852. ISBN 0521585058. Cambridge, UK: Cambridge University Press, December 2003.

Lamy, P., D. A. Biesecker, and O. Groussin 2003. SOHO/LASCO observation of an outburst of Comet 2P/Encke at its 2000 perihelion passage. *Icarus* **163**, 142–149.

Lamy, P. L., I. Toth, Y. R. Fernandez, and H. A. Weaver 2004. The sizes, shapes, albedos, and colors of cometary nuclei. *Comets II*, 223–264.

Lisse, C. M., J. VanCleve, A. C. Adams, M. F. A'Hearn, Y. R. Fernández, T. L. Farnham, L. Armus, C. J. Grillmair, J. Ingalls, M. J. S. Belton, O. Groussin, L. A. McFadden, K. J. Meech, P. H. Schultz, B. C. Clark, L. M. Feaga, and J. M. Sunshine 2006. Spitzer Spectral Observations of the Deep Impact Ejecta. *Science* **313**, 635–640.

Llebaria, A., P. Lamy, and J.-F. Danjard 2006. Photometric calibration of the LASCO-C2 coronagraph for Solar System objects. *Icarus* **182**, 281–296.

Llebaria, A., and A. Thernisien 2001. Highly accurate photometric equalization of long sequences of coronal images. In J.-L. Starck and F. D. Murtagh (Eds.), *Proc. SPIE Vol. 4477, p. 265-276, Astronomical Data Analysis, Jean-Luc Starck; Fionn D. Murtagh; Eds.*, Volume 4477 of *Presented at the Society of Photo-Optical Instrumentation Engineers (SPIE) Conference*, pp. 265–276.

Lowry, S., A. Fitzsimmons, P. Lamy, and P. Weissman 2008. *Kuiper Belt Objects in the Planetary Region: The Jupiter-Family Comets*, pp. 397–410. The Solar System Beyond Neptune.

MacQueen, R. M., and O. C. St. Cyr 1991. Sungrazing comets observed by the Solar Maximum Mission coronagraph. *Icarus* **90**, 96–106.

Mäkinen, J. T. T., J.-L. Bertaux, M. R. Combi, and E. Quémerais 2001. Water Production of Comet C/1999 S4 (LINEAR) Observed with the SWAN Instrument. *Science* **292**, 1326–1329.

Mäkinen, J. T. T., J.-L. Bertaux, H. Laakso, T. Pulkkinen, T. Summanen, E. Kyrölä, W. Schmidt, E. Quémerais, and R. Lallement 2000. Discovery of a

comet by its Lyman-α emission. *Nature* **405**, 321–322.

Mäkinen, J. T. T., J.-L. Bertaux, T. I. Pulkkinen, W. Schmidt, E. Kyrölä, T. Summanen, E. Quémerais, and R. Lallement 2001. Comets in full sky L_{alpha} maps of the SWAN instrument. I. Survey from 1996 to 1998. *A&A* **368**, 292–297.

Marcus, J. N. 2007a. Comet C/2006 P1 (McNaught). *IAU Circ.* **8793**.

Marcus, J. N. 2007b. Forward-scattering enhancement of comet brightness. I. Background and model. *Int. Comet Quart.*, 39–66.

Marcus, J. N. 2007c. Forward-scattering enhancement of comet brightness. II. The Light Curve of C/2006 P1 (McNaught). *Int. Comet Quart.*, 119–130.

Marcus, J. N., and D. A. J. Seargent 1986. Dust forward scatter brightness enhancement in previous apparitions of Halley's Comet. In *ESLAB Symposium on the Exploration of Halley's Comet. Volume 2: Dust and Nucleus*, Volume 250 of *ESA Special Publication*, pp. 359–362.

Marsden, B. G. 1967. The sungrazing comet group. *AJ* **72**, 1170–1183.

Marsden, B. G. 1989. The sungrazing comet group. II. *AJ* **98**, 2306–2321.

Marsden, B. G. 2005. Sungrazing Comets. *ARA&A* **43**, 75–102.

Marsden, B. G., and K. Battams 2008a. COMETS C/2007 C11, 2007 D4, 2007 D5, 2007 E4, 2007 E5, 2007 F5, 2007 Y10. *Minor Planet Electronic Circulars*, F38.

Marsden, B. G., and K. Battams 2008b. COMETS C/2007 L2, 2007 L3, 2007 L13, 2007 V4 (SOHO). *Minor Planet Electronic Circulars*, G4.

Marsden, B. K., B. G., and K. Baldwin 2008. COMETS C/2007 F2, 2007 S5 (SOHO). *Minor Planet Electronic Circulars*, G15.

Meech, K. J., O. R. Hainaut, and B. G. Marsden 2004. Comet nucleus size distributions from HST and Keck telescopes. *Icarus* **170**, 463–491.

Meyer, M. 2003. New Groups of Near-Sun Comets. *International Comet Quarterly*, 115–122.

Meyer, M., D. Hammer, and B. G. Marsden 2002. COMET C/2002 C3 (SOHO). *Minor Planet Electronic Circulars*, C28.

Michels, D. J., N. R. Sheeley, R. A. Howard, and M. J. Koomen 1982. Observations of a Comet on Collision Course with the Sun. *Science* **215**, 1097–1102.

Morrill, J. S., C. M. Korendyke, G. E. Brueckner, F. Giovane, R. A. Howard, M. Koomen, D. Moses, S. P. Plunkett, A. Vourlidas, E. Esfandiari, N. Rich, D. Wang, A. F. Thernisien, P. Lamy, A. Llebaria, D. Biesecker, D. Michels, Q. Gong, and M. Andrews 2006. Calibration of the Soho/Lasco C3 White Light Coronagraph. *Sol. Phys.* **233**, 331–372.

Newton, I. 1687. *Philosophiae Naturalis Principia Mathematica, Book 3, Prop. 41.* London: Streater.

Ney, E. P. 1982. Optical and infrared observations of bright comets in the range 0.5 micrometers to 20 micrometers. In L. L. Wilkening (Ed.), *IAU Colloq. 61: Comet Discoveries, Statistics, and Observational Selection*, pp. 323–340.

Ney, E. P., and K. M. Merrill 1976. Comet West and the scattering function of cometary dust. *Science* **194**, 1051–1053.

Oates, M., R. Kracht, K. Battams, and B. G. Marsden 2005. Comets C/2005 E3, 2005 E4 (soho). *Minor Planet Electronic Circulars*, E87.

Oates, M., and B. G. Marsden 2005. Comets C/2005 E3 (SOHO) and C/2005 E4 (SOHO). *IAU Circ.* **8494**.

Ohtsuka, K., S. Nakano, and M. Yoshikawa 2003. On the Association among Periodic Comet 96P/Machholz, Arietids, the Marsden Comet Group, and the Kracht Comet Group. *PASJ* **55**, 321–324.

Otterstedt, H., K. Battams, B. G. Marsden, and P. Chodas 2004. Comets C/2004 V9, 2004 V10 (soho). *Minor Planet Electronic Circulars*, X73.

Povich, M. S., J. C. Raymond, G. H. Jones, M. Uzzo, Y.-K. Ko, P. D. Feldman, P. L.

Smith, B. G. Marsden, and T. N. Woods 2003. Doubly Ionized Carbon Observed in the Plasma Tail of Comet Kudo-Fujikawa. *Science* **302**, 1949–1952.

Preston, G. W. 1967. The spectrum of Ikkeya-Seki (1965f). *ApJ* **147**, 718–742.

Rauch, K. P., and D. P. Hamilton 2002. The HNBody Package for Symplectic Integration of Nearly-Keplerian Systems. In *Bulletin of the American Astronomical Society*, Volume 34 of *Bulletin of the American Astronomical Society*, pp. 938.

Raymond, J. C., S. Fineschi, P. L. Smith, L. Gardner, R. O'Neal, A. Ciaravella, J. L. Kohl, B. Marsden, G. V. Williams, C. Benna, S. Giordano, G. Noci, and D. Jewitt 1998. Solar Wind at 6.8 Solar Radii from UVCS Observation of Comet C/1996Y1. *ApJ* **508**, 410–417.

Raymond, J. C., M. Uzzo, Y.-K. Ko, S. Mancuso, R. Wu, L. Gardner, J. L. Kohl, B. Marsden, and P. L. Smith 2002. Far-Ultraviolet Observations of Comet 2P/Encke at Perihelion. *ApJ* **564**, 1054–1060.

Rickman, H., and C. Froeschle 1988. Cometary dynamics. *Celestial Mechanics* **43**, 243–263.

Schleicher, D. G. 2007. Deep Impact's target Comet 9P/Tempel 1 at multiple apparitions: Seasonal and secular variations in gas and dust production. *Icarus* **190**, 406–422.

Schulz, R., A. Owens, P. M. Rodriguez-Pascual, D. Lumb, C. Erd, and J. A. Stüwe 2006. Detection of water ice grains after the DEEP IMPACT onto Comet 9P/Tempel 1. *A&A* **448**, L53–L56.

Sekanina, Z. 1967a. Definitive orbit of Comet Pereyra (1963 V). *Bulletin of the Astronomical Institutes of Czechoslovakia* **18**, 229–232.

Sekanina, Z. 1967b. On the origin of the Kreutz family of sun-grazing comets. *Bulletin of the Astronomical Institutes of Czechoslovakia* **18**, 198–199.

Sekanina, Z. 1977. Relative motions of fragments of the split comets. I - A new

approach. *Icarus* **30**, 574–594.

Sekanina, Z. 1978. Relative motions of fragments of the split comets. II - Separation velocities and differential decelerations for extensively observed comets. *Icarus* **33**, 173–185.

Sekanina, Z. 1982. The problem of split comets in review. In L. L. Wilkening (Ed.), *IAU Colloq. 61: Comet Discoveries, Statistics, and Observational Selection*, pp. 251–287.

Sekanina, Z. 2000a. Secondary Fragmentation of the Solar and Heliospheric Observatory Sungrazing Comets at Very Large Heliocentric Distance. *ApJ* **542**, L147–L150.

Sekanina, Z. 2000b. Solar and Heliospheric Observatory Sungrazing Comets with Prominent Tails: Evidence on Dust-Production Peculiarities. *ApJ* **545**, L69–L72.

Sekanina, Z. 2002a. Runaway Fragmentation of Sungrazing Comets Observed with the Solar and Heliospheric Observatory. *ApJ* **576**, 1085–1089.

Sekanina, Z. 2002b. Statistical Investigation and Modeling of Sungrazing Comets Discovered with the Solar and Heliospheric Observatory. *ApJ* **566**, 577–598.

Sekanina, Z. 2003. Erosion Model for the Sungrazing Comets Observed with the Solar and Heliospheric Observatory. *ApJ* **597**, 1237–1265.

Sekanina, Z., and P. W. Chodas 2002a. Common Origin of Two Major Sungrazing Comets. *ApJ* **581**, 760–769.

Sekanina, Z., and P. W. Chodas 2002b. Fragmentation Origin of Major Sungrazing Comets C/1970 K1, C/1880 C1, and C/1843 D1. *ApJ* **581**, 1389–1398.

Sekanina, Z., and P. W. Chodas 2004. Fragmentation Hierarchy of Bright Sungrazing Comets and the Birth and Orbital Evolution of the Kreutz System. I. Two-Superfragment Model. *ApJ* **607**, 620–639.

Sekanina, Z., and P. W. Chodas 2005. Origin of the Marsden and Kracht Groups of

Sunskirting Comets. I. Association with Comet 96P/Machholz and Its Interplanetary Complex. *ApJS* **161**, 551–586.

Sekanina, Z., and P. W. Chodas 2007. Fragmentation Hierarchy of Bright Sungrazing Comets and the Birth and Orbital Evolution of the Kreutz System. II. The Case for Cascading Fragmentation. *ApJ* **663**, 657–676.

Sheeley, N. R., Jr., R. A. Howard, M. J. Koomen, and D. J. Michels 1982. Coronagraphic observations of two new sungrazing comets. *Nature* **300**, 239–242.

Slaughter, C. D. 1969. The Emission Spectrum of Comet Ikeya-Seki 1965-f at Perihelion Passage. *AJ* **74**, 929–943.

Snodgrass, C., A. Fitzsimmons, O. Hainaut, M. Hamuy, D. Hutsemekers, E. Jehin, M. Jones, and J. Manfroid 2007. Comet C/2006 P1 (McNaught). *Central Bureau Electronic Telegrams* **832**.

St. Cyr, O. C., J. Burkepile, A. Stanger, D. Pitone, B. Twambly, and B. G. Marsden 1989. Comet 1989x (SMM 10). *IAU Circ.* **4884**.

Strom, R. 2002. Daytime observations of sungrazing comets in Chinese annals. *A&A* **387**, L17–L20.

Su, H., K. Battams, and B. G. Marsden 2005. Comet C/2005 w1 (soho). *Minor Planet Electronic Circulars*, W7.

Sunshine, J. M., O. Groussin, P. H. Schultz, M. F. A'Hearn, L. M. Feaga, T. L. Farnham, and K. P. Klaasen 2007. The distribution of water ice in the interior of Comet Tempel 1. *Icarus* **190**, 284–294.

Tancredi, G., J. A. Fernández, H. Rickman, and J. Licandro 2006. Nuclear magnitudes and the size distribution of Jupiter family comets. *Icarus* **182**, 527–549.

Tancredi, G., V. Motta, and C. Froeschlé 2000. Dynamical taxonomy of comets and asteroids based on the Lyapunov indicators. An analysis of the relevance of splitting. *A&A* **356**, 339–346.

Thernisien, A. 2003. Photometric Calibration of C3 Using Stars and LAS Color Correction: Summary of the Results. *private communication*.

Thernisien, A. F., J. S. Morrill, R. A. Howard, and D. Wang 2006. Photometric Calibration of the Lasco-C3 Coronagraph Using Stars. *Sol. Phys.* **233**, 155–169.

U. S. Naval Observatory, and Royal Greenwich Observatory 1999. *The Astronomical almanac for the year 2000*. The Astronomical almanac for the year 2000 Washington : Issued by the Nautical Almanac Office, United States Naval Observatory by direction of the Secretary of the Navy and under the authority of Congress : For sale by the Supt. of Docs., U.S. G.P.O. ; London : For sale by Her Majesty's Stationery Office,.

Uchina, M., B. Zhou, H. Su, R. Matson, K. Battams, B. G. Marsden, and R. Kracht 2008. Comets C/2008 G5, 2008 G6, 2008 H2, 2008 H3 (soho). *Minor Planet Electronic Circulars*, L29.

Uzzo, M., J. C. Raymond, D. Biesecker, B. Marsden, C. Wood, Y.-K. Ko, and R. Wu 2001. Results from UVCS and LASCO Observation of the Sungrazing Comet C/2000 C6. *ApJ* **558**, 403–410.

Watanabe, J.-i., H. Kawakita, R. Furusho, and M. Fujii 2003. Heliocentric Dependence of the Sodium Emission of Comet 153P/Ikeya-Zhang. *ApJ* **585**, L159–L162.

Weidenschilling, S. J. 2004. *From icy grains to comets*, pp. 97–104. Comets II.

Weissman, P. R. 1980. Physical loss of long-period comets. *A&A* **85**, 191–196.

Weissman, P. R., and S. C. Lowry 2003. The Size Distribution of Jupiter-Family Cometary Nuclei. In S. Mackwell and E. Stansbery (Eds.), *Lunar and Planetary Institute Conference Abstracts*, Volume 34 of *Lunar and Planetary Institute Conference Abstracts*, pp. 2003.

Yeomans, D. K. 1991. *Comets. A chronological history of observation, science, myth, and folklore*. New York: Wiley, 1991.

Yuan, S., R. Kracht, A. Kubczak, H. Su, K. Battams, and B. G. Marsden 2008. Comets C/2007 Y3, 2007 Y4, 2007 Y5, 2007 Y6, 2007 Y7 (soho). *Minor Planet Electronic Circulars*, B49.

Zhou, B., H. Su, K. Battams, B. G. Marsden, and S. Hoenig 2005. Comets C/2005 W4, 2005 W5 (soho). *Minor Planet Electronic Circulars*, X14.

Zhou, X.-M., H. Su, R. Kracht, K. Battams, and B. G. Marsden 2008. Comets C/2002 Q8, 2008 E4, 2008 F1 (soho). *Minor Planet Electronic Circulars*, F32.